Energy & Environmental Science

Multiscale Factors in Designing Alkali-Ion (Li, Na, and K) Transition Metal Inorganic Compounds for Next-Generation Rechargeable Batteries

Journal:	*Energy & Environmental Science*
Manuscript ID	EE-REV-04-2020-001277.R1
Article Type:	Review Article
Date Submitted by the Author:	n/a
Complete List of Authors:	Lee, Wontae; Sungkyunkwan University, Department of Energy Science Kim, Jaeyoung; Sungkyunkwan University - Suwon Campus, Energy Science Yun, Soyeong; Sungkyunkwan University, Department of Energy Science Choi, Woosung; Sungkyunkwan University, Department of Energy Science Kim, Haegyum; Lawrence Berkeley National Laboratory, Material Sciences Division Yoon, Won-Sub; Sungkyunkwan University, Department of Energy Science

Energy & Environmental Science

Guidelines for Reviewers

Thank you very much for agreeing to review this manuscript for *Energy & Environmental Science*.

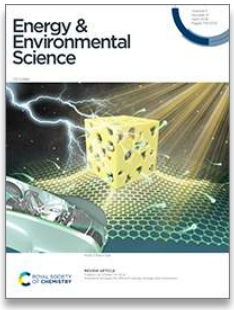

Energy & Environmental Science is an international journal dedicated to publishing exceptionally important and high quality, agenda-setting research tackling the key global and societal challenges of ensuring the provision of energy and protecting our environment for the future. For work to be published it must be linked to the energy-environment nexus and be of significant general interest to our community-spanning readership. Further information on scope can be found on the journal's website: rsc.li/ees.

Energy & Environmental Science's Impact Factor is **33.250** (2018 Journal Citation Reports®)

The following manuscript has been submitted for consideration as a

REVIEW

Review articles are detailed, balanced, state-of-the-art and authoritative current accounts of the selected research field. Review articles normally comprise 10,000 or more words of text, together with supporting figures and tables. They should be timely and add to the existing literature, rather than duplicate existing articles, and should be of general interest to the journal's wide readership.

When preparing your report, please:

- Focus on the originality, importance, impact and reliability of the science. English language and grammatical errors do not need to be discussed in detail, except where it impedes scientific understanding.
- Use the journal scope and expectations to assess the manuscript's suitability for publication in *Energy & Environmental Science.*
- State clearly whether you think the article should be accepted or rejected and include details of how the science presented in the article corresponds to publication criteria.
- Inform the Editor if there is a conflict of interest, a significant part of the work you cannot review with

Best regards,

Professor Joseph T. Hupp
Editorial Board Chair
Northwestern University, USA

Dr Sam Keltie
Executive Editor
Royal Society of Chemistry

Contact us

Please visit our reviewer hub for further details of our processes, policies and reviewer responsibilities as well as guidance on how to review, or click the links below.

What to do when you review

Reviewer responsibilities

Process & policies

Response to Reviewers
(Manuscript ID: EE-REV-04-2020-001277)

Title: Multiscale Factors in Designing Alkali-ion (Li, Na, and K) Transition Metal Inorganic Compounds for Next-Generation Rechargeable Batteries

Wontae Lee[a,†], Jaeyoung Kim[a,†], Soyeong Yun[a], Woosung Choi[a], Haegyeom Kim[b], and Won-Sub Yoon[a*]*

[a]Department of Energy Science, SungKyunKwan University, Suwon 440-746, South Korea, E-mail: wsyoon@skku.edu

[b]Materials Sciences Division, Lawrence Berkeley National Laboratory, Berkeley, CA 94720, USA, E-mail: haegyumkim@lbl.gov

[c]The Institute of New Paradigm of Energy Science Convergence, Sungkyunkwan University, Suwon 16419, Republic of Korea.

†These authors contributed equally to this work

Dear editor.

We would like to express our sincere gratitude to you for the time to consider our manuscript (Review, manuscript number: **EE-REV-04-2020-001277**) for publication in Energy & Environmental Science. We are also grateful to the reviewers for the precious and fruitful comments, which certainly helped us to improve the quality of our manuscript. In the revised manuscript, we have addressed the reviewer's comments point by point and hope that the manuscript is now ready for publication in *Energy & Environmental Science*. The revised text in the manuscript is highlighted with different background color as yellow. The changes and response to the reviewer's comments are as follows:

Reviewer #1: The reviewer enjoyed reading this review article. It has a very good balance between various aspects of the field. The authors described very nicely what are the parameters that are important in designing next generation alkali metal compounds cathode materials. With careful attention to practicality (cost and safety) to material structure (atomistic, molecular and crystal). The authors address the importance of the interface and morphology in various systems. Overall this review is a very good summary, and gives useful introduction and perspective to the community.

Response to the overall comments

➔ We appreciate the reviewer's encouraging comments on our manuscript.

Reviewer #2: The review article "Multiscale Factors in Designing Alkali-Ion Transition Metal Inorganic Compounds for Next-Generation Rechargeable batteries" provides a detailed and very comprehensive review on different aspects of cathode materials, mainly for Li-ion batteries, with several inserts describing sodium and potassium materials.
Review has been submitted based on invitation and authors replied properly to set of comments and questions from previous reviewers. Although, as a reviewer I should concentrate only on rebuttal letter and corrections, I take a privilege to read very carefully whole manuscript and provide additional comments and suggestions, which in my opinion will help authors to further improve this review article. Once this is done I suggest that it is accepted and published since field needs such deep understanding that is provided in this work.
My comments and suggestions are:

Additional comments:

Nevertheless, I have read this manuscript and i was happy with the contents and discussions. I was impressed by the amount of information and the way that authors organized the ideas: I like in particular the scope covering from atoms to crystals and to particle size and morphology. Such a kind of comprehensive review covering the different scales is not so frequent in battery materials science. I also like the choice of figures and illustrations. However, a negative point: the authors do not address the topic of formulation. Electrodes formulation (i.e. the inactive phases such as carbon additives and binder surrounding the active material particles) will also affect the overall activity of the active material particles, and not only then their shape, size and crystallinity. But it is understandable that the authors cannot cover this, their review is already long and cover many aspects. Then it is a matter of the authors' choice. I think also that the topic is timely and can raise interest from the battery audience. I would recommend it for publication.

Response to the overall comments

➔ We thank to the reviewer's comments that are helpful to improve the quality of our review article. Moreover, we appreciate the reviewer for understanding why we do not cover the contents like as an electrode formulation, and many thanks again for sharing a good idea with us to improve our manuscript. The answers to the reviewer's valuable comments are described below.

1. P.8: authors compare lithium, potassium and sodium cobalt oxide and reference for Li_xCoO_2 reports probably the worst behavior of compound that runs most of mobile phones. I am not sure it that this is fair comparison

Response

➔ We would like to thank the reviewer for the kind comment on the suitability of Li_xCoO_2 reference for the comparison. The main point of page 8 is indeed that Li_xCoO_2 can provide better cycling stability despite larger strain than Na- and K-analogues. When all the points of our main idea and reviewer's comment on this are considered, we believe that comparing only the P2-K_xCoO_2 with the P2-Na_xCoO_2 is better than before. In this case, the variable can be minimized for the comparison as excluding the different structure types like O2- or O3-Li_xCoO_2. Hence, we have modified the related content in the revised manuscript as follows:

"It is widely believed that the insertion of larger alkali-ions into the cathode hosts leads to a larger lattice strain and faster capacity degradation. For example, $K_{0.6}CoO_2$ retains only ~60% of the initial capacity after 120 cycles. However, the opposite trend is observed when we compare the cycling stability and lattice change of A_xCoO_2 **(Revised:** (A= Na and K).**)** P2-K_xCoO_2 shows only ~3.5% change in c lattice between charged and discharged states, **(Revised:** but P2-Na_xCoO_2 exhibits ~4.0% of c lattice change, respectively.**)** In this comparison, we found that larger lattice strain provides better cycling stability **(Revised:** even after 1000 cycles: P2-K_xCoO_2 (60% after 120 cycles), P2-Na_xCoO_2 (94% after 1000 cycles).**)**

2. P.8 – section 2.1.2 – authors state that transition metal ions function as a main electron source and major component of constructing framework of the electrode material – this is old school and can kill creativity of young people. There are many examples that change of redox state in TM is lower compared to anionic activity. Besides that, polyanionic materials are constructed based on polyanionic network.

Response

➔ We appreciate the reviewer's thoughtful advice on the part of transition metal ions perspective in our manuscript. We agree that the original sentence is rather misleading. The transition metal ion is one of the electron sources and the components of constructing framework of the electrode material. The effects of anion framework and anion redox are described in Page 12 and Page 16 in the original manuscript. Thus, we have modified the original sentence in the revised manuscript as follows:

"From the point of view of a cathode, the above requirements are highly dependent on the transition metal ions. **(Revised:** The transition metal ions function as a one of the main electron sources and one of the major components of constructing framework of the electrode materials.**)** The important thing to consider when designing electrode materials is how many available electrons and how high redox potential couples are there in the **(Revised**: electron sources**)**, which is directly linked

to the energy and power density."

3. P.8 – structural polymorphism have influence on potential, from small shown on case of phosphates and silicates to substantial shown in the case of tavorite phase as shown in Fig7.

Response

➔ We would like to thank the reviewer for the kind comment on the relationship between structural polymorph and redox potential. We believe that the reviewer's comment can make our manuscript more fruitful. However, when considering the proper place, we have added the related contents to the chapter of polymorph in the 'molecular to crystallographic scale' rather than to the chapter of redox potential in the 'atomic to molecular scale' in the revised manuscript as follows:

"Crystal polymorphs are defined as compounds that have same nominal chemical formula but exist in more than one crystal structure. Polymorphism is of particular importance in the polyanion compounds, as a lot of polyanion compounds sometimes have more than one crystal form and their electrochemical properties vary depending on the crystal structure. **(Revised:** For example, the structural polymorphism has an impact on the redox potential as shown in Fig. 7.**)** **(Revised:** More specifically,**)** all two structures, tavorite structure of $LiFe_{0.9}Mn_{0.1}SO_4F$ and triplite structure of $LiFe_{0.9}Mn_{0.1}SO_4F$, have similar close-packing structures that maintain the underlying framework of the sulfate tetrahedra. However, the reaction potential increases in the order of $LiFe_{0.9}Mn_{0.1}SO_4F$ in the tavorite phase (3.6 V) and $LiFe_{0.9}Mn_{0.1}SO_4F$ in the triplite phase (3.9 V) while they use the same $Fe^{2+/3+}$ redox"

4. P.12 – dissolved metals can accumulate on the surface of electrode materials – but it is even more important to mention that metal ions can be reduced on the negative electrode making passive film conductive, and that consumes electrolyte, or in worst case can lead to short circuit.

Response

➔ We really appreciate the reviewer's comments. As the reviewer pointed out, the issues that the reduction of dissolved metal ions can make a passive film on the negative electrode, and that consumes electrolyte, or in worst case can lead to short circuit are important topic to know. In response to the helpful advice of the reviewer, we have added the related contents and references in the revised manuscript as follows:

"Even worse, the dissolved ions can be accumulated on the surface of electrode materials or block the pores of separator, leading an increase in internal resistance. **(Revised:** Furthermore, the dissolved transition metal ions can travel to the negative electrode and form a passive film by the reduction reaction at there, and that consume electrolytes, or in worst case can result in short circuit. [Ref. R1]**)** In the case of Cr^{4+} ion, the three Cr^{4+} ions are easily changed to two Cr^{3+} and one Cr^{6+} ion by the disproportionation reaction because Cr ion is more stable in the electron configurations of Cr^{3+} and Cr^{6+} ions than that of Cr^{4+} ion (*i.e.,* $3Cr^{4+} \rightarrow 2Cr^{3+} + Cr^{6+}$)."

Reference

[Ref. R1] C. Zhan, T. Wu, J. Lu, K. Amine, *Energy Environ. Sci.*, 2018, **11**, 243

5. P.16 – section 2.2. Explain better which crystallographic properties are fundamentally linked to the changes in the constituent elements and interactions.

Response

➔ We are very grateful to the reviewer for helping us to further improve our manuscript. We agree that it would be better to explain the content in detail as the reviewer pointed out. Thus, we have added the examples to the revised manuscript as follows:

"The crystallographic properties and behaviors of insertion cathode materials are fundamentally linked to the changes in the constituent elements and interactions among them. **(Revised:** For example, in the case of crystallographic properties like as lattice parameters and unit cell volume largely depend on the size of constituent atoms. Therefore, in some cases, we can control the parameters by changing the ratio of constituent elements. Moreover, in the Ni-based layered materials, the atomic position of Li^{+} and Ni^{2+} ions can be easily exchanged due to the similar ion size of the two ions, making disordered structure, and that can lead to impede the diffusion of mobile ions.**)** The manipulation of molecular scale factors has obviously crystallographic effects, and the ongoing technical development in the structural analysis is providing detailed information on the corresponding results."

6. Figure 9 – one phase reaction should be replaced with solid state solution

Response

➔ We would like to thank the reviewer for the valuable comment. We have modified the sentence in the Figure 9 in the revised manuscript as follows:

"One phase reaction → **Revised:** Solid solution reaction"

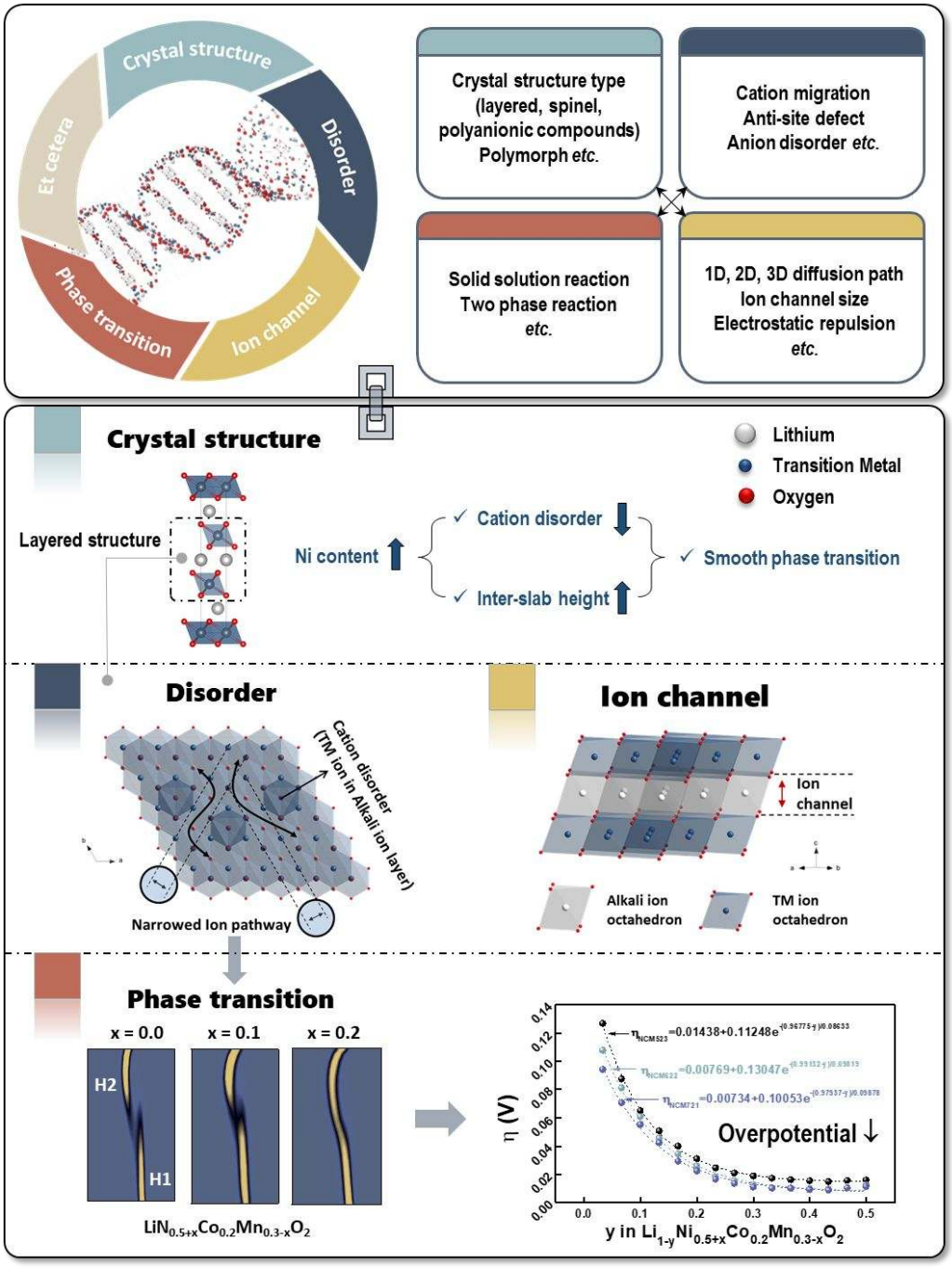

7. P.27 last sentence where flourophosphate is mentioned – I don't see the reason for this comparison except previously discussed completely different type of cathodes

Response

➔ The reason we put the flourophosphate is that we want to show that large and inactive ions in the ion channel can provide beneficial effect on the migration of alkali-

ions in not only layered oxides but also other type cathodes such as polyanions. In response to the reviewer's comment, we revised the manuscript as follow:

➔ **(Revised:** Similar effect can also be observed in other type cathodes. As an example,) in the case of fluorophosphates ($Li_{1.1}Na_{0.4}VPO_{4.8}F_{0.7}$) cathode material, Park *et al.* suspected that a large size of Na^+ ion maintains a larger framework and it provides beneficial environment for Li-ion diffusion.**)**

8. P.27 – yellow highlighted paragraph – language revision needed –"Li layer is also can be…."

Response

➔ We really appreciate the reviewer's precious and kind comments. We have modified the sentence in the revised manuscript as follows:

"**(Revised:** As migrated transition metal ion in tetrahedral site in the Li layer can also be considered as mobile ion which experience the electrostatic repulsion between transition metal layer**)**, Eum *et al.* experimentally corroborated that O2-type $Li_{0.83}(Li_{0.1}Ni_{0.2}Mn_{0.6})O_2$ with ABCBA oxygen stacking can mitigate additional cation migration from the fact that TM ions in the LiO_6 octahedra are subject to strong electrostatic repulsion through the face-shared LiO_6 octahedra and TMO_6 octahedra."

9. P.29 – what is discussed here is not only effect of ionic radius but also effect of bonding and electron distribution

Response

➔ We really appreciate the reviewer's delicate inspection of our manuscript. As the reviewer pointed out, the contents include the effect of ionic radius as well as that of bonding and electron distribution. Hence, we have modified the subheading in the revised manuscript as follows:

"Effect of ionic radius → **Revised:** *Effect of ionic radius, bonding and electron distribution*"

10. P.32 – it would be great if they can include short paragraph about Li1+xMO2Fx rock salt materials when talking about anion disorder

Response

➔ Thanks for the suggestion. In response to the helpful advice of the reviewer, we have added the related contents and references in the revised manuscript as follows:

"As the result, the anion disordered $KVPO_4F$ structure exhibits a smooth voltage profile and better rate capability. **(Revised:** In a broad sense, the fluorination in disordered rock-salt materials can be regarded as the introduction of disorder in the anion lattice. When the oxygen ion is replaced by fluorine ion in locally Li-rich environment within the disordered rock-salt oxides matrix, the capacity and cyclability can be improved. [Ref. R2-5] For example, the Li percolation is restored and enhanced as the amount of F ion is increased in the $Li_xMn_{2-x}O_{2-y}F_y$ disordered rock-salt system, affecting the Li-ion transport properties of the material. [Ref. 6] In addition, the fluorination leads to the increase in the ratio of low-valent transition metal ions functioning as an electron source. This enables the fluorinated disordered rock-salt materials to have increased transition metal redox capacity without a restriction of Li excess condition which is essential for the bulk Li percolation, reducing the dependence on O ion redox. Thus, the capacity and cycle life can be improved.[Ref. R7])"

References

[Ref. R2] J. Lee, D. A. Kitchaev, D.-H. Kwon, C.-W. Lee, J. K. Papp, Y.-S. Liu, Z. Lun, R. J. Clément, T. Shi, B. D. McCloskey, J. Guo, M. Balasubramanian and G. Ceder, *Nature*, 2018, **556**, 185–190.

[Ref. R3] R. A. House, L. Jin, U. Maitra, K. Tsuruta, J. W. Somerville, D. P. Förstermann, F. Massel, L. Duda, M. R. Roberts and P. G. Bruce, *Energy Environ. Sci*., 2018, **11**, 926–932.

[Ref. R4] J. Lee, J. K. Papp, R. J. Clément, S. Sallis, D. H. Kwon, T. Shi, W. Yang, B. D. McCloskey and G. Ceder, *Nat. Commun.,* 2017, **8**, 981

[Ref. R5] Z. Lun, B. Ouyang, D. A. Kitchaev, R. J. Cle´ment, J. K. Papp, M. Balasubramanian, Y. Tian, T. Lei, T. Shi, B. D. McCloskey *et al. Adv. Energy Mater.*, 2019, **9**, 1802959.

[Ref. R6] Z. Lun, B. Ouyang, Z. Cai, R. J. Clément, D. H. Kwon, J. Huang, J. K. Papp, M. Balasubramanian, Y. Tian, B. D. McCloskey, H. Ji, H. Kim, D. A. Kitchaev and G. Ceder, *Chem*, 2020, **6**, 153–168.

[Ref. R7] R. J. Clément, Z. Lun and G. Ceder, *Energy Environ. Sci.*, 2020, **13**, 345–373.

11. P.37 – irreversible phase transition can be also amorphisation for certain materials when alkali ions are completely removed, another type of irreversible transition is connected with transition of material to more stable thermodynamic state which can not accommodate alkali metal

Response

➔ We would like to thank for the valuable comments on the part of irreversible phase transition of cathodes in our manuscript. We agree that the original sentences may mislead reader. Cathode materials also experience irreversible phase transition and can be amorphized at severe condition such as completely de-inserted state. Hence, we have modified the original sentences in the revised manuscript as follows:

"**(Revised:** Like the negative electrode materials which lose crystallinity and become amorphous due to conversion or alloying reaction, an irreversible phase transition of the material in the bulk can occur for insertion cathode materials if certain unstable and harsh conditions exist.**)** One example that shows irreversible phase transition in the cathode is *Immm*-Li_2NiO_2, in which Li and Ni occupies the center of the tetrahedral site and rectangle site respectively between oxygen layers. In more specifically, during the 1st de-insertion of Li-ion, the bulk crystalline structure collapses and transforms into a layered *R*-3*m* with some degree of amorphization or very small crystallite size accompanying the oxygen evolution. **(Revised:** Consequently, it never recovered again because NiO_6 octahedrons in the layered structure is more stable thermodynamic state than NiO_4 square plane in the pristine state. That is, the changed stable state cannot accommodate mobile ions as in the original state.**)** These irreversible phase transitions in the bulk come from the intrinsic property tending to be an energetically favorable state from original metastable state. **(Revised:** Layered transition metal oxides also experience the irreversible phase transition when the material suffers from repeated cycling or at highly charged states. $LiMnO_2$ layered material is a good example for the former one.**)** In the layered $LiMnO_2$, the capacity decays during initial few cycles because of the transformation into the spinel-like phase **(Revised:** at the surface.**) (Revised:** Irreversible phase transition in the bulk is more common for layered materials which have relatively large possibility of slab gliding owing to intrinsic property (*e.g.* Na compounds) or almost complete de-insertion process (*e.g.* typical $LiCoO_2$). [Ref. R8-10]**)** The irreversible phase transition may result in the collapse of the structure and formation of the defects at the boundaries between the various domains, and therefore, it remains as a challenge. This fact reiterates the importance of the stable and rigid host structure with or without mobile ions as like polyanion materials."

References

[Ref. R8] J. N. Reimers and J. R. Dahn, *J. Electrochem. Soc.,* 1992, **139**, 2091.

[Ref. R9] G. G. Amatucci, J. M. Tarascon, and L.C. Klein, *J. Electrochem. Soc.*, 1996, **143**, 1114–1123.

[Ref. R10] X. Lu, Y. Sun, Z. Jian, X. He, L. Gu, Y. S. Hu, H. Li, Z. Wang, W. Chen, X. Duan, L. Chen, J. Maier, S. Tsukimoto and Y. Ikuhara, *Nano Lett.*, 2012, **12**, 6192–6197.

References

[Ref. R1] C. Zhan, T. Wu, J. Lu, K. Amine, *Energy Environ. Sci*., 2018, **11**, 243-257

[Ref. R2] J. Lee, D. A. Kitchaev, D.-H. Kwon, C.-W. Lee, J. K. Papp, Y.-S. Liu, Z. Lun, R. J. Clément, T. Shi, B. D. McCloskey, J. Guo, M. Balasubramanian and G. Ceder, *Nature*, 2018, **556**, 185–190.

[Ref. R3] R. A. House, L. Jin, U. Maitra, K. Tsuruta, J. W. Somerville, D. P. Förstermann, F. Massel, L. Duda, M. R. Roberts and P. G. Bruce, *Energy Environ. Sci*., 2018, **11**, 926–932.

[Ref. R4] J. Lee, J. K. Papp, R. J. Clément, S. Sallis, D. H. Kwon, T. Shi, W. Yang, B. D. McCloskey and G. Ceder, *Nat. Commun.,* 2017, **8**, 981

[Ref. R5] Z. Lun, B. Ouyang, D. A. Kitchaev, R. J. Cle´ment, J. K. Papp, M. Balasubramanian, Y. Tian, T. Lei, T. Shi, B. D. McCloskey *et al. Adv. Energy Mater.*, 2019, **9**, 1802959.

[Ref. R6] Z. Lun, B. Ouyang, Z. Cai, R. J. Clément, D. H. Kwon, J. Huang, J. K. Papp, M. Balasubramanian, Y. Tian, B. D. McCloskey, H. Ji, H. Kim, D. A. Kitchaev and G. Ceder, *Chem*, 2020, **6**, 153–168.

[Ref. R7] R. J. Clément, Z. Lun and G. Ceder, *Energy Environ. Sci.*, 2020, **13**, 345–373.

[Ref. R8] J. N. Reimers and J. R. Dahn, *J. Electrochem. Soc.,* 1992, **139**, 2091.

[Ref. R9] G. G. Amatucci, J. M. Tarascon, and L.C. Klein, J. Electrochem. Soc., 1996, **143**, 1114–1123.

[Ref. R10] X. Lu, Y. Sun, Z. Jian, X. He, L. Gu, Y. S. Hu, H. Li, Z. Wang, W. Chen, X. Duan, L. Chen, J. Maier, S. Tsukimoto and Y. Ikuhara, Nano Lett., 2012, **12**, 6192–6197.

Reviewer #3: This review summarized some key factors that could influence the properties and performance of cathode materials of alkali-ion transition metal compounds, encompassing a wide scope from atomic to microscopic levels. The topic of this review is of general interest and the review is also timely.

But there are some details that need to be fully explained and supplemented. Therefore, I suggest a major revision and following questions need to be answered.

Response to the overall comments

➔ We really appreciate the reviewer for taking the time out of the reviewer's busy schedule to review our manuscript. The reviewer's constructive comments on our review work is enormously helpful to us. Moreover, we are much grateful to the reviewer for appreciating the value of our work. The answers to the reviewer's comments are described below.

1. In Figure 3, the authors show the gravimetric and volumetric energy of cathode materials. However, the energy densities only based-on discharge profiles probably give a confusion for readers. As Figure 3 illustrated, for example, NCM cathode displays an energy density of almost 900 Wh Kg-1, which is much higher than the practical energy density of around 300 Wh kg-1. The comparisons of voltage and specific capacity play a key role in comprehending the energy density of cathode materials, which is necessary to be added as an important information.

Response

➔ We suspect the reviewer is confused on the energy density of the cathode in the manuscript. The energy density in our manuscript is calculated based on cathode weight only. The practical energy of around 300 Wh/kg should be about cell level. In addition, we do agree with the reviewer that voltage vs specific capacity curve is also important aspect. However, what we would like to show in Figure 3 is that the electrochemical performance, energy density, is largely affected by alkali ion species and the trends vary depending on the cathode structure. Lastly, we believe that the plot of several voltage vs capacity curves with different type cathodes and alkali ion species will make the figure too busy and it will not be helpful for readers to capture our insights.

2. The authors concluded internal factors of designing cathode materials for alkali-ion batteries from atomic, molecular and crystallographic scale. However, in the part of

Transition metal ions perspective and Anions perspective, much content about Li and Na ions-battery are summarized, conversely, almost no content of K-ions battery is involved.

Response

➔ We have discussed K-ion battery in alkali ion perspective in detail. In addition, we do not think that transition metal ions and anion perspectives will significantly vary depending on alkali ion species. Therefore, there is no reason to separately discuss K-ion battery in transition metal ions and anion perspectives.

3. The content of the annotation of figures is too long and complexed, which is nor beneficial for readers. For instant, in Figure 8, the explanation of this figure should be explained in the text, not in the caption.

Response

➔ We appreciate the reviewer's valuable comment that make our manuscript better. We agree with the reviewer's comment that the annotation of Figure 8 is too long and complexed. Thus, we have modified the annotation of Figure 8 in the revised manuscript as follows:

"**(Revised:** Fig. 8 (a) The crystal structure focusing on slab of $Li_{1/3}M_{2/3}O_2$ and the relevant parts of its band structure. Taking Mott–Hubbard splitting into account, the Li_2MO_3 band structure is further classified under three cases (b–d), depending on the interplay between the d–d Coulomb repulsion term U and the charge transfer term Δ. (e) Schematic electronic structures for $LiMO_2$ (x = 0), Li_2MO_3 (x = 1/3) and Li_5MO_6 (x = 2/3) where the $|O_{2s}$ and $|O_{2p}$ lone-pair states are highlighted by red bands.**)**"

4. The authors claimed that electrochemically inactive magnesium ion in the alkali-ion layer can supporting the ion channel, please illustrate this point in detail in the revised manuscript.

Response

➔ We are very grateful to the reviewer for helping us to further improve our manuscript. In response to the reviewer's comment, we have illustrated that point in detail in the revised manuscript as follows:

"**(Revised:** Contrariwise, the presence of heterogeneous atoms in alkali-ion channel in layered materials can have positive aspects.**)** For the $LiNiO_2$ layered system, the Ni^{2+} ion in the Li layer can be oxidized, and it causes local collapses of the structure. This

local collapse hinders the Li-ion diffusion in the Li layers and reinsertion of Li-ion into the six sites around the oxidized Ni ion in Li layers. **(Revised:** However, since cation disorder can mitigate the electrostatic repulsion forces between the TM layer by occupying the Li sites, it can act as a pillar role in supporting the ion channel in between transition metal layers as well as preventing the additional migration of TM ions from TM layer to Li layer. Therefore, the introduction of an inactive ion, which can play a similar pillar role and prevent local collapse of Li slab, can provide beneficial effect on the migration of alkali-ions. For example, a Mg-substituted $LiNiO_2$ cathode material exhibits a higher reversible capacity than that of pure $LiNiO_2$ cathode, which is explained by the pillar effect of Mg^{2+} ions in Li layer owing to its size similarity to lithium and constant valence.)"

5. Fig.13a, fig.21b and c, fig25b and fig.27a referenced in this draft are not clear, the authors should provide pictures with higher resolution.

Response

➔ We would like to thank the reviewer for the comment on the figure resolution. We have modified the figures with high resolution in the revised manuscript as follows:

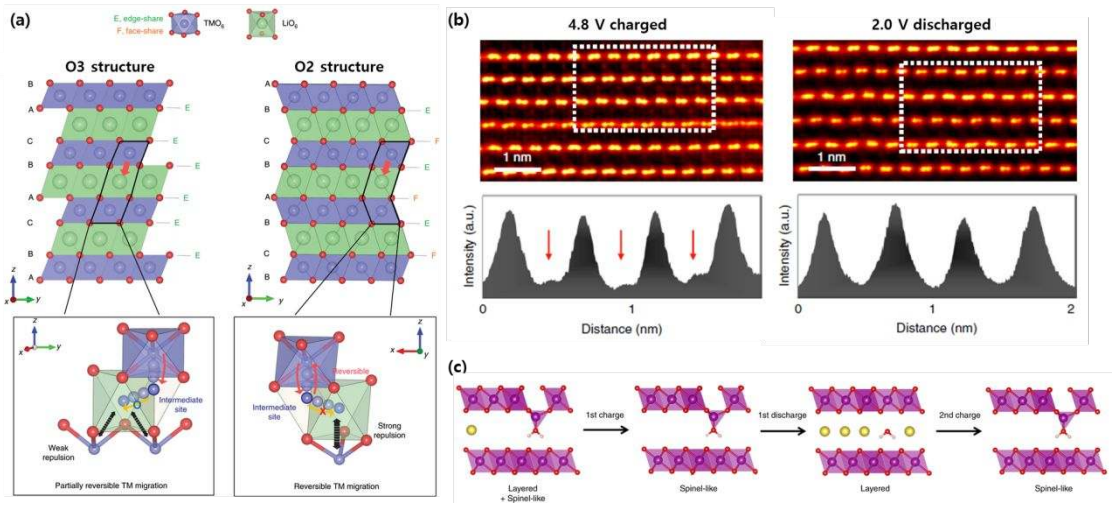

Fig. 13 (a) Schematic illustrations of crystal structure and cation migration paths of O3-type and O2-type Li layered oxides. (b) HAADF-STEM images and signals along the $[1\bar{1}0]$ zone axis for 4.8 V charged and 2.0 V discharged state of O2-type $Li_{0.83}(Li_{0.1}Ni_{0.2}Mn_{0.6})O_2$. (c) Schematic illustrations for the structural changes during sodiation/desodiation of partially dehydrated Na-birnessite material.

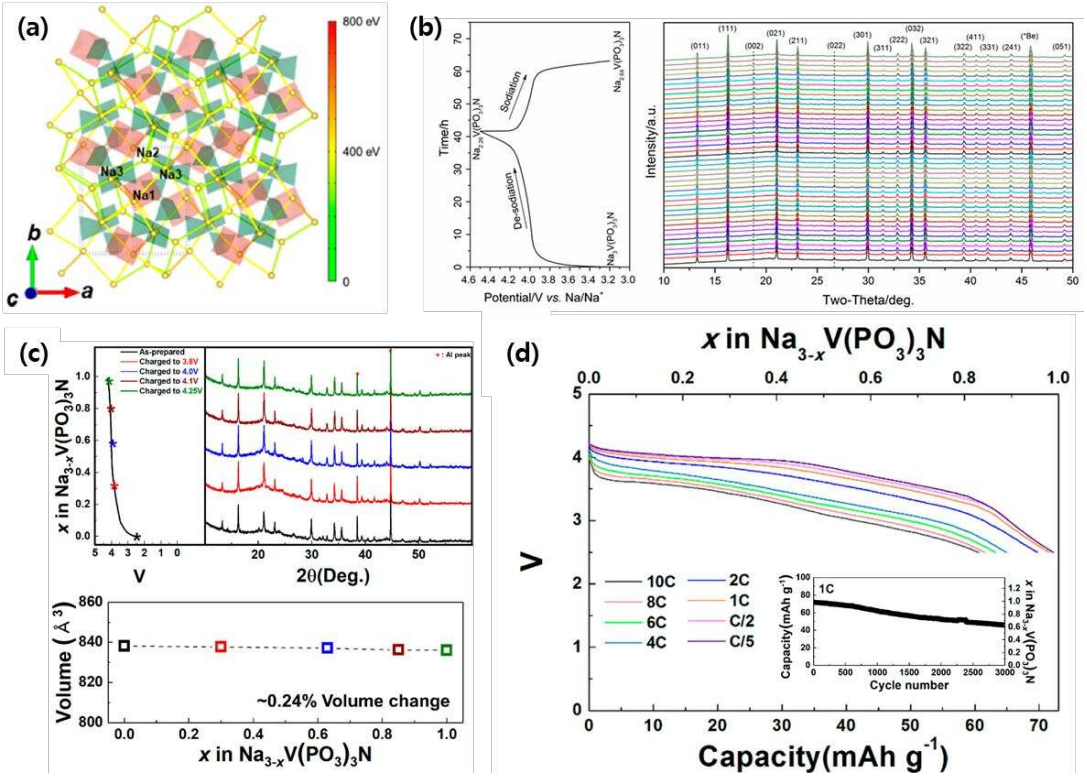

Fig. 21 (a) Illustration of the three-dimensional Na-ion diffusion pathways in $Na_3V(PO_3)_3N$. Note that the Na1−Na2 pathways are excluded in this figure because of their high activation barriers (~800 eV). (b) Voltage profile and in situ XRD patterns of $Na_3V(PO_3)_3N$ during the first cycle. (c) Ex situ XRD patterns and volume changes of $Na_{3-x}V(PO_3)_3N$ ($0 \le x \le 1$). (d) Electrochemical performances of various discharge capacities of $Na_3V(PO_3)_3N$ at different current rates (C/5, C/2, 1C, 2C, 4C, 6C, 8C, and 10C in the 2.5−4.25 V window, 1C = 73 mAh g−1). Inset graph is cyclability test result at 1C during 3000 cycles.

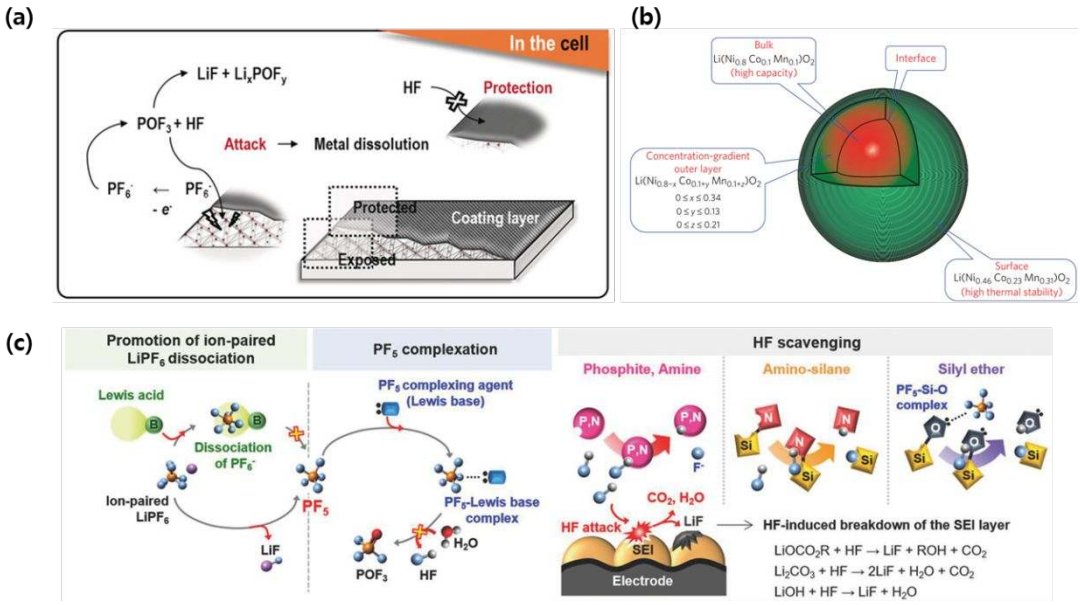

Fig. 25 Schematic illustration of (a) surface coating method, (b) surface modification method by inducing deviation of composition at the surface, (c) scavenging mechanisms of different electrolyte additives.

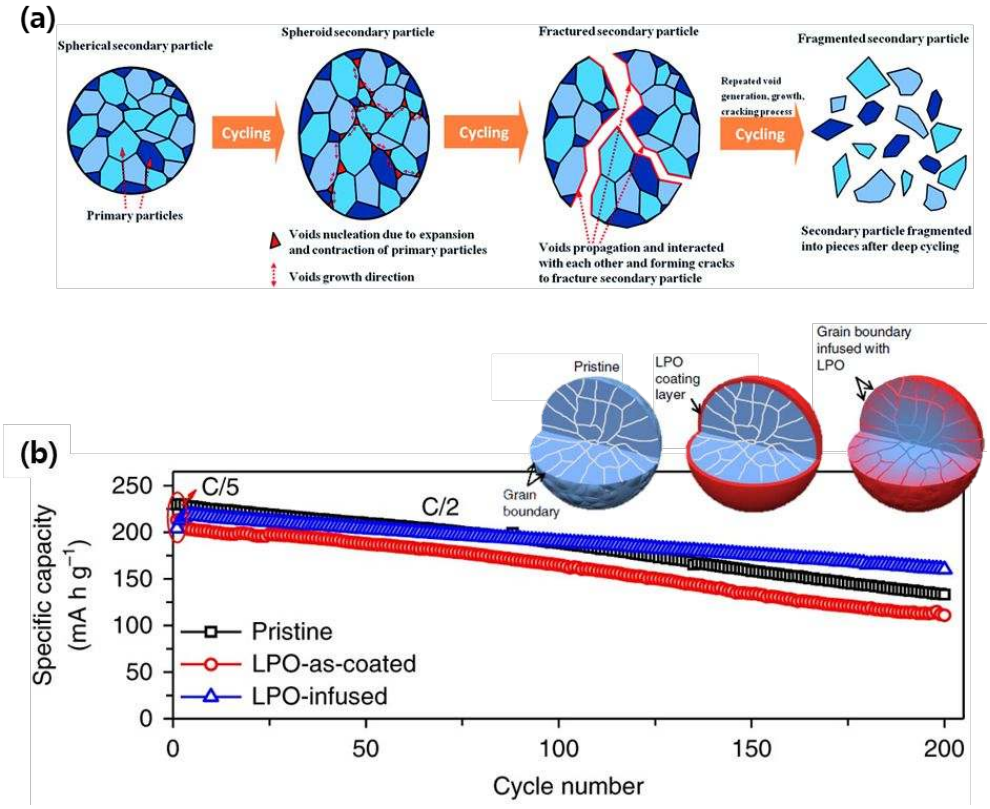

Fig. 27 (a) Schematic illustration of crack formation and fragmentation mechanisms of secondary particle during cycling. (b) Cycling performance of $LiNi_{0.76}Mn_{0.14}Co_{0.10}O_2$ at 60 ℃ with different surface treatment. LPO-infused material shows best performance by preventing crack formation along the grain boundaries.

Title: Multiscale Factors in Designing Alkali-Ion (Li, Na, and K) Transition Metal Inorganic Compounds for Next-Generation Rechargeable Batteries

Wontae Lee[a,c†], Jaeyoung Kim[a,†], Soyeong Yun[a], Woosung Choi[a], Haegyeom Kim[b*] and Won-Sub Yoon[a*].

[a]Department of Energy Science, SungKyunKwan University, Suwon 440-746, South Korea, E-mail: wsyoon@skku.edu

[b]Materials Sciences Division, Lawrence Berkeley National Laboratory, Berkeley, CA 94720, USA, E-mail: haegyumkim@lbl.gov

[c]The Institute of New Paradigm of Energy Science Convergence, Sungkyunkwan University, Suwon 16419, Republic of Korea.

†These authors contributed equally to this work

Abstract

The demand for 'more energy and less carbon' is one of the most important challenges facing humanity. Exploring not only more efficient renewable energy systems, but also advanced energy conversion and storage materials is an essential requisite to achieve the task. Since the emergence of alkali-ion rechargeable batteries, the development of cathode materials has been considered as a core that improves the overall performance of batteries. In this respect, understanding the underlying science of what are the factors affecting the properties and performance of cathode materials and how to ameliorate them have made remarkable progress. There has been considerable reporting about factors ranging from nano- to micrometer scale, and now it is time to build an infrastructure to design advanced cathode materials with a selective and comprehensive perspective on those factors. In this Review article, we discuss the key factors contributing the properties and performance of cathode materials with a comprehensive perspective on various alkali-ion transition metal compounds. It covers a wide scope of the factors from atomic to microscopic levels as follows: atomic, electronic, crystal and particle structures.

Broader context

The effective utilization of renewables is an optimum approach for implementing environmentally and sustainable development. Accordingly, the importance of energy storage devices is being emphasized more and more. The energy storage devices conserve the generated energy by converting it to electricity. With unceasing technology innovations in the fields of renewables and electric vehicles, the reliance on the batteries has been increasing in recent years and will remain. The technology of alkali-ion rechargeable batteries is proving to be the most promising candidate for satisfying the recent extensive requirement of energy storage devices especially for energy, power, safety, life and cost. Moreover, the cathode is always being mentioned as the key component enabling the enhancement of rechargeable battery performance and boosting its growth potential. Thus, understanding of the factors affecting the properties and performance of alkali-ion cathode materials is essential. Herein, various factors with a wide scope ranging from atomic, molecular, crystallographic, and microscopic scale are discussed.

1. Introduction

One of the greatest challenges in the energy system of our time is to solve the complex problem of reducing carbon emissions while meeting increasing energy demands. Although the increase rate is slower compared to the previous 40 years (see Fig. 1a), the overall energy demand in a global world is expected to grow steadily.[1] Furthermore, the trend of global energy generation is shifting to renewables gaining share with chiefly lowering the portion of fossil fuels. The renewable energy is the fastest growing source of energy, and its share in the global energy sector is expected to increase to around 30%, overtaking the coal by 2040 as shown in Fig. 1b. As renewable energy grows to a

significant level, electricity systems will demand greater flexibility, and thus the role of the energy storage devices is likely to take on great significance. More directly, the electrical energy storage device can enable the electric vehicles (EVs) to dominate the transport part, facilitating deep decarbonization.[2] Over the past 20 years, alkali-ion batteries have been proven to be the most powerful technology for supplying high energy and power demands. As a result, the batteries have dominated the global operational electricity storage power capacity. There are numerous electricity storage technologies, but the alkali-ion batteries have capture the largest portion (around 70%) of whole technologies due to the high power and energy densities (Fig. 1c).[3] Such alkali-ion rechargeable batteries are a fruition of the researchers awarded the 2019 Nobel Prize in Chemistry and now provide an attractive solution for a range of energy and environmental problems. The important parameters for the performance of rechargeable batteries can be represented by five aspects: energy, power, safety, cost, and life (Fig. 1c). The electrochemical performance of the rechargeable batteries is determined by whole cell components including cathode, anode, electrolyte and others (Fig. 1d). In current state of development, cathode materials have been regarded as the bottleneck in the advance of alkali-ion batteries due to the limited capacity and capacity fading at high voltage, compared to the high capacities in anode materials.[4–6] While the electrochemical performance is notwithstanding the integrated results of whole components, the advance in the performance of rechargeable batteries is more likely to come from the trials of various approaches to the underlying science of cathode materials. In addition, the cost of cathodes has the biggest part of the total cost structure of the cells, more emphasizing the importance of cathodes.[7]

Cathode materials can be roughly divided into those which operate on the basis of insertion or non-insertion reactions. In the latter case, the cathode materials have high theoretical capacities benefiting from a conversion reaction, offering a relatively large amount of charge carrier ion storage sites. From the energy density point of view, these types of cathodes are fascinating as a candidate for the post-rechargeable batteries. However, their huge changes in the crystal structure that entails a breaking and recombining chemical bond result in the low reversibility between reactants and products during electrochemical reaction, making it hard to achieve complete commercialization in the near future. [4,8] On the other hand, for insertion reaction materials, there are confined charge carrier ion storage sites in the crystal structure and consequently the cathodes which undergo insertion reactions have a bounded theoretical capacity level. In other words, the insertion-based cathodes are based on host-guest reactions without a significant repetitive chemical bond breaking and forming, which leads to relatively stable and reversible electrochemical reactions.[8,9] In addition to this, recently, the discovery of anionic redox chemistry has extended the reach of electron resource species, and thus the alkali-ion insertion cathode materials have been re-evaluated for its potential in terms of impact on a new paradigm for designing high energy cathode materials toward next-generation rechargeable batteries.[10,11]

There has been a significant progress in the development of cathode materials for alkali-ion batteries. Numerous insightful and admirable review papers on the cathode materials have been published vigorously, and it substantiates once more the importance of alkali-ion transition metal based inorganic compounds for the rechargeable batteries. Hence, fundamental understanding of factors determining battery performance is essential for surpassing the limit of cathode materials researched to date. Thus, this review does not simply reiterate the previous research findings with a clichéd view classified in accordance with materials, rather focus on a design factor that can optimize material characteristics. This comprehensive and unique attempt will provide useful information and refresh reader's insight. This review aims to build a bridge to the constructive future of the alkali-ion batteries for the tentatively named 'near-post-rechargeable batteries'. Accordingly, we will cover various factors affecting the properties and performance of the high-energy cathode materials regarding alkali-ion transition metal compounds. The main contents will be pieced together as follows.

i) Atomic to molecular scale

ii) Molecular to crystallographic scale

iii) Crystallographic to microscopic scale

The alkali-ion transition metal compounds can be dismantled as three parts on the basis of the host structure (framework: cations for 3*d*, 4*d*

and 5*d* transition metal ions and anions for pnictogens, chalcogens, and halogens or complex *etc.*) and guest ion (mobile ion: Li, Na, and K) viewpoint. Therefore, the factors in the first section will be dealt with based on alkali-ions, transition metal ions, and anions perspective. After that, numerous factors affecting the crystal structure, ion channel, disorder, and phase transition *etc.* and various outcomes that resulted from the change in above-mentioned things will be addressed. Lastly, diverse factors corresponding to the level from crystallographic to microscopic scale such as surface, grain boundary, particle size, and morphology aspect will be handled. For the upper large scales including composite electrodes and various cell designs, it is highly complex electrochemical system where whole reactions are nonlinearly combined across a space and time scales encompassing both (electro)chemical and mechanical processes. On account of the complexity, multiscale modeling which is a combination process of models that are established based on the theoretical and experimental results are utilized to investigate the reactions in the system. This method not only provides clues to the unpredictable phenomena, but also derives important key information, which has a positive effect on development of rechargeable batteries.[12–18] In the case of the formulation and manufacturing of composite electrodes at the industrial level are also an important topic. Regarding this, there are already some insightful review papers on this topic specifically for the Li-ion batteries.[19–22] And it is commonly expected that a similar manufacturing process can be applied to Na- an K-ion batteries, which make them promising candidates for next-generation rechargeable batteries. Our aim is to provide the inner control factors of the materials by comparing and sorting out commonalities and differences among them. Hence, this review will not cover the topic related to the upper level scales, and instead refer to other excellent review works.[17,19–23]

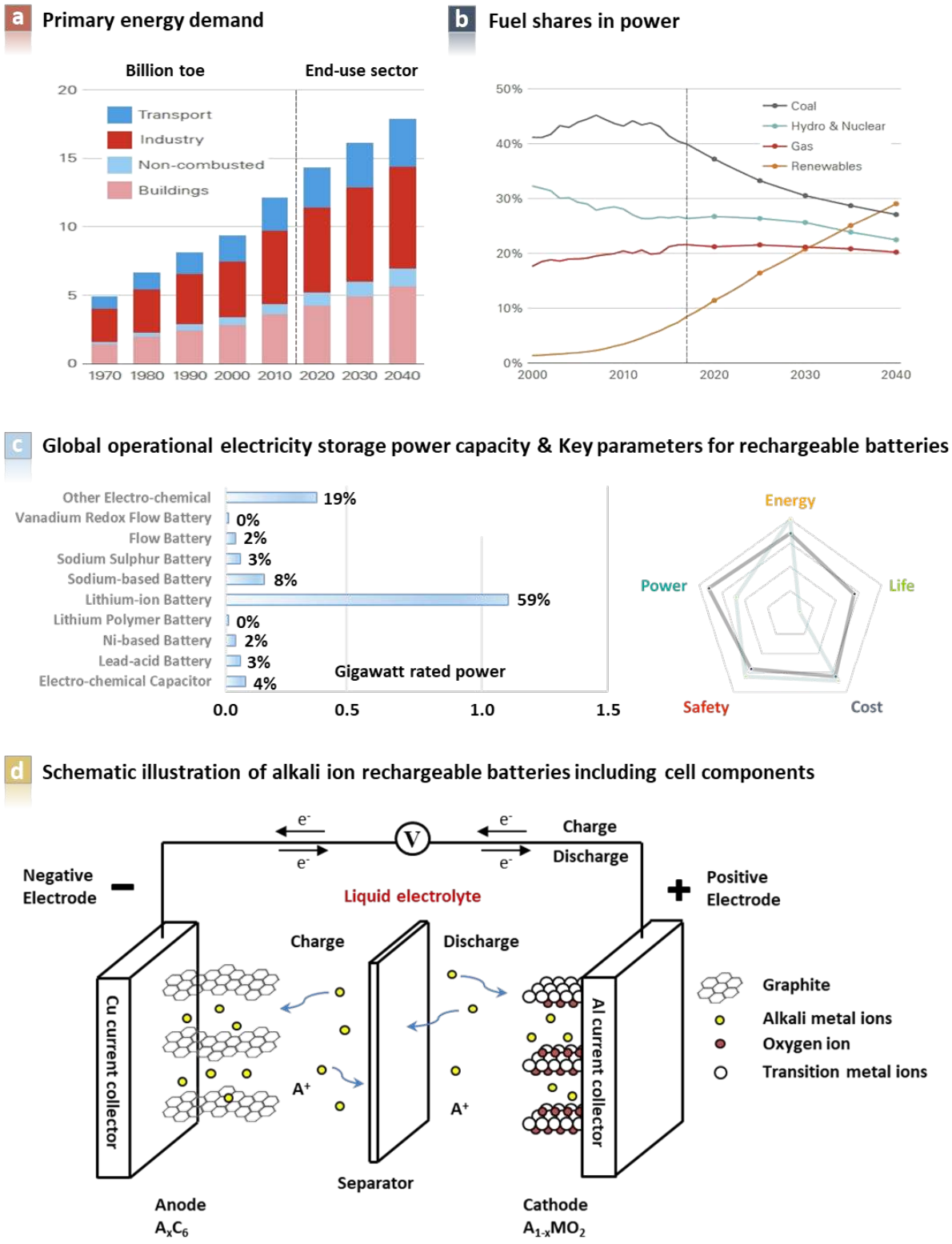

Fig. 1 (a) The outlook of primary energy demand and (b) fuel shares in power.[1] (c) Global operational electricity storage power capacity[2] and key parameters for rechargeable batteries. (d) Schematic illustration of alkali ion rechargeable batteries including cell components.

2. Factors in the design of alkali-ion transition metal compounds for cathode materials

2.1. Atomic to molecular scale

The electrochemical potential, crystal structure and dynamics are fundamentally attributed to the element that constitutes the electrode materials. The alkali-ion transition metal compounds for insertion materials can be divided into three sections on the basis of host-guest chemistry. (guest: alkali-ions, host: cations for transition metal ions and anions for single component or multiple complex of nonmetal, halogen, and metalloid ions). The accessible level now reaches the atomic scale due to the advance of synthesis and analysis techniques, and consequently with no limits on the control of the constituents of the alkali-ion transition metal compounds when designing electrode materials. Hence, atomistic approaches will provide the theoretical route to predicting the properties of target materials. In this part, the considerable factors that contribute to material's properties will be presented from three main perspectives. (Periodic table with electronegativity and ionic radius is displayed in the end of this chapter, see Fig. 2)

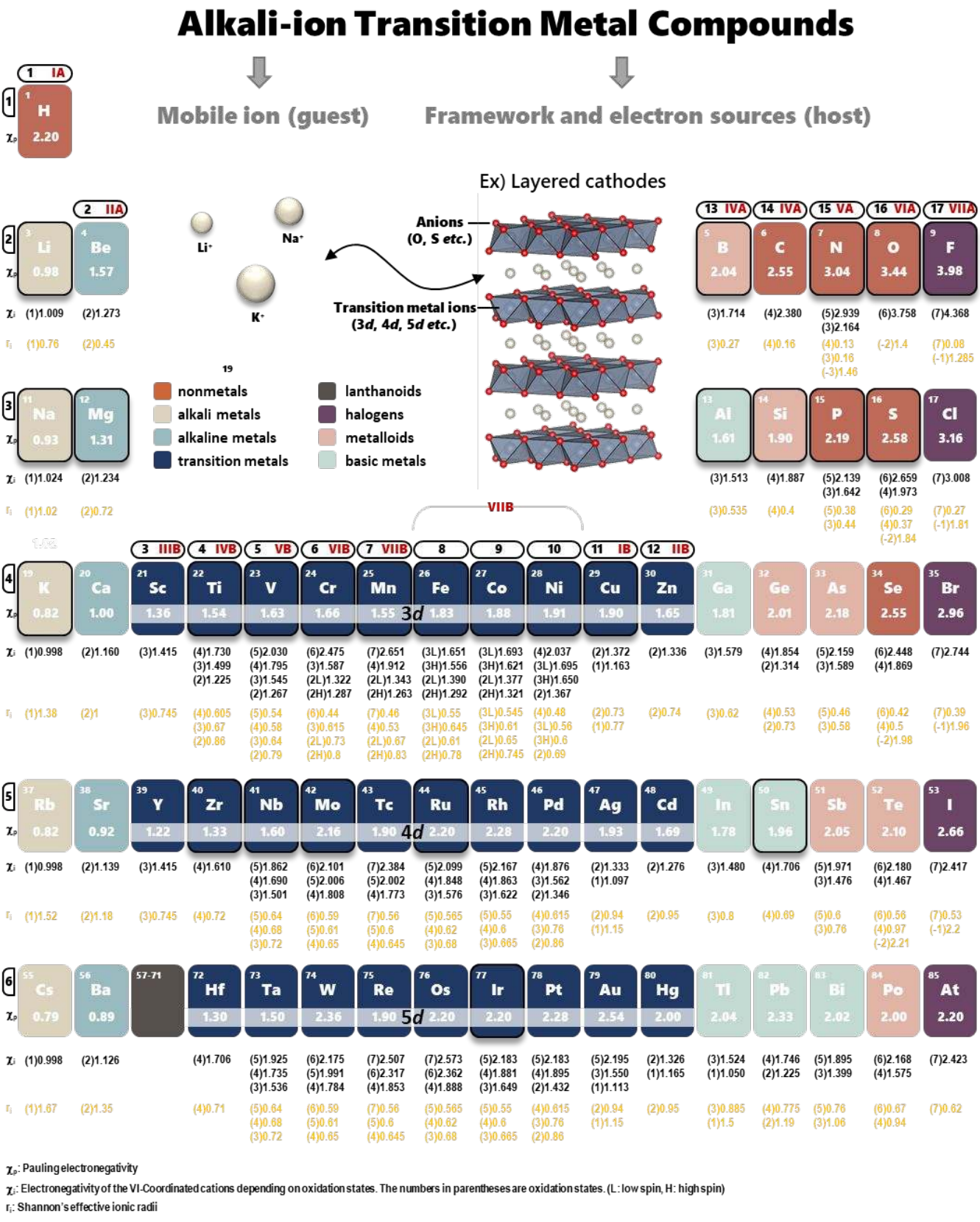

Fig. 2 Periodic tables with electronegativity and ionic radius. χ_P: Pauling electronegativity, χ_i: Electronegativity of the VI-Coordinated cations depending on oxidation states. The numbers in parentheses are oxidation states. (L: low spine, H: High spine).[24] r_i: Shannon's effective ionic radii.[25]

2.1.1. Alkali-ion perspective: Li, Na, K *etc.*

Insertion ion species influences the electrochemical properties of cathode materials, including average voltage, voltage curve, specific capacity, cycling stability, and rate capability. This insertion ion-property relationship significantly impacts on the choice of cathode materials in alkali- (Li, Na, and K) ion batteries. For example, in Li-ion batteries, there is no doubt that the layered oxides (*i.e.,* $LiCoO_2$, $LiNi_{0.8}Co_{0.1}Mn_{0.1}O_2$, $LiNi_{0.8}Co_{0.15}Al_{0.05}O_2$) are better than other candidates because of their high gravimetric and volumetric energy (see Fig. 3).[26–50] In contrast, the layered oxides do not always outperform polyanions and Prussian blue analogues (PBAs) in Na and K systems. In the Na system, some polyanions (*i.e.,* $Na_3V_2(PO_4)_2F_3$) and PBAs can deliver higher gravimetric energy than layered oxides and this trend becomes more obvious in the K system: most of the K-polyanions and PBAs deliver higher energy than K-layered oxides.

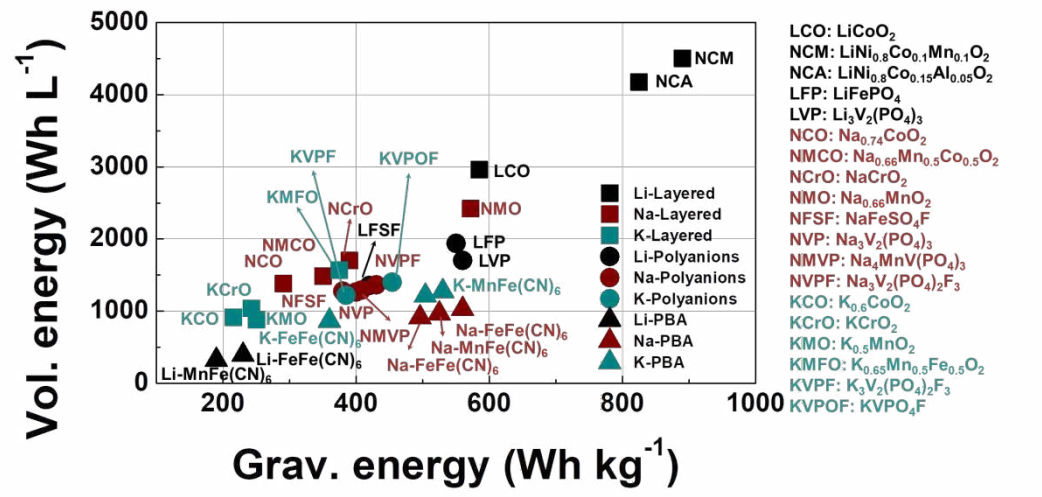

Fig. 3 Gravimetric *vs.* Volumetric energy of cathode materials for Li, Na, and K-ion batteries. The gravimetric energy density is calculated from the discharge profile in literature.[26–51] For volumetric energy density estimation, we used theoretical density of cathode materials.

What is the root cause why the performance of cathode materials depends on the insertion ion species? Fundamental understanding of such underlying origin would provide insights for the design of high energy cathodes for each Li-, Na-, and K-ion battery. In the layered oxides, both the gravimetric and volumetric energy linearly decrease as a larger alkali-ion is inserted. There are two main reasons. First, larger and heavier insertion ion increases both the mass and volume of cathodes. Second, interaction between alkali-ions gets stronger considerably as their size increases.[52] In the layered structure, the alkali-oxygen bond length increases in larger alkali-ion system and the alkali-alkali interaction becomes less effectively screened by electron clouds in oxygen anions, which is the main reason of stronger K-K interaction than Na-Na and Li-Li. Such strong K-K interaction changes thermodynamic energy of the layered oxides as a function of K content more significantly than the Na and Li systems, resulting in much sloped voltage curves. Because the cathode should be cycled within the electrolyte stability window, the achievable specific capacity and voltage are limited once the voltage slope is determined by alkali-alkali interaction. The strong K-K interaction results in another disadvantage in K-layered oxides: almost all the K-layered oxides have K-deficient composition ($x < 1.0$ in K_xMO_2, M = transition metals).[27,31,38,44] The use of K-deficient cathodes requires pre-potassiation process. In this respect, polyanions and PBAs are better cathode candidates for Na and K systems because they generally have 3-dimensional alkali-ion arrangements, which would reduce the Na-Na (or K-K) interaction. As a result, polyanions and PBAs have Na (or K)-rich compositions and exhibit much platter charge-discharge curves, and thus high energy.

It is widely believed that the insertion of larger alkali-ions into the cathode hosts leads a larger lattice strain and faster capacity degradation.[27] For example, $K_{0.6}CoO_2$ retains only ~60% of the initial capacity after 120 cycles. However, the opposite trend is observed when we compare the cycling stability and lattice change of A_xCoO_2 (A= Na, and K). P2-K_xCoO_2 shows only ~3.5% change in *c* lattice between charged and discharged states, but P2-Na_xCoO_2 exhibits ~4.0% of *c* lattice change, respectively.[27,43] In this comparison, we found that larger lattice strain provides better cycling stability even after 1000 cycles: P2-K_xCoO_2 (60% after 120 cycles),[27] P2-Na_xCoO_2 (94% after 1000 cycles)[54]. In polyanion, K_xVPO_4F (x~0) for example, a large K ion insertion exhibits similar capacity retention with Li and Na insertion.[55] In fact, there are many other parameters affecting cycle life, including anode stability, electrolyte stability, and electrode composition. For example, in many cases, the choice of electrolytes improves the cyclability considerably. For specific, $Na_{0.7}CoO_2$ could provide almost no capacity decay with $NaPF_6$ in EC/DMC electrolyte, while only ~61% of capacity is retained after 40 cycles when $NaClO_4$ in EC/DMC electrolyte is used.[43] Therefore, more comprehensive investigations are required to understand how size of insertion ion determines the cycle life of cathode materials.

The size of insertion ions also determines the rate capability of cathode materials by tuning their migration pathways and corresponding barriers. It is intuitively accepted that a larger moving ion would be more difficult to migrate through a cathode material. However, there are some counter-intuitive examples and they demonstrate that the correlation between insertion ion size and rate capability is more complicated than ones believe. For example, Kim and his colleagues show that the migration of a relatively small Li ion in K_xVPO_4F (x ~ 0) is more difficult than large Na and K ions by both experiments and theoretical calculations.[55] They proved that Li ions are located at under-coordinated sites, which are different from Na and K sites, because of relatively small ionic radius of Li compared to void space in the K_xVPO_4F (x ~ 0) framework. And Li ions have unique migration pathways wherein Li ions go through unstable Li sites, which significantly increase Li migration barrier (~0.442 eV for Li *vs.* 0.222 eV for Na and 0.195 eV for K). Similar results are also observed by Nikitina *et al* and Fedotov *et al.*[56,57] One can find a similar behavior in K_xFeSO_4F: Li insertion shows larger polarization than Na insertion.[58] In addition, Komaba *et al.* claimed that, in the layered oxide frameworks, the diffusion of Na ions would be faster than that of Li because longer alkali-oxygen bonding results in reduced electrostatic interaction.[59] Similarly, Ong and his colleagues show a slightly lower Na migration barrier in $NaCoO_2$ than Li migration in $LiCoO_2$.[60] These examples clearly demonstrate that the insertion ion size itself is not the sole factor determining rate capability of cathode materials. Instead, one might need to finely tune void size along the migration paths to develop high rate cathode materials because it is likely that there is an optimized void size for facile migration of each alkali ion.

2.1.2. Transition metal ions perspective: 3*d*, 4*d*, 5*d*, *etc.*

Energy density, power density, cycle life, safety and cost are primary requisite performance of rechargeable batteries. From the point of view of a cathode, the above requirements are highly dependent on the transition metal ions. The transition metal ions function as a one of the main electron sources and one of the major components of constructing framework of the electrode materials. The important thing to consider when designing electrode materials is how many available electrons and how high redox potential couples are there in the electron sources, which is directly linked to the energy and power density. In addition, the physicochemical stability of the host structure that is composed of transition metal ion compounds largely contributes the cycle life and safety of the cathode materials. Therefore, understanding unique roles and properties of transition metal ions in the cathode materials is essential to design advanced electrodes.

Redox potential

The coordination of transition metal ions in silicates, borates and phosphates is tetrahedral (4), triangular pyramid (5) and octahedral (6), respectively, and as coordination numbers decrease, fewer steric hindrances create more stable covalent M-O bonds. More covalent M-O bonds generate quantum orbital repulsion between bonding and antibonding states, bringing the antibonding orbitals closer to the Fermi level of lithium, decreasing the voltage. As a result, systems containing transition metal ions with high coordination numbers provide higher redox potentials. The redox potential also depends on the transition metal species itself in the polyanion system. For example, the discharge

potential values for $M^{2+/3+}$ are 3.4 V (Fe), 4.0 V (Mn), 4.8 V (Co), and 5.2 V (Ni) for olivine phosphates $LiMPO_4$ materials.[61] This transition metal dependent redox potential can also be found in various polyanion cathode groups ($LiMP_2O_7$, $LiMPO_4$, $LiMBO_3$, $LiMSiO_4$), where the redox potential changes in order of Ni > Co > Mn > Fe.[62]

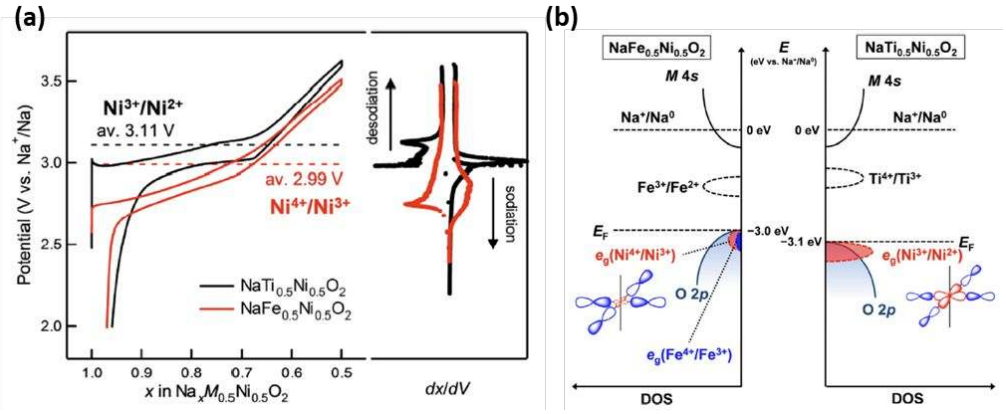

Fig. 4 (a) Potential profiles as a function of x in $Na_xTi_{0.5}Ni_{0.5}O_2$ and $Na_xFe_{0.5}Ni_{0.5}O_2$. The dx/dV plots are also shown for comparison. (b) Schematic electronic structures of $Na_xM_{0.5}Ni_{0.5}O_2$ (M = Ti, Fe). Oxygen 2*p* and Ni e_g orbitals hybridize well to delocalize holes over both Ni and oxygen in $Na_xTi_{0.5}Ni_{0.5}O_2$. For $Na_xFe_{0.5}Ni_{0.5}O_2$, the frontier orbital with a dominant oxygen 2*p* character does not reflect the Ni^{4+}/Ni^{3+} character significantly. Reproduced from Refs.[63] With permission of ACS.

It is indispensable to understand the factors that determine the redox potential of electrode materials. Intuitionally, it is thought that a higher redox couple will show a higher redox potential (*i.e.,* $E(M^{3+}/M^{2+}) < E(M^{4+}/M^{3+})$), therefore, the valence state of the redox active transition metal ion is believed to govern the operating voltage of the materials. However, it is not always the case. For example, the redox potential of $E(Ni^{3+}/Ni^{2+})$ in $NaTi_{0.5}Ni_{0.5}O_2$ is higher than that of $E(Ni^{4+}/Ni^{3+})$ in $NaFe_{0.5}Ni_{0.5}O_2$ (Fig. 4).[63] The authors claimed that the reason for the aforementioned redox paradox lies in the hybridization between the 2*p* orbital of oxygen and 3*d* orbital of transition metal ions. In the case of $NaTi_{0.5}Ni_{0.5}O_2$, the 2*p* orbital of oxygen ion and e_g of 3*d* orbital of nickel ion are well hybridized, delocalizing the hole over both oxygen and nickel ion. In contrast, in the case of $NaFe_{0.5}Ni_{0.5}O_2$, the frontier orbital exhibits dominantly oxygen 2*p* character with not reflecting the Ni^{4+}/Ni^{3+} character. Consequently, it leads to a large contribution of oxygen orbital to the redox reaction, resulting in the apparent redox potential paradox of $E(Ni^{4+}/Ni^{3+})$. Thus, considering the orbital level (*e.g.,* hybridization state of materials) is important to design electrode materials and tune their redox potential.

Transition metal ion migration into alkali-ion sites

The host structure needs to maintain its crystal structure upon extraction and insertion of alkali-ions to exhibit stable cycle life. If the host framework is deformed by a migration of transition metal ions, available insertion sites for alkali-ions diminish and the substituted sites by transition metal ions even obstruct the alkali-ion movement. For example, in AMO_2 layered structure compounds, the transition metal ions entering the alkali-ion layer block the alkali-ion pathway and consequently reduce the mobility of alkali-ion. In order to have a high rate and large electrode capacity, it is necessary to minimize the degree of transition metal migration into alkali-ion sites. Since transition metal ion migration usually proceeds through the tetrahedral site, the generation of Mn-based compounds that prefer octahedral site reduces the number of cases where transition metal/alkali-ion mixing occurs, resulting in sustain the high alkali-ion mobility. For $LiNi_{0.5+\sigma}Mn_{0.5-\sigma}O_2$ (σ > 0) cathode materials, not only for Mn^{4+} ions present here but also the low spin Ni^{4+}, Ni^{3+} and Ni^{2+} observed as the cycling also shows high

octahedral site preference. Therefore, $LiNi_{0.5+\sigma}Mn_{0.5-\sigma}O_2$ ($\sigma > 0$) cathode has less possibility of the transition metal ion migration to the alkali-ion sites during battery cycling and presents the high rate and high capacity rechargeable batteries.[64] In contrast, Fe^{4+} ions easily migrate into Na site through relatively stable tetrahedral sites upon charge from $NaFeO_2$ and it leads to low capacity and rapid capacity degradation.[65]

Jahn-Teller distortion

In the case of octahedral complexes of transition metals, certain electron configurations cause a geometrical distortion (reduction in the degree of symmetry of the complex and removal of the degeneracy), lowering the energy of a system.[66,67] This is referred to as a Jahn-Teller distortion or effect, and the ions which have this phenomenon are called as Jahn-Teller active ions. The phenomenon depends greatly on the number of electrons where those are located. Specifically, the electron configuration of the d^9, low-spin d^7, and high-spin d^4 in octahedral complexes of transition metals leads to odd number occupation of electron in the e_g orbitals, and it lifts the degeneracy of the orbitals, with the system having a large energetic stabilization. In the rechargeable batteries, many studies have found that numerous electrochemical properties and performance are closely linked to this phenomenon, and the Jahn-Teller active ions could be deemed a curate's egg due to having both pros and cons depending on situations.

The phenomenon is commonplace in six-coordinate Mn^{3+} (high spin $t_{2g}^3e_g^1$) complexes such as AM_2O_4 spinel type materials. During charge and discharge process, the spinel AMn_2O_4 materials are suffering a large and anisotropic volume changes due to a phase transition from cubic to tetragonal originated from the Jahn-Teller distortion of Mn^{3+} ion.[68] The continuous stress from the lattice mismatch between different phases (*i.e.,* the cubic and tetragonal lattice) can influence the mobile ion diffusion channels and lead to pulverization, resulting in the deterioration of performance of the cathode materials.[69] In the layered structure system, the strong cooperative Jahn-Teller active Mn^{3+} ion in AMO_2 compounds causes a monoclinic distortion, which destabilizes the rhombohedral structure.[70] Similar with the $LiMn_2O_4$ case, the phase transition between distorted monoclinic and rhombohedral structure, occurring in Li_xMnO_2 during charge-discharge, might affect its electrochemical performance, but the most critical issue in the layered Li_xMnO_2 is the irreversible structure transformation to the spinel.[71] For the polyanion system, while $LiMnPO_4$ can be considered as a good cathode candidate because of its high working voltage at 4.1 V vs Li^+/Li,[72] its low achievable capacity and poor cycling stability, resulting from low electronic and ionic conductivity and structural distortions, caused by Jahn-Teller Mn^{3+} cation, are the big hurdles.[73]

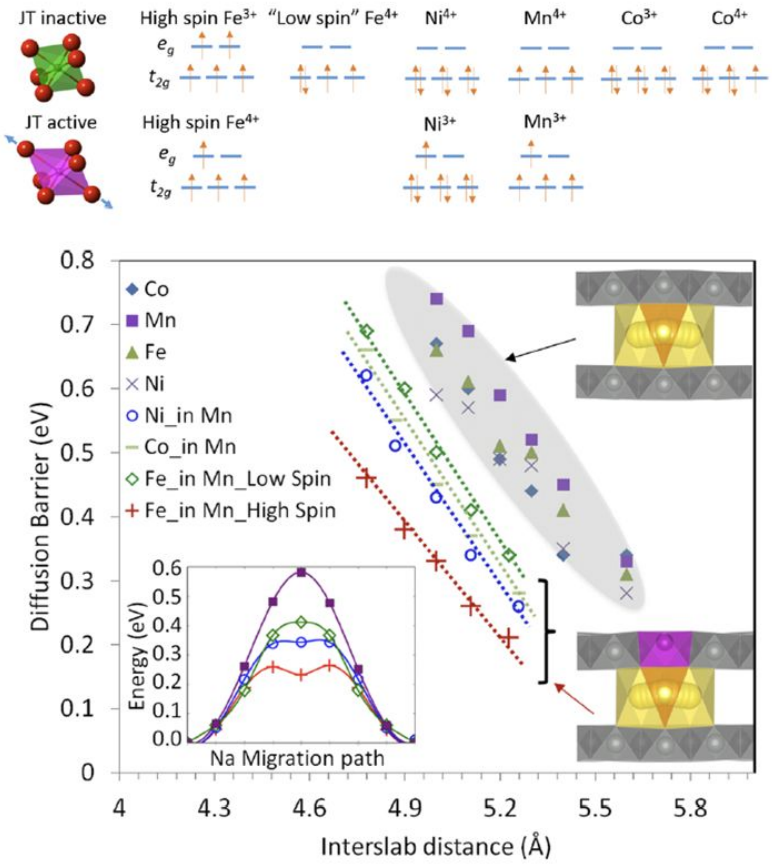

Fig. 5 Top: Electronic structures of Jahn−Teller inactive (top row) and active (bottom row) transition metal oxide octahedrons. Bottom: DFT calculated Na activation energies in layered $NaTMO_2$ with different transition metal combinations at various interslab distances. The labels of Mn, Fe, Co, and Ni in the legend stand for the transition metal cations TM in the $NaTMO_2$. Ni_in Mn stands for an isolated Ni (adjacent to the Na migration path) embedded in the Mn surroundings, etc. For Fe_in Mn, both high spin and low spin electronic configurations of Fe are calculated. The upper right inset shows the calculated Na diffusion path for $NaTMO_2$ with a single type of transition metal (gray). The lower right inset shows the Na diffusion path when Fe (purple octahedra) embedded in Mn surroundings (gray) is face-sharing with the activated state. Obvious buckling of Fe can be observed. The lower left inset shows the calculated profiles for Na migration at the inter-slab distance of 5.1 Å. Reproduced from Refs.[74] With permission of ACS.

On the positive aspects, the Jahn-Teller distortion can facilitate the diffusion of alkali-ions. In the case of the Jahn-Teller inactive Fe^{3+} (high spin $t_{2g}^3e_g^2$) ion in $NaMO_2$ layered system, the FeO_6 octahedron can be distorted at high voltage region due to the Fe^{4+} (high spin $t_{2g}^3e_g^1$) ion which exhibits a strong Jahn-Teller effect. Ceder group demonstrated that the distortion of FeO_6 octahedron in a $Na_x(Mn,Fe)O_2$ layered system results in the increase in the distance between Fe and Na ion when the Na ion goes through the face-sharing tetrahedral site, lowering the activation energy for the migration of the alkali-ions (Fig. 5).[74] Similarly, Kim and colleagues showed that the Na migration barrier can be significantly affected by a local distortion due to the electronic structure of the transition metal ions.[75,76] According to their reports, in $Na_4Fe_3(PO_4)_2(P_2O_7)$ and $Na_4Mn_3(PO_4)_2(P_2O_7)$ materials, the activation barriers of Na migration path are changed after the oxidation of transition metal ions. In the former case, a local distortion occurs in P_2O_7 dimers after Fe oxidation and the Na diffusion channels are narrowed, which increases the activation barriers for Na migration paths. However, in the latter case, a Jahn-Teller distortion occurs after Mn oxidation (due to the electronic configuration of Mn^{3+} ion), and it increases the Mn-O bond length along the *c*-direction, opening up the Na diffusion channel. As a result, the activation barriers for Na migration paths decrease, improving the rate capability.

Disproportionation

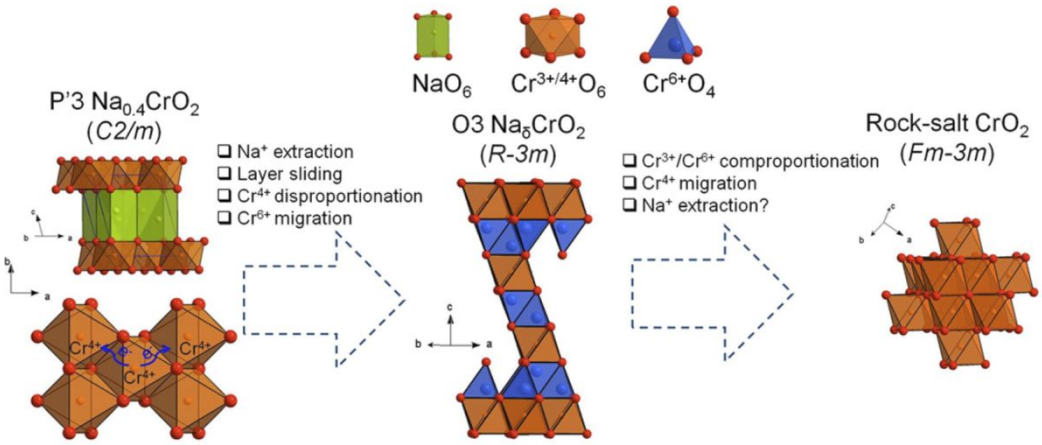

Fig. 6 Proposed schematics of the layered P′3 $Na_{0.4}CrO_2$ to rock-salt CrO_2 structural transition. Reproduced from Refs.[77] with permission of ACS.

The disproportionation is a kind of redox reaction that transition metal ions whose valence states are the same turn into different oxidation states by exchanging electrons with each other (one is higher and the other is lower than the intermediate states). This phenomenon is regarded as a negative factor for the cycle life of electrode materials. Mn^{3+} and Cr^{4+} ions are the representative ions with the disproportionation reaction in the alkali-ion transition metal compounds. For example, the two Mn^{3+} ions are converted to Mn^{2+} and Mn^{4+} ion by the disproportionation reaction (*i.e.,* $2Mn^{3+} \rightarrow Mn^{2+} + Mn^{4+}$). In this case, the Mn^{2+} ion can easily dissolve in electrolytes, meaning that a loss of electroactive species.[78,79] Even worse, the dissolved ions can be accumulated on the surface of electrode materials or block the pores of separator, leading an increase in internal resistance.[78] Furthermore, the dissolved transition metal ions can travel to the negative electrode and form a passive film by the reduction reaction at there, and that consume electrolytes, or in worst case can result in short circuit.[80] In the case of Cr^{4+} ion, the three Cr^{4+} ions are easily changed to two Cr^{3+} and one Cr^{6+} ion by the disproportionation reaction because Cr ion is more stable in the electron configurations of Cr^{3+} and Cr^{6+} ions than that of Cr^{4+} ion (*i.e.,* $3Cr^{4+} \rightarrow 2Cr^{3+} + Cr^{6+}$).[81] For instance, in the chromium-based layered structure materials (*i.e.,* $NaCrO_2$), this disproportionation reaction degrades the reversible capacities[82] because the Cr^{6+} ion, formed by the disproportionation reaction, prefers to occupy tetrahedral sites owing to the small ionic size and the absence of electrons in 3d orbitals of Cr^{6+}. The 4-coordinated Cr^{6+} ions in the tetrahedral site can migrate reversibly into octahedral sites,[83] but in the worst case there is a reversion to the Cr^{4+} ions by a comproportionation reaction of Cr^{6+} ion with neighboring two Cr^{3+} ions. In this case, the regenerated Cr^{4+} ions can move to near octahedral sites in the Na layer, resulting in the layered to rock-salt transformation (Fig. 6).[77]

Metal-metal dimerization

Utilizing a property of transition metal ions whose are prone to interact between each other can be utilized to increase the capacity of the cathode materials by stabilizing anion redox reaction. For example, Reeves *et al.*[84] claimed that the unpaired electron (low spin d^4) contributes to the formation of Ru-Ru dimerization in a Li_2RuO_3 compound. The generated Ru-Ru dimer bonding gets stronger during the Li extraction due to increase of Ru oxidation state from Ru^{4+} to Ru^{5+}. The stronger Ru-Ru dimer structure effect to the Ru-O bonding and bond length, and thus the $O_2^{-/2-}$ peroxo-like dimer is stabilized. As a result, the reversible oxygen redox reaction is stabilized which increases the capacity.[84]

2.1.3. Anions perspective: O, S, F, PO_4 *etc.*

Anions are one of the key structural components in constructing the framework of host structures together with transition metal ions. The anion itself has important abilities that can modify the redox potential of transition metal ions through an inductive effect, augment the capacity of cathodes by an anionic redox chemistry, and improve the structural and chemical stability by an incorporation of anions. (For convenience, the alkali-ion is fixed as Li-ion when the redox potential *vs.* anion species is discussed, see Fig. 6).

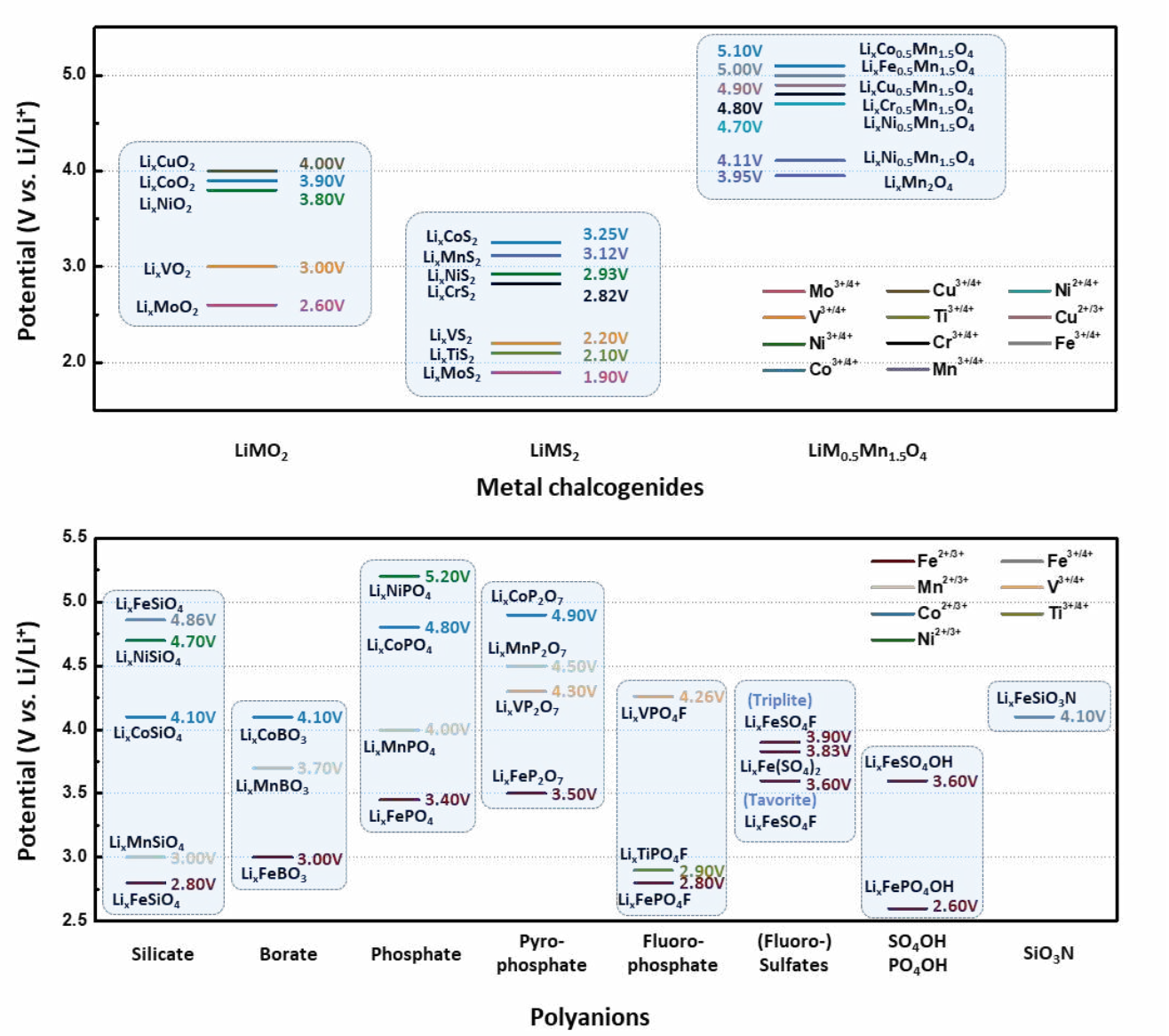

Fig. 7 Redox potential *vs.* anions of cathode materials for Li-ion batteries. Top: Li-ion transition metal chalcogenide compounds.[6,85–97] Bottom: Li-ion transition metal polyanion compounds.[62,98–104]

Redox potential

The difference in redox potential of transition metal ions by anion species is observed between oxide and sulfide materials. The redox potential of $V^{3+/4+}$ in $LiVO_2$ is 3.0 V, but the $V^{3+/4+}$ redox potential in lithium vanadium sulfide ($LiVS_2$) is 2.2 V (Fig. 7).[90,96] The redox potential

of $Mo^{3+/4+}$ in $LiMoO_2$ is 2.6 V, whereas the redox potential of $LiMoS_2$ is 1.9 V.[86,92] These indicate that the redox potential of sulfide materials is generally lower than that of oxide counter parts, which is likely due to higher electronegativity of O^{2-} than S^{2-}.Similarly, the Fe-polyanion compounds show distinct discharge potential of $Fe^{2+/3+}$ according to polyanion species, with 3.5 V for $Li_2FeP_2O_7$, 3.4 V for $LiFePO_4$, 3.0 V for $LiFeBO_3$, and 2.8 V for Li_2FeSiO_4 (Fig. 8). This exhibits a strong association between Fe-O covalent bonding and redox couple energy of $Fe^{2+/3+}$ according to the polyanion groups (silicates, borates, phosphates, and pyrophosphates). The discharge potential values of the polyanion compounds also show the general trend of $(P_2O_7)^{4-} > (PO_4)^{3-} > (BO_3)^{3-} > (SiO_4)^{2-}$ in the same transition metals. Other examples are hydroxyl-phosphates, N-substituted silicates, and flurophosphates. Redox potential of $Fe^{2+/3+}$ in hydroxy-phosphate is lower than that of phosphate groups. The redox potential of $Fe^{2+/3+}$ in $LiFePO_4$ is reported as 3.45 V, while the redox potential of $Fe^{2+/3+}$ in Li_2FePO_4OH is reported as 2.6 V.[98,105] First principles calculations also reported that the de-insertion of Li-ion voltage associated with the $Fe^{3+/4+}$ redox couple was decreased by N substitution in silicates (4.86 V in Li_2FeSiO_4, 4.7 V in $Li_2FeSiO_{3.5}N_{0.5}$ and 4.1 V in Li_2FeSiO_3N).[104] Substituted N is located in the adjacent Fe ion tetrahedral, yielding a strong covalent Fe-N bond due to the lower electronegativity of N. The more covalent Fe-N bonds render the lowering redox potential of $Fe^{2+/3+}$. The vanadium oxy/flurophosphate $Na_3V_2(PO_4)_2F_{3-2y}O_{2y}$ ($0 \le y \le 1$) system has been reported to have $V^{3+/4+}$ (y = 0) or $V^{4+/5+}$ (y = 1) redox couples, depending on the different anion configurations.[106] The $V^{3+/4+}$ redox couple in $Na_3V_2(PO_4)_2F_3$ occurs at higher voltage (average redox potential: ~3.9 V) than the $V^{4+/5+}$ in $Na_3V_2(PO_4)_2FO_2$ (average redox potential: ~3.8 V) due to the stronger inductive effect of the more electronegative F^- compared to O^{2-}.

Structural change behavior

The difference of electronegativity between the transition metal ion and anion can affect the different structural change behavior, for example, variation of $c_{hex.}$-lattice parameter and inter-slab distance. In the layered oxides of $Li_xNi_{1.02}O_2$ (LNO), which exhibits a strongly ionic character as the Li-ions are removed from the structure, electrostatic effects prevail, resulting in a continuous increase in the inter-slab distance and $c_{hex.}$-lattice parameter during extraction of Li ions ($0.3 < x < 1$). [107] On the other hand, for $x < 0.3$, completely different behavior is observed: the collapse of the slab distance and decrease of the $c_{hex.}$-lattice parameter in the highly de-inserted state is observed. In contrast, $c_{hex.}$ parameter keeps increasing as Li ions intercalate into the more covalent compounds, Li_xTiS_2 and Li_xZrS_2 systems.[107] The increase in $c_{hex.}$-lattice parameter during Li insertion can be explained by the steric effects of the Li-ions in more covalent sulfides systems. In more covalent systems, steric effect becomes stronger than electrostatic one between anions. That is why sulfide compounds have different c_{hex}-parameter change behavior compared to oxides. NiO_2 can also be assumed to be very covalent due to the high oxidation states of Ni^{4+} and, therefore it is well understood that a decrease in the $c_{hex.}$-lattice parameter at the top of the charge in LNO.

Origin of Anionic redox

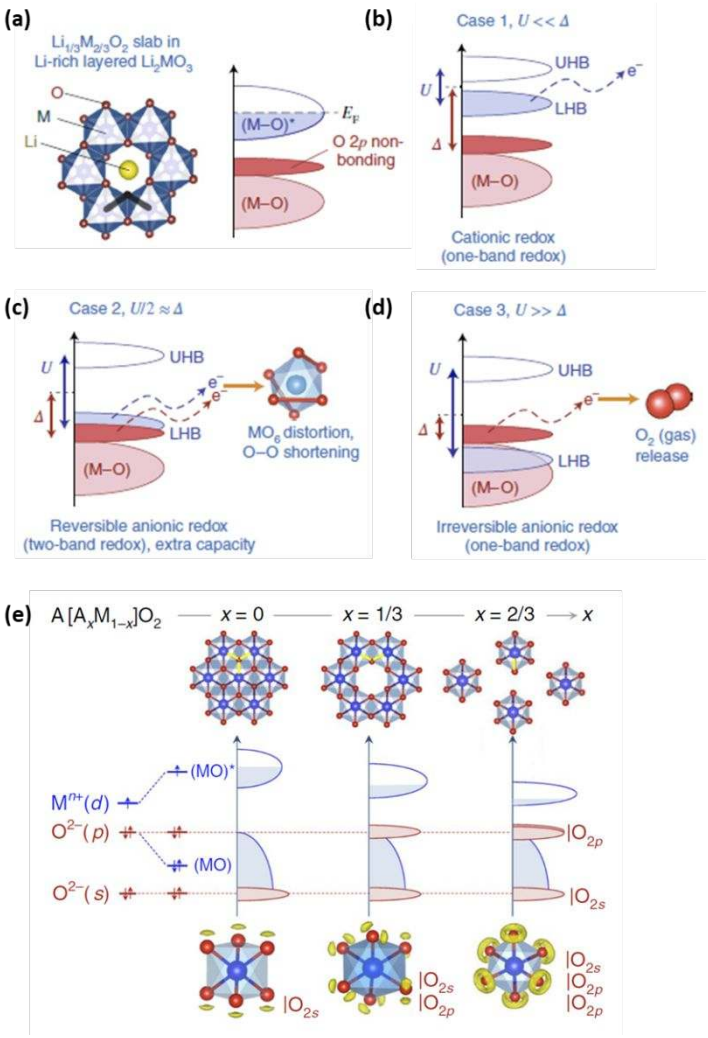

Fig. 8 (a) The crystal structure focusing on slab of Li1/3M2/3O2 and the relevant parts of its band structure. Taking Mott–Hubbard splitting into account, the Li2MO3 band structure is further classified under three cases (b–d), depending on the interplay between the d–d Coulomb repulsion term U and the charge transfer term Δ. (e) Schematic electronic structures for LiMO2 (x = 0), Li2MO3 (x = 1/3) and Li5MO6 (x = 2/3) where the |O2s and |O2p lone-pair states are highlighted by red bands. Reproduced from Refs.[10,11]With permission of NPG.

Anionic redox activity has been reported in a variety of systems ranging from conventional layered $LiMO_2$[108,109] to Li-rich layered and cation-disordered rock-salts $Li_{1+x}M_{1-x}O_2$ (M = Mn, Co, Ni, Fe, V, Nb, *etc.*),[110–114] Li_2MO_3 (M = Mn, Ru, Ir, *etc.*),[115–118] Li_3MO_4 (M = Nb, Ru, Ir, *etc.*),[119] and Li_4MO_5 (M = Mo).[120,121] There have been debating reports that anionic redox chemistry is highly associated with covalency of transition metal and anion, non-bonding of anion *p* bands, and cation migration during the charge and discharge.[122,123] A recent work by Assat *et al.* claimed that the presence of strong covalent M-O bond or the presence of ligand non-bonding of anion *p* bands is not individually sufficient condition to ensure reversible anionic redox (Fig. 8a-d).[10] They introduce the anionic redox mechanism depending on the interplay between the *d-d* Coulomb repulsion term U and the charge transfer term Δ by focusing on slab of $Li_{1/3}M_{2/3}O_2$ (Fig. 8a). The charge transfer, the difference in energy between (M–O) and (M–O)*, depends on the electronegativity difference between cation and anion. The *d–d* Coulomb interaction term U is related to the on-site electron repulsion within the d orbital which is frequently used in solid-state physics. According to their report, for U << Δ, electrons are exchanged from the partially filled (M-O)* band as cationic redox reaction in conventional layered oxides with highly ionic bonds of M-O during the electrochemical cycle (Fig. 8b). In contrast, electrons are exchanged directly from the non-

bonding O 2*p* states, which means the irreversible anionic redox in highly covalent bonds of M-O case (U >> Δ) (Fig. 8d). The intermediate state of U/2 ≈ Δ results in overlapping (M-O)* bands and O 2*p* non-bonding bands, which can introduce the reversible cationic and anionic redox (Fig. 8c). Such a redox process is triggered depending on the relative position of non-bonding O 2*p* band and partially filled (M-O)* band.[10] Based on previous fundamental understanding of anionic redox, Yahia *et al.* recently developed the unified picture of anionic redox by figuring out that the number of holes per oxygen, h^O, is a significant parameter for the reversible anionic redox in A-rich-TMOs.[11] They described the anionic redox process in terms of h^O; $h^O \leq x$ (x in $A[A_xM_{1-x}]O_2$) is required for the reversible anionic redox, and $h^O = 1/3$ is suggested as the upper limit for achieving reversible anionic capacity in $A[A_xM_{1-x}]O_2$ ($0 < x \leq 1/3$) electrodes (Fig. 8e). For example, Fe and Te ions, which are inactive during electrochemical cycling in $Li_{4.27}Fe_{0.57}TeO_6$ materials, maintain Fe^{3+} and Te^{6+} oxidation states, and only oxygen participates in the redox process. The only anionic redox reaction occurs during charge process, accompanied by the evolution of O_2 gas as well as the formation of peroxo-like species.[124] Li_3MO_4 is another good example system with an O/M ratio of 4 to increase oxygen lone pairs in non-bonding O 2*p* orbitals associated with anionic redox.[119,125] More specifically, Perez *et al.* demonstrated large amount of Li extraction (> 2.5 Li) from Li_3IrO_4, utilizing anion redox without participation of iridium redox during the 1st delithiation. The authors explained that the instability of the oxygen network due to such increased O/M ratio with low coordination number of oxygen with transition metal (not Li-ions) can be stabilized through high Ir-O bond covalency.[119]

In $Li_{1.17}Ni_{0.21}Co_{0.08}Mn_{0.54}O_2$ (Li and Mn-rich NCM) materials, a strong correlation between cation migration and anionic redox was identified.[126] The partially reversible migration of transition metal in the bulk structure leads to a change in the local oxygen coordination environment, confirming that O 2*p* states shift to higher energy states as well as reshuffling the anionic and cationic redox potential. This anionic redox mechanism means that the anionic redox reaction does not occur as rigid O^{2-}/O^- but rather as a reaction of dynamic reshuffling of O redox states with TM migration.[126] In similar way, it has been reported that cation migration is closely related to anionic redox in $Li_2Ir_{1-x}Sn_xO_3$ system.[118] Multivalent hybridized Ir-O redox contributes to the total capacity of Li_2IrO_3 in the de-insertion process without Ir migration and anionic redox. However, as the amount of Sn increases in the $Li_2Ir_{1-x}Sn_xO_3$ system, the anionic redox reaction is activated by Sn migration during the charge process. Cation vacancies are formed by Sn migration and dangling bonds of O are generated through Sn-O de-coordination. They claimed that the mechanism of anionic redox can be described by ligand-to-metal charge transfer (LMCT) reaction to form shortened Ir=O double bond (1.76-1.79 Å) or O-O dimers (~1.44 Å) by donating lone-pair electrons of dangling bond oxygen to Ir or O during charge process.[118] However, substitution of electrochemically inactive M (M = Mn^{4+}, Sn^{4+}) into the $A[A_xM_{1-x}]O_2$ materials invariably leads to partial irreversibility of the anionic process with voltage hysteresis and cation migration due to the increase of h^O. This allows us to understand the anionic redox with cation migration in the reported $Li_{1.17}Ni_{0.21}Co_{0.08}Mn_{0.54}O_2$ and $Li_2Ir_{1-x}Sn_xO_3$ systems.

2.2. Molecular to crystallographic scale

The crystallographic properties and behaviors of insertion cathode materials are fundamentally linked to the changes in the constituent elements and interactions among them. For example, in the case of crystallographic properties like as lattice parameters and unit cell volume largely depend on the size of constituent atoms. Therefore, in some cases, we can control the parameters by changing the ratio of constituent elements. Moreover, in the Ni-based layered materials, the atomic position of Li^+ and Ni^{2+} ions can be easily exchanged due to the similar ion size of the two ions, making disordered structure, and that can lead to impede the diffusion of mobile ions. The manipulation of molecular scale factors has obviously crystallographic effects, and the ongoing technical development in the structural analysis is providing detailed information on the corresponding results. The scope of what will be dealt with is extended to crystallographic scale such as crystal structure, disorder, ion channel, phase transition point of view. In this part, what governs the characteristics of each of those factors, and the consequences arising from the changes in those factors will be addressed. The comprehensive approach will facilitate the understanding of how each factor can be controllable, and how they are linked together and influence each other.

Batteries are operated by the movement of mobile ions so that the most important determinant of performance is the kinetic nature of the mobile ions in electrode material. The transport properties in the cathode material are determined by the two major components which are mobile ion and host structure. As elucidated in chapter 2.1, even though host structure of the cathode has same structure, it exhibits different electrochemical characteristics when using different mobile ions. Also even small changes in the host structure may significantly affect performance. Electrochemical performance in many cathode materials has been identified as a collective outcome, where a functional relationship between mobile ion and host structure has been interacted. Therefore, the correlation between host material and mobile ions must be taken into account when designing a new material.

In chapter 2.2, the scope of what will be dealt with is extended from the molecular scale covered in chapter 2.1 to crystallographic scale beginning with the representative crystal structure explanation. In addition, kinetic properties based on local and bulk structural changes will be explained based on three key words: disorder, ion channel, and phase transition. Disorder is a factor that directly affects the ion channel, and the phase transition is a fundamental element directly or indirectly affected by the other two factors, all of which are not independent and are quite closely multi-correlated (Fig. 9). Consequently, decoupling all the detailed factors that influence battery performance is not easy. Nevertheless, an approach through systematic classification will provide an in-depth understanding of the kinetics of complex electrodes that are directly related to performance.

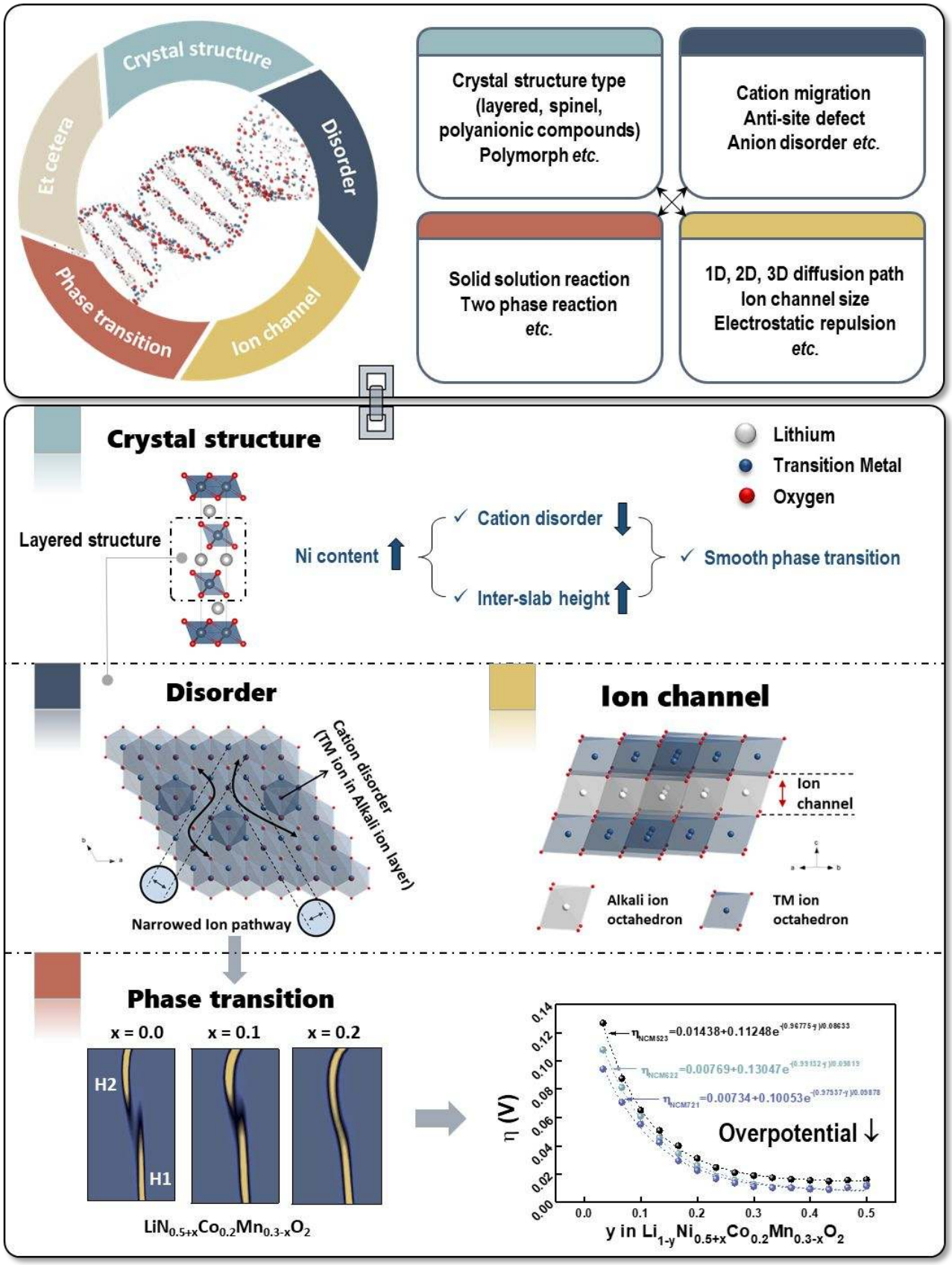

Fig. 9 Schematic illustration of one of the examples for the multi-correlated factors such as crystal structure, disorder, ion channel, phase transition and electrochemical property.[127]

2.2.1. Crystal structure

There are a large number of crystal structures in alkali-ion transition metal compounds on the basis of the combination of three parts as alkali metal ions (A), transition metal ions (M), and anions (X). Considering that the transition metal ions can have multivalence states, any one of these the A-M-X phase diagram will have various stable phases. Despite various constraints (for example, X is only a halide, oxide, or chalcogenide ion), more than 10,000 combinations of A, M, and X are available.[128] Among these numerous types of crystal structure, the majority of current promising insertion cathode materials can be categorized into layered, spinel, olivine, tavorite, Prussian blue analogues crystal structures and so on. The reaction potential, dimension of alkali-ion diffusion paths, and reaction mechanisms can be variable depending on their crystal structures despite the same chemical composition.

Metal oxide compounds

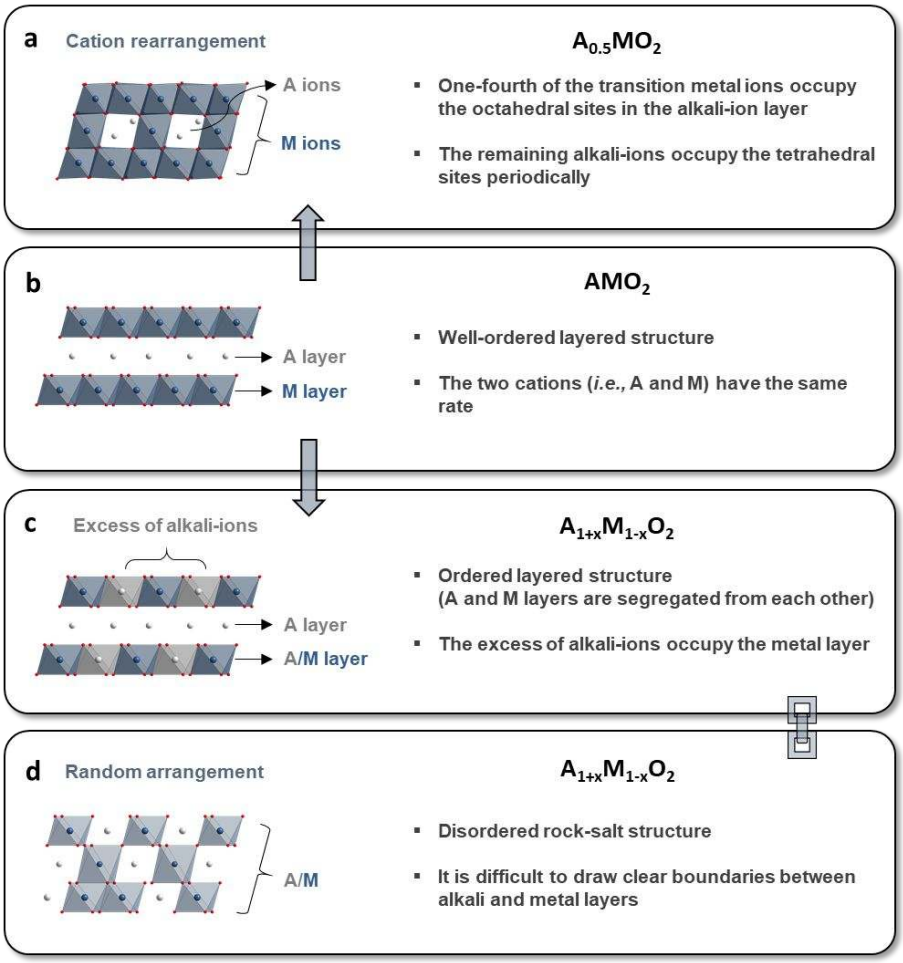

Fig. 10 Schematic illustration and descriptions of (a) spinel, (b-c) layered and (d) disordered rock-salt crystal structures.

The pure layered structure material (*e.g.*, $R\bar{3}m$, $LiMO_2$) is composed of two repeated layers where alkali-ion and transition metal layers are well separated from each other (Fig. 10b). Sometimes, when the ionic radius of alkali-ion and transition metal ions are similar, there are cation disorders: extra transition metal ions occupy the alkali-ion layer or each ion exchanges their position. The layered structure materials have a 2-dimensional ion diffusion channel which formed between two transition metal layers, so the diffusivity of alkali-ions is greatly

influenced by the environment of alkali-ion layers.[129]

When the proportion of alkali-ions surpasses that of transition metal ions in the layered structure (*e.g.,* $Li_{1+x}M_{1-x}O_2$), the excess alkali-ions are inevitably located in the transition metal layer. If the alkali-ions are present in the transition metal layer and the alkali-ion and transition metal layers are well separated, the material can be labeled as alkali-ion rich layered structure cathodes (*e.g.,* Li-rich layered materials, Fig. 10c). The crystal structure, specifically in the case of Li-rich layered materials, has both a rhombohedral symmetry of $LiMO_2$ phase (M = Ni, Co, or Mn *etc.*) and a monoclinic symmetry of $Li_2M'O_3$ phase (M' = Mn, Ru, or Sn *etc.*), so the Li-rich layered materials have been denoted by two chemical formulas: $(1-x)Li_2M'O_3$-$xLiMO_2$ (nanocomposite) and $Li_{1+x}M_{1-x}O_2$ (solid solution). There have been numerous research efforts to identify the crystal structure of the materials, but the debate about the initial structure of Li-rich layered materials is not yet complete.[9] Leaving the controversial issue aside, the most important feature of this type of materials is the activity of anionic redox chemistry due to a distinctive local structure originated from a higher ratio of alkali-ion than transition metal ion. For example, when extra Li-ions are located in a transition metal layer and an oxygen ion is surrounded by four Li-ions and two transition metal ions, the oxygen ion can have linear bonding with two Li-ions as a Li-O-Li configuration. In this case, the O 2*p* orbitals along the Li-O-Li configurations are unhybridized, thus the energy of electrons of O 2*p* states in the Li-O-Li configuration are higher than those of the other O 2*p* states. As a result, it allows the oxygen to participate in the charge compensation at a reasonable voltage window (< 4.5V vs Li).[123] However, the excess alkali-ion environment is a sufficient requirement but not necessary condition for the activity of anionic redox chemistry. For instance, the $Na_{2/3}(Mg_{0.28}Mn_{0.72})O_2$ layered structure material shows an extra capacity which is unable to be explained by the electrons originated from transition metal based redox chemistry. In this case, the Mg^{2+} ion in the transition metal layer promotes the oxygen redox by weakening the ionic Mg-O bonds (similar to Li-O) due to the relatively high energy of Mg^{2+} 3*s* state compared to O 2*p*.[130]

Contrary to the ordered layered structures, if the two cations (*i.e.,* A and M ions) are randomly distributed in the crystal structure and the two layers are not obviously distinguished, the cathode can be called as the disordered rock-salt materials (Fig. 10d). In general, disordered structures are reckoned to be inappropriate to the insertion materials because the cation disorder obstructs the alkali-ion diffusion. However, a highly reversible insertion reaction is observed despite the increase in the level of disorder of the crystal structure, which is attributed to the presence of a percolating 0-TM network.[131] Further details of the disordered structure materials will be dealt with at the "disorder & ion channel" chapter.

From a simplistic view, the spinel structure can be seen as a derivative of layered structure material (Fig. 10a). After a removal of half the amount of alkali-ion from the layered structure (*e.g.,* $Li_{0.5}MO_2$) and a cation rearrangement that one-fourth of the transition metal ions occupy the octahedral sites in the alkali-ion layer and the remaining alkali-ions occupy the tetrahedral sites periodically, the final structure can be expressed in a spinel structure (*e.g.,* $Fd\bar{3}m$, $Li_{0.5}MO_2$ = 1/2 LiM_2O_4, M: 16d sites, Li: 8a sites). The alkali-ion diffusion channel of the spinel crystal structure is in the form of a 3-dimensional migration pathway. Thus, the host structure with this high degree of the dimensional migration path in the open framework can provide the mobile ions with a fast diffusion environment. The two representative structure of the spinel type materials are ordered and disordered spinel. In the case of the ordered spinel (e.g., $P4_332$, $Li_xNi_{0.5}Mn_{1.5}O_4$) structure, there are distinctive positions for the Ni and Mn ions where each element is located in 4*a* and 12*d* sites respectively. However, in the case of the disordered spinel (*e.g.,* $Fd\bar{3}m$, $Li_xNi_{0.5}Mn_{1.5}O_{4-\delta}$) structure, the two transition metal ions are randomly distributed in 16*d* sites. Due to the deficiency of oxygen ion in the disordered structure, there is a certain degree of Mn^{3+} in the lattice, which contributes to the plateau voltage profile around 4.0 V.[9,132]

Polyanion compounds

Polyanion materials are composed of a union of multidimensional connected network among transition metal polyhedra and polyanionic groups like phosphates, sulfates, silicates, and borates *etc.* Numerous host structures (*i.e.,* polyanionic framework) can be created from combinations of diverse transition metal ions and polyanionic compounds. Representative crystal structures of polyanion materials are

NASICON, olivine, and tavorite *etc.* (Fig. 11).

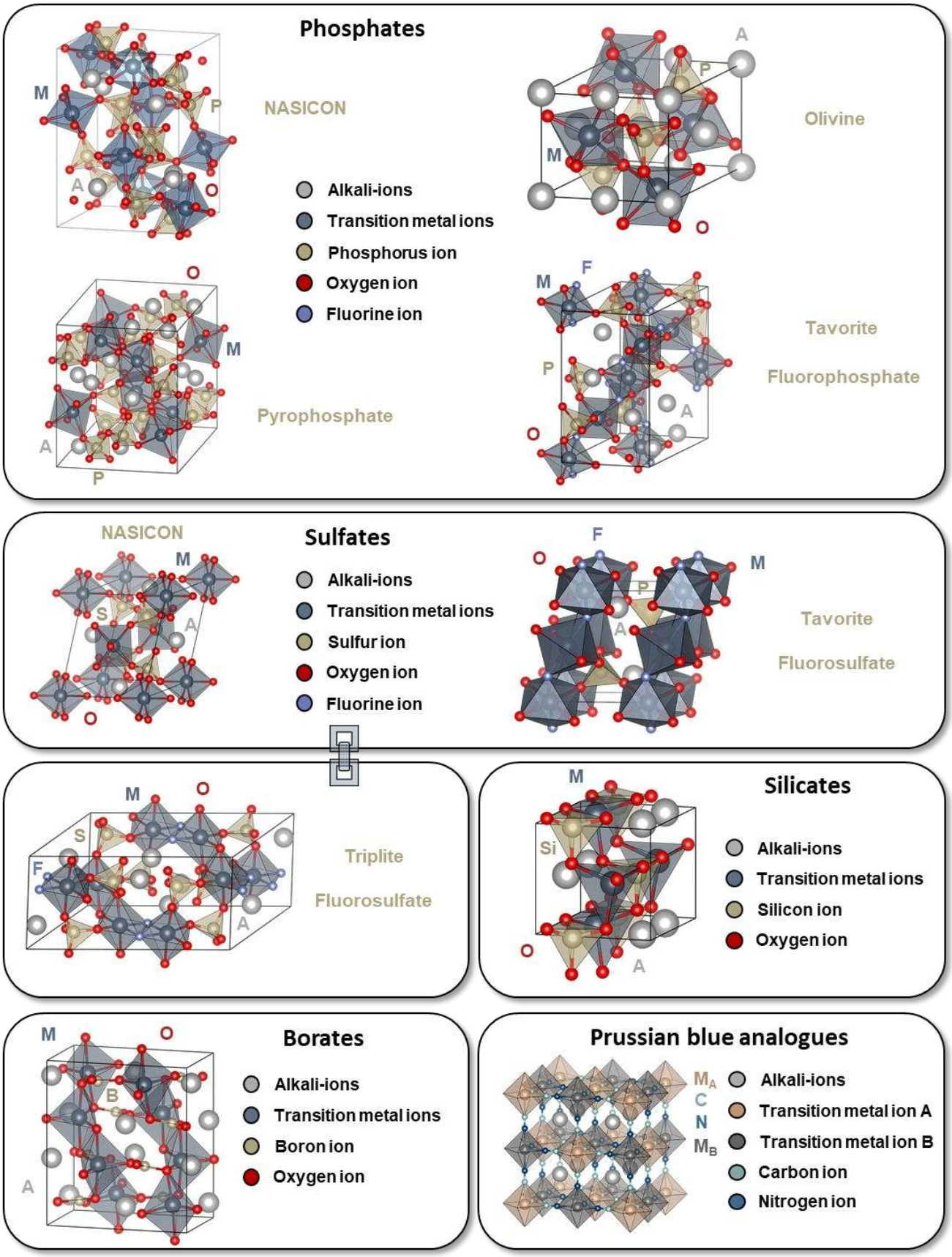

Fig. 11 Schematic illustration of phosphates, sulfates, silicates, borates and Prussian blue analogues crystal structures.[133–140]

Phosphates

The NASICON (Na Super Ionic CONductor) type materials have a three-dimensional framework of MO_6 octahedrons corner shared with XO_4 tetrahedrons. The basic unit of this structure, so-called "lantern unit", is comprised of three tetrahedral connected with two octahedrons. Each unit is connected to six adjacent units and forms a large space that can accommodate alkali-ions, and the weak binding between alkali-ions and the framework can lead to the easiness of the mobile ion migration.[141,142]

A representative olivine type material is a triphylite $LiFePO_4$ cathode which has orthorhombic symmetry with *Pnma* space group. The phosphorous forms polyanion with oxygen ions (PO_4^{3-}), and Li^+ and Fe^{2+} ions are located in the octahedral sites, making 1D pathways for Li transport along [010] direction. Structurally, the FeO_6 octahedron is connected with PO_4 tetrahedral groups (one edge-shared and four corner-shared). In this respect, Rousse *et al.* claimed that elongated and weakened Fe-O bond because of the repulsion between Fe and P ions leads to boosting up of the operation voltage.[143]

Polyphosphates such as pyrophosphates have attracted much attention due to their interesting and promising electrochemical performance.[144] The crystal structure of pyrophosphates (*e.g.,* $Li_2MP_2O_7$, M = Mn, Fe, Co) is represented by 3D framework built of M_2O_9 blocks of edge-shared distorted MO_6 octahedrons and MO_5 bipyramids interconnected with P_2O_7 polyanion group. These blocks and groups form tunnels along [100] and [010] directions where alkali-ions are accommodated. In this structure, alkali-ion exists in two distinct coordination polyhedrons: tetrahedral AO_4 and distorted square pyramid AO_5. Examples of pyrophosphates are $Li_2MnP_2O_7$ (space group $P2_1/a$), $Li_2FeP_2O_7$ (space group: $P2_1/c$)and $Li_2CoP_2O_7$ (space group: $P2_1/c$).[145]

The $LiVPO_4F$ is the first fluorophosphates which is used for the cathode materials, and has a tavorite-based arrangement in the crystal structure.[146] The host framework is composed of one-dimensional VO_4F_2 octahedrons chains where each octahedron is connected by corner-sharing with fluorine atoms. Due to the presence of fluorine with high electronegativity, the redox potential of V^{3+}/V^{4+} redox couple in $LiVPO_4F$ is 0.4 V higher than in fluorine-free $Li_3V_2(PO_4)_3$ (*i.e.,* 4.2 V for $LiVPO_4F$[146] and 3.8 V for $Li_3V_2(PO_4)_3$[147] respectively, *vs* Li/Li^+).

Sulfates

The first reported sulfate-based material for Li insertion is $Fe_2(SO_4)_3$ with a flat voltage of 3.6 V vs Li^+/Li.[148] The crystal structure of monoclinic $Fe_2(SO_4)_3$ represents NASICON-type ordering and lithium intercalation occurs through two-phase reaction.[149] Later, Reynaud *et al.* developed the lithiated iron sulfate, $Li_2Fe(SO_4)_2$, which has a monoclinic unit cell with space group $P2_1/c$.[102] It delivers even higher voltage of ~3.83 V vs Li^+/Li. These iron sulfate is built of isolated FeO_6 octahedrons interconnected with six SO_4 tetrahedrons forming large channels along [100] direction where Li-ions accommodate.

In the case of fluorosulfates, the $LiFeSO_4F$ was firstly reported in 2010.[150] The crystal structure of $LiMSO_4F$ fluorosulfates (M = Fe, Co, Ni) belong to *P*-1 space group and it is similar to phosphate-based tavorite materials. The host structure is composed of the chains of corner-shared FeO_6 octahedrons interconnected by SO_4 tetrahedrons forming a 3D framework with large spaces for Li ion occupation. Another important member of $LiMSO_4F$ (M = Fe, Mn) fluorosulfates family is represented by triplite-based materials.[151,152] Triplite based materials are crystallized into a monoclinic cell with *C*2/*c* space group and structurally differs from tavorite $LiMSO_4F$ fluorosulfates. The triplite $LiMSO_4F$ crystal structure is composed of edge-sharing chains of MO_4F_2 octahedrons interconnected with sulfate tetrahedrons whereas for tavorite structure octahedrons are corner-shared. In the triplite $LiMSO_4F$, these MO_4F_2-SO_4 chains run along the [101] or [010] direction, which is distinct from the single chain running along [100] direction in tavorite. Fluorine atoms are located on the same edge (cis-configuration) of MO_4F_2 octahedrons in a triplite structure while in a tavorite structure they are located on axial positions (trans-configuration). The most

important difference between triplite and tavorite is a random distribution of Li and Fe on metal sites creating more stable six-fold coordination for Li-ions.[153] In fact, $LiFeSO_4F$ can be obtained either in tavorite or triplite and these phases can be considered as ordered and disordered polymorphs, respectively. Also, partial substitution of Fe for Mn in $LiFe_{1-x}Mn_xSO_4F$ leads to transformation of tavorite phase to disordered triplite, resulting in an increase of Fe^{2+}/Fe^{3+} potential.[152]

Fluorine-free materials with high transition metal redox potential are objects of intense investigation due to the safety and environmental concerns. The introduction of hydroxyl groups also increases the ionicity of M-X bonding but the effect is weaker than for fluorine contained materials: 3.6 V and 3.2 V vs Li^+/Li for Fe^{2+}/Fe^{3+} redox couple in tavorite-$LiFeSO_4F$ and tavorite-$LiFeSO_4OH$, respectively. Recently, $LiMSO_4OH$ (M = Fe, Mn, Co) with layered structure has also been reported.[154] In this structure, FeO_6 octahedra share edges to form zigzag chains along the [010] direction. These chains are connected by vertices to form a layered structure. SO_4 tetrahedra are linked via vertices to the FeO_6 octahedra on each side of the layer. Li-ions are tetrahedrally coordinated by oxygen atoms and locate in the space between the layers.

Silicates

Silicate-based materials are very attractive due to the widespread and low cost of silicon oxide. One of the features of any silicate materials is its rich polymorphism. Various polymorphs are known for Li_2MSiO_4 materials with slightly different electrochemical performance.[155–157] It challenges the synthesis of single phase material because all polymorphs have similar formation energy. Depending on the synthesis temperatures, Li_2MSiO_4 crystallizes more than 8 different polymorphs, and they can be categorized into two groups as β- and γ- forms respectively.[158] The structure consists of distorted hexagonal close packing of oxygen ions where the half of tetrahedral sites is occupied by cations. Cations can be distributed into two possible sets of available tetrahedral sites.

Borates

One of the polyanionic compounds drawbacks is a “mass penalty”. Phosphate, sulfate, silicate and other anionic groups bring inactive mass to the cathode material reducing the specific capacity. Reducing the mass of the anion group is one of the ways to increase the capacity of the polyanionic materials. $LiMBO_3$ (M = Mn, Fe, Co) containing the lightest polyanion group $(BO_3)^{3-}$ was firstly considered as a cathode material in 2001.[136] The crystal structure of $LiMBO_3$ (M = Fe, Co) is described in the monoclinic *C2/c* group and composed of a 3D framework formed from chains of edge-sharing MO_5 hexahedrons along the [-101] direction, linked with corner-shared planar BO_3 groups.[159] Li-ion occupies two distinct tetrahedral sites Li1 and Li2 forming edge-sharing chains of paired face-sharing LiO_4 octahedrons along the [001] direction. On contrary, the crystal structure of $LiMnBO_3$ is described in hexagonal *P*-6 and composed of chains of edge-sharing square pyramids connected through borate groups and forming the 3D framework with Li-ion in tetrahedral sites. In both types of crystal structures, the 3D framework also forms a 1D channel for Li-ion diffusion.

Prussian blue analogues

The cyanide group (-CN) anions can make open framework together with transition metal ions for hosting the alkali-ions. Generally, the Prussian blue analogues (PBAs) have six-cyanide group anions in a nominal formula (*i.e.,* $A^+M_A^{2+}[M_B^{3+}(CN)_6]$, so it is also known as Hexacyanometallates. A large interstitial site for accommodating alkali-ions which is surrounded by the cyanide ligands can be constructed by a chain of M_A-N≡C-M_B that is arranged along the <001> direction of the cubic unit cell. Each transition metal ion is coordinated by N and C respectively, forming M_AN_6 and M_BC_6 octahedrons. The host structure creates 3D diffusion pathway for the migration of alkali-ions.[52] The cyano-bridging ligand which has stretching and vibrational modes contributes to the structural flexibility of PBAs.[160] These host structure can accommodate the alkali-ions such as Li, Na, and K, and they can be used as insertion cathode materials. For the Li-PBAs, the voltages are comparable to or slightly lower than those of Na-PBAs, but the specific capacities are much lower than those of Na-PBAs.[48,49,52,161] Compared with the Na-PBAs, the specific capacities of K-PBAs are lower than those of Na-PBAs due to the heavier K^+ ions, but they exhibit higher voltages.[52] As a result, the PBAs are receiving much attention as K-cathode materials.[52]

Polymorph

Crystal polymorphs are defined as compounds that have same nominal chemical formula but exist in more than one crystal structure. Polymorphism is of particular importance in the polyanion compounds, as a lot of polyanion compounds sometimes have more than one crystal form and their electrochemical properties vary depending on the crystal structure. For example, the structural polymorphism has an impact on the redox potential as shown in Fig. 7. More specifically, all two structures, tavorite structure of $LiFe_{0.9}Mn_{0.1}SO_4F$ and triplite structure of $LiFe_{0.9}Mn_{0.1}SO_4F$, have similar close-packing structures that maintain the underlying framework of the sulfate tetrahedra. However, the reaction potential increases in the order of $LiFe_{0.9}Mn_{0.1}SO_4F$ in the tavorite phase (3.6 V) and $LiFe_{0.9}Mn_{0.1}SO_4F$ in the triplite phase (3.9 V) while they use the same $Fe^{2+/3+}$ redox.[152] Significant degree of atomic disorder occurs from the tavorite phase to the triplite phases and it results in a difference in redox potential.[98] Another example can be found in pure $LiFeSO_4F$ that has two different polymorphs: one is ordered $LiFeSO_4F$ (Tavorite, space group: *P*-1) and the other is disordered $LiFeSO_4F$ (Triplite, *C*2/*c*). The disordered $LiFeSO_4F$ exhibits relatively slower Li-ion diffusion as indirectly witnessed by the larger polarization in the voltage profiles.[151] While it has been believed that the Li/Fe disorder in the lattice considerably reduce the mobility of Li-ions,[162,163] a recent work by Seo and his colleagues demonstrated that Li migration barrier inside the triplite $LiFeSO_4F$ phase is indeed relatively low (< 400 meV).[164] They further showed the Li migration through domain boundaries is slow because of its high activation barrier (> 700 meV) and experimentally demonstrated that the particle size reduction to minimize the amount of domain boundaries can significantly improve the achievable capacity and rate capability of the triplite $LiFeSO_4F$.

We can find another example in $Li_2Fe(SO_4)_2$ materials: they have orthorhombic phase and monoclinic *marinate* polymorphs. The orthorhombic phase has higher material density because of the short Fe-Fe distance, resulting from the difference in the ordering of FeO_6 and SO_4. In addition, the two polymorphs exhibit different Li (de)insertion behaviors. The monoclinic $Li_2Fe(SO_4)_2$ has a single plateau during Li extraction/insertion while orthorhombic $Li_2Fe(SO_4)_2$ have 2 distinct plateaus during charge and discharge process.[165,166] The 2 distinct plateaus in the orthorhombic phase is attributable to the formation of a stabilized intermediate phase of $Li_{1.5}Fe(SO_4)_2$..[165,166]

Polymorphs can be also found in oxide systems. β-Li_2IrO_3 (*Fdmm*), unlike α-Li_2IrO_3 (*C*2/*m*), is built on three-dimensional structure in which IrO_6 octahedra are connected in a 3D edge-sharing structure that can accommodate Li-ion migration via interconnected paths. β-Li_2IrO_3 exhibits high capacity retention owing to the absence of shear stresses related with the gliding of the planes as is often the case with α-Li_2IrO_3 polymorph.[167]

2.2.2. Ion channel & Disorder

Alkali-ions of the insertion materials travel through a pathway called the ion channel. If the ion channel becomes obstructed and proper (de)insertion process is disturbed, it leads to significant performance deterioration of rechargeable batteries. In this respect, the ion channel can be equated to the blood vessel, so the factors that influence the environment of ion channel should be considered to understand the nature of ion migration and ways of controlling it. The word “disorder” generally has a negative connotation, but it has ambilateral effect on the insertion cathode materials. In this chapter, a wide range of aspect for the disorder will be addressed including local and bulk disorder. In fact, there is no such thing as a perfect crystal in nature. Crystalline imperfections such as interstitials, vacancies, and atomic occupancy are always present and they are usually classified as a defect. The amount of structural imperfections in crystal is dependent on the material property and the synthesis condition, all of which are related with the intrinsic and extrinsic regime such as defect formation energy, ion migration energy and ion trapping energy. Presence of a defect is a factor that destroys the symmetry and changes the ordering of the local environment within the crystal structure so it will be referred to as a “disorder” in this review. Local disorders are not only present intrinsically after synthesis but also acquired by external factors such as cell operating conditions. Local disorder has a physical and chemical effect on the structure, and as mentioned at the beginning of chapter 2.2, it is directly related to the ion channel. Since cathode materials were originally developed using ordered type with a clear order of mobile ion and host structure as elucidated in chapter of crystal structure,

disorder in crystalline structure was considered as a stereotype that may cause performance degradation. Recently, however, several papers have reported that disorder is not necessarily in an adverse way and a representative example of which is the bulk disorder type, disordered rock-salt cathode material. Therefore, in this part, the consequences based on the classification of local disorders and bulk disorders will be described.

Size of channels

In typical two-dimensional layered structure cathode materials (so called O3-type layered), alkali-ions migrate from its original octahedral position to another octahedral site by passing through an intermediate tetrahedral site which abuts onto both octahedral sites. In this regard, when a mobile cation moves into the tetrahedral site, the mobile cation repels electrostatically with a transition metal cation in a nearby the tetrahedral site. As a result, an activation barrier for mobile alkali-ions varies with a size of the tetrahedral site and the species of transition metal cations. The activation energies derived from these two factors should be lowered to achieve a high ionic conductivity.[129] For example, on the basis of *ab initio* calculations, the activation barriers for Li-ion migration can be reduced due to the release of compression on the activated Li-ion site when the height of Li slab increases.[129] Understandably, in addition to this, low valence state cations such as Ni^{2+} and Cu^{2+} in the $LiMO_2$ (M = transition metal ions) layered structure results in a lower migration barrier for alkali-ions because of the reduced electrostatic repulsion between low valence cations and Li.[168]

As a way of increasing the Li slab is to control the composition ratio of each element in the multi-component layered system. For example, in the Co-fixed $LiNi_{0.5+x}Co_{0.2}Mn_{0.3-x}O_2$ (x = 0, 0.1, and 0.2) layered materials,[127] the height of Li slab increases when the Ni concentration increases. As total amount of Ni increases, average distance of TM-O decreases because the Ni^{3+} content in mixed Ni^{2+} and Ni^{3+} states increases, given that Co and Mn ion are 3+ and 4+, respectively. The decrease in the distance of TM-O results in the increased electrostatic forces between TMO_6 slabs, which elongates Li slab distance and improves Li diffusivity.

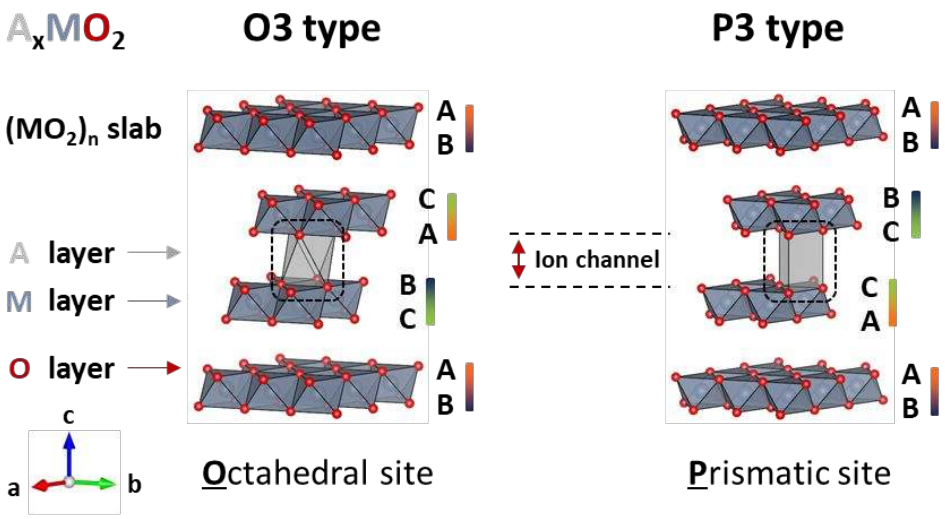

Fig. 12 Schematic illustration of two types of A_xMO_2 layer oxides such as O3 and P3 (A: Alkali-ions, M: transition metal ions, O: oxygen ion).[9]

The type of alkali-ion sites can also influence the diffusion of migrating ions. For example, in the layered structure materials, there are two representative types of alkali-ion sites such as octahedral (O) and prismatic (P) sites (Fig. 12). In the O3-type layered oxides where alkali-ions occupy octahedral sites, the alkali-ions migrate through face-shared tetrahedral sites. On the contrary, alkali-ions migrate between face-sharing prismatic sites through a large rectangular space in the P3-type layered oxides where alkali-ions sit in prismatic sites. Specifically, in the case of a large ionic size of alkali-ion such as Na^+ ion, the migration from one octahedral site to another octahedral site via an intermediate

tetrahedral site, occurring in O3-type, is energetically unfavorable due to the small size of tetrahedral site. In contrast to this, the ion channel in P3-type structure, which is composed of prismatic sites, can provide direct paths with a low diffusion barrier for large alkali-ions.[169,170]

Generally, a large ion channel is considered good for fast ion diffusion. However, an overlarge migration channel can lead to high alkali-ion migration barrier. For example, as mentioned above in the alkali-ion perspective part, the Li-ion migration barrier is the highest value among the three alkali-ions in a A_xVPO_4F (A = Li, Na, K) framework due to a different migration path and low coordination intermediate states. Therefore, a suitable void space and transition states for each mobile ions should be designed in order to achieve high rate performance of alkali-ion insertion cathode materials.[55]

Defects and Channels

In 2D layered structure materials, the cation (generally transition metal ions) in the alkali-ion layer is considered injurious to the movement of mobile ions. The extra transition metal ions in the alkali-ion layer reduce the space of inter-slab (*i.e.,* alkali-ion diffusion channel) and the high valence state of transition metal ions entail electrostatic repulsions with alkali-ions (*e.g.,* Li^+, Na^+, and K^+ *etc.*), leading to difficult situations in the (de)insertion of alkali-ions.[36,171–176] Therefore, controlling the transition metal ions in the alkali-ion layer is one of the key factors to improve the electrochemical performance of layered cathode materials. For instance, in the Ni-based layered cathode materials, the nickel content in the Li layer can be controlled by regulating the total quantity of Ni^{2+} and Ni^{3+} ions. A certain amount of nickel ions can occupy the Li layer due to the similarity of the ionic radius between Li^+ (0.76 Å) and Ni^{2+} (0.69 Å) ion. Therefore, reducing the absolute amount of Ni^{2+} ions is a way of lowering the chance of cation disorder. Specifically, in the case of Ni-Co-Mn three component layered system, one can simply increase the Ni concentration in Co-fixed $LiNi_{0.5+x}Co_{0.2}Mn_{0.3-x}O_2$ (x = 0, 0.1, and 0.2) layered materials to generate more Ni^{3+} than Ni^{2+}.[127] Such increase in Ni content leads to lower the cation disorder (*e.g.,* Ni^{2+} in the Li layer, NCM523 > NCM622 > NCM721).[127]

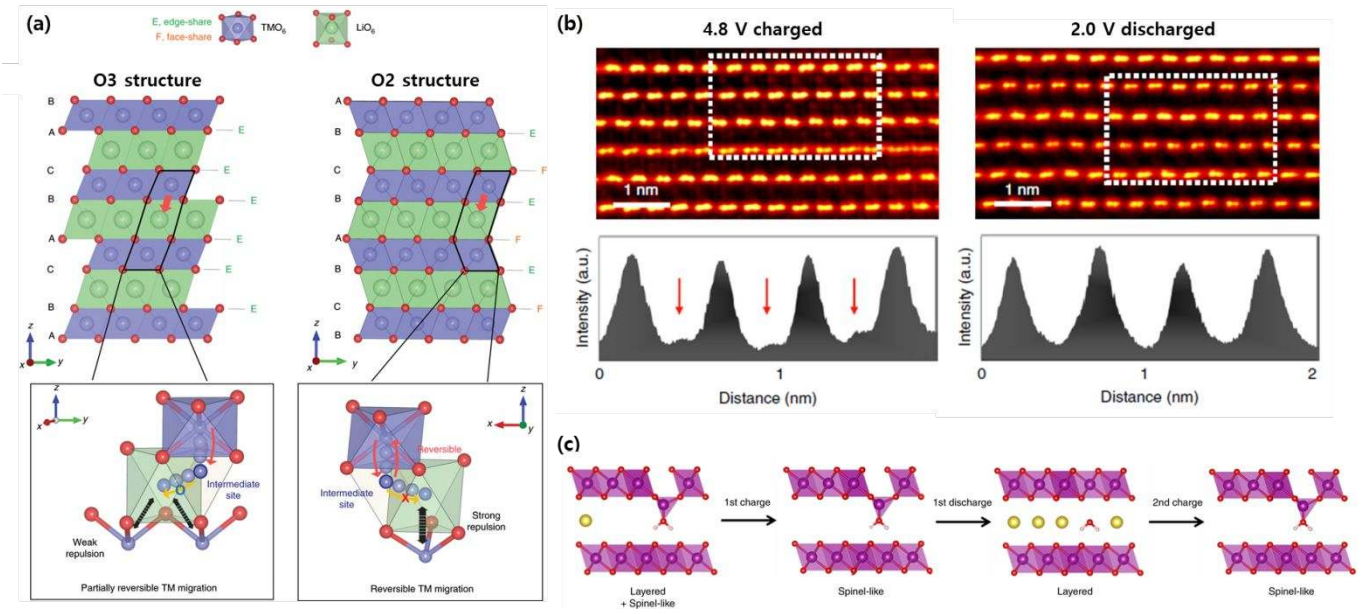

Fig. 13 (a) Schematic illustrations of crystal structure and cation migration paths of O3-type and O2-type Li layered oxides. (b) HAADF-STEM images and signals along the $[1\bar{1}0]$ zone axis for 4.8 V charged and 2.0 V discharged state of O2-type $Li_{0.83}(Li_{0.1}Ni_{0.2}Mn_{0.6})O_2$. (c) Schematic illustrations for the structural changes during sodiation/desodiation of partially dehydrated Na-birnessite material. Reproduced from Refs.[182,183] With permission of NPG.

Contrariwise, the presence of heterogeneous atoms in alkali-ion channel in layered materials can have positive aspects. For the $LiNiO_2$ layered system, the Ni^{2+} ion in the Li layer can be oxidized, and it causes local collapses of the structure.[177] This local collapse hinders the Li-ion diffusion in the Li layers and reinsertion of Li-ion into the six sites around the oxidized Ni ion in Li layers.[178,179] However, since cation disorder

can mitigate the electrostatic repulsion forces between the TM layer by occupying the Li sites, it can act as a pillar role in supporting the ion channel in between transition metal layers as well as preventing the additional migration of TM ions from TM layer to Li layer. Therefore, the introduction of an inactive ion, which can play a similar pillar role and prevent local collapse of Li slab, can provide beneficial effect on the migration of alkali-ions. For example, a Mg-substituted $LiNiO_2$ cathode material exhibits a higher reversible capacity than that of pure $LiNiO_2$ cathode, which is explained by the pillar effect of Mg^{2+} ions in Li layer owing to its size similarity to lithium and constant valence.[177] Similar effect can also be observed in other type cathodes. As an example, in the case of fluorophosphates ($Li_{1.1}Na_{0.4}VPO_{4.8}F_{0.7}$) cathode material, Park *et al.* suspected that a large size of Na^+ ion maintains a larger framework and it provides beneficial environment for Li-ion diffusion.[180]

Although the cation disorder in layered materials was considered as stationary or partially reversible, novel cases of overcoming the disadvantages of layered materials by controlling reversible cation disorders have been recently reported. In case of conventional O3-type Li-rich layered materials, it undergoes high-voltage anionic redox chemistry accompanying the voltage decay. The origin of this phenomena is regarded as the irreversible cation migration from the transition metal layer to vacant Li layer to form antisite cation-vacancy defect pairs,[181–183] that is thermodynamically favorable process during charging. To be more concrete, migrated transition metal ions from TM layer to adjacent tetrahedral site of the Li layer move permanently again to octahedral Li site. As migrated transition metal ion in tetrahedral site in the Li layer can also be considered as mobile ion which experience the electrostatic repulsion between transition metal layer, Eum et al. experimentally corroborated that O2-type $Li_{0.83}(Li_{0.1}Ni_{0.2}Mn_{0.6})O_2$ with ABCBA oxygen stacking can mitigate additional cation migration from the fact that TM ions in the LiO_6 octahedra are subject to strong electrostatic repulsion through the face-shared LiO_6 octahedra and TMO_6 octahedra.[184] Thereby, reversible TM ion migration to original TM layer during re-lithiation as well as prevention of the movement in the intra-layer of Li slab was observed resulting in enhanced electrochemical performances (Fig. 13a-b). Reversible inter-layer TM migration was also found in Na layered material in a similar way by controlling the migration barrier energy of Mn ions in Na-birnessite containing crystal water in the Na layer ($Na_xMnO_2{\cdot}yH_2O$). Exploiting the X-ray absorption spectroscopy with X-ray diffraction and first-principle calculations, Jo et al. reported that pristine sample, which shows the coexistence of spinel-like structure and layered structure due to the Mn migration into the Na layer, transforms to spinel-like phase and to layered structure during cycling reversibly (Fig. 13c).[185] The authors elucidated that the crystal water contents controlled through the dehydration process resulted in the reversible movement of Mn ions, resulting in the enhanced ion diffusion kinetics and improve its structural stability.

The cation disorder (so called antisite) critically detriments the Li-ion transport in olivine type cathode materials because the antisite blocks the 1D Li ion pathway. Therefore, it is vital to reduce the antisite defect in the olivine cathodes. The antisite defect can be reduced by the introduction of non-stoichiometric character in the olivine crystal structure. The antisite defect of the non-stoichiometric $LiFe_{0.5-x}Mn_{0.5-x}PO_{4-\sigma}$ material is reduced by half in comparison with that of stoichiometric $LiFe_{0.5}Mn_{0.5}PO_4$ material (*i.e.,* the values declined from 3.2 % to 1.6 %), showing better rate performance.[186]

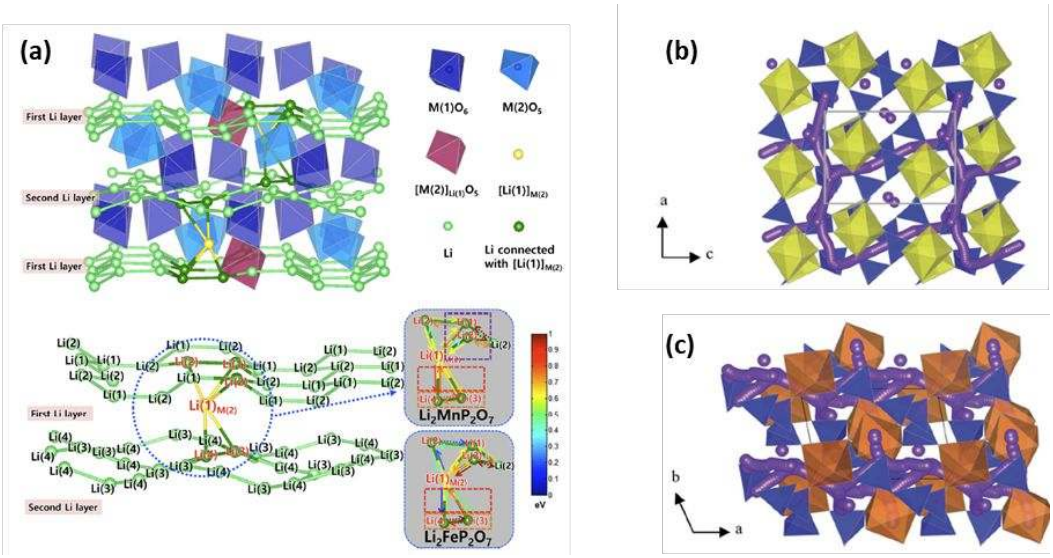

Fig. 14 (a) Structure and Li-ion network of $Li_2MP_2O_7$ with M(2)-Li(1) antisites. (b) Calculated paths for long-range Na^+ migration within $Na_2FeP_2O_7$ (c) $Na_2MnP_2O_7$ along the a-axis, b-axis and c-axis directions. Reproduced from Refs.[187, 188] With permission of ACS.

Contrary to this, the antisite defects sometimes can play a role in promoting alkali-ion diffusion by percolating the crossover pathway between the ion channels. For example, the $LiMnBO_3$ with a one-dimensional transport along the *c*-axis can be converted from one-dimensional to three dimensional Li conduction pathways when a considerable amount of antisite defects is present and the antisite defects act as bridging sites for crossover between different Li-ion channels.[189] For more specific, a partial Fe and Mg substitution to Mn increases the antisite disorder in $LiMBO_3$ (M = transition metal ions) crystal structure, enabling the material to have a cross-channel diffusion with a three-dimensional percolating pathway.[189] Likewise, the antisite defects in the pyrophosphate $Li_2MP_2O_7$ (M = Fe or Mn) crystal structure reduce activation barriers for Li hopping and creates a new path for Li-ion diffusion. Specifically, the defect site which is in between two Li layers is connected with all four Li sites which are in Li layers and it enables the material to have three-dimensional diffusion pathway in the structure (Fig. 14a). Thus, the increase in the antisite defect concentration can lead to the percolation of the diffusion channels, permitting better ionic conductivity than low defects crystal structure.[187] Similarly, in $Na_2MP_2O_7$ (M = Fe or Mn), the formation of antisite defects are favorable and the antisites lower migration energies along to the *a*, b, *c*-axes, making 3D Na^+ diffusion pathways (Fig. 14b-c).[188] Kang's group also discovered that Li-excess in the olivine $Li_{1+x}Fe_{1-x}PO_4$ creates extra Li in Fe sites but near-zero Fe in Li sites.[190] In such unique antisite configuration, the extra Li in Fe sites lowers the Li migration barrier to 0.82 eV along [101] direction, which is blocked for Li migration because of very high barrier (> 2 eV) in normal $LiFePO_4$. Therefore, the extra Li in Fe sites creates a new path for Li ion migration and makes 3D Li diffusion paths in $LiFePO_4$.

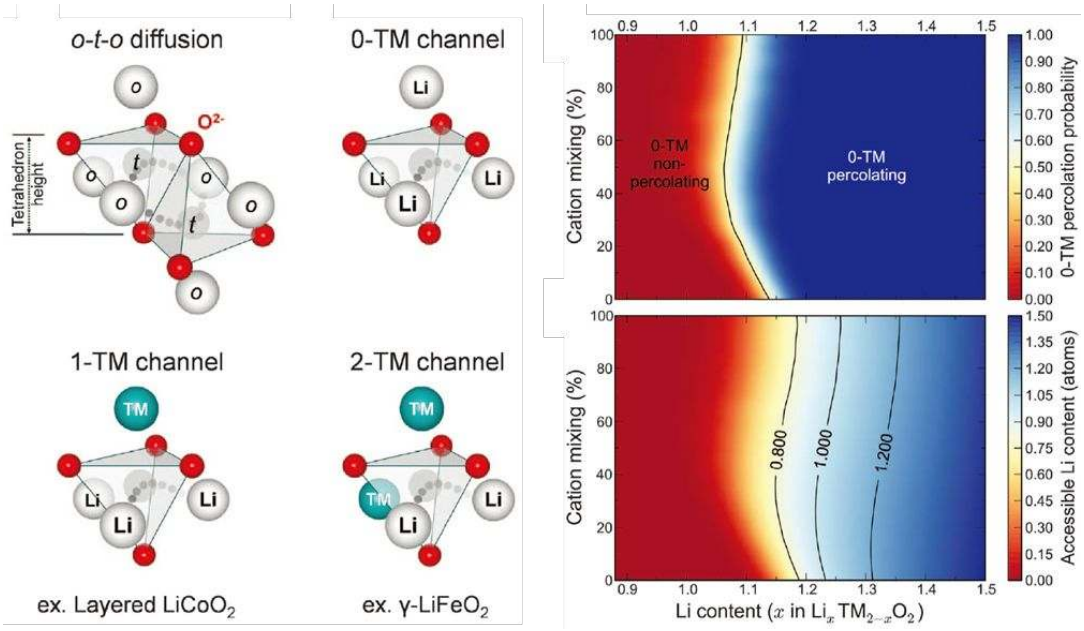

Fig. 15 Possible environments for an *o-t-o* hop (alkali-ion diffusion proceeds by hopping from one octahedral site to another octahedral site via an intermediate tetrahedral site) and the probability of finding a percolating network of 0-TM channels in the rock-salt oxides. Reproduced from Refs.[131] With permission of AAAS.

A recent study demonstrated that cation disordering can provide good alkali ion mobility when some requirements are met (i.e. Li-rich environment).[131] As discussed briefly in the crystal structure part, disordered structure can accommodate the alkali-ions reversibly during the electrochemical reaction. What makes it possible for this highly reversible insertion of alkali-ions is due to the presence of a 0-TM percolating network (Fig. 15).[131] The 0-TM channel signifies that there are no transition metal ions around the intermediate tetrahedral site which has four face-sharing octahedral sites. Thus, owing to no face-sharing transition metal ions, the migration barriers along 0-TM channel is lower than other channels such as 1-TM channel (typical layered structure, *e.g.,* $LiCoO_2$). More importantly, to enable facile macroscopic diffusion of alkali-ion, the 0-TM channels should be connected through the entire crystal structure continuously without loss in the connectivity by other 1-TM or 2-TM channel, and finally this is called the "a percolating network of 0-TM channels. In addition, the 0-TM channels must have locally alkali-ion rich environment, so the ratio of alkali-ion should be higher than that of transition metal ion (*e.g.,* $A_xM_{2-x}O_2$, x >1)

Effect of ionic radius, bonding and electron distribution

The ionic radius of cations (i.e., transition metal ions) and anions can have a significant effect on cycling stability and rate capability of the cathodes. In $Li_2Ru_{1-x}M_xO_3$ (M = Ti, Ru, Sn), when ionic radii of M increases in order of Ti^{4+} (0.60Å), Ru^{4+} (0.62Å), Sn^{4+} (0.69Å), cation (M) migration through an intermediate tetrahedral site is reduced. Because the voltage decay in this type of materials is an intrinsic property and is highly associated M trapping in the interstitial tetrahedral sites, the fastest voltage decay is observed for the smallest cation (Ti^{4+}) among the $Li_2Ru_{1-y}M_yO_3$ samples.[191]

Alkali-ion migration barriers in electrode materials can be considerably affected by anion species. For instance, in the layered structure materials, the Li migration barriers are significantly reduced when the anion is changed from oxygen ($LiCoO_2$ or $LiTiO_2$) to sulfur ($LiCoS_2$ or $LiTiS_2$). The underlying reason of the reduction in the activation barrier is a larger electron density of the sulfur ion, providing better screening effect which functions as a shield reducing the electrostatic interaction between a migrating alkali-ion and a transition metal ion.[168]

Bulk disorder

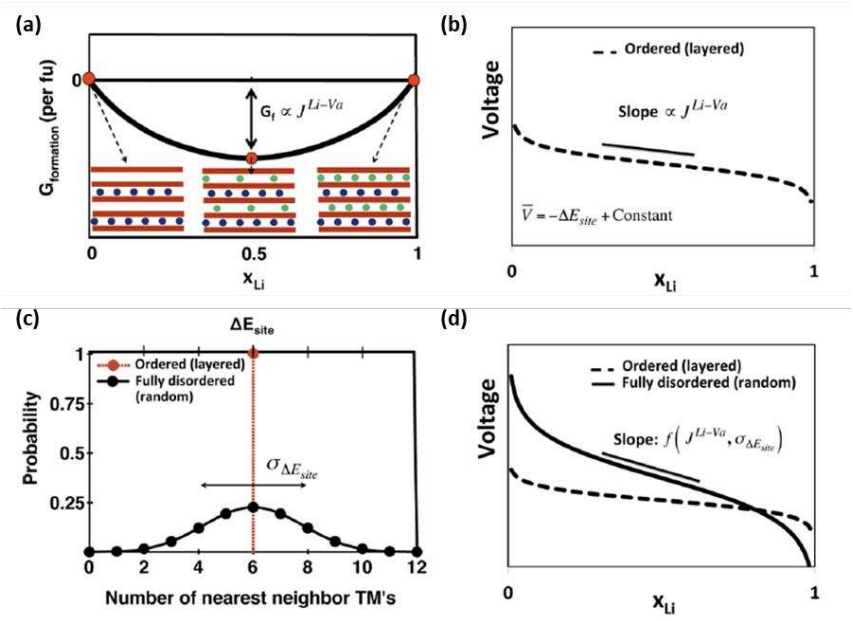

Fig. 16 Factors that contribute to the increase of the voltage slope upon cation disorder in lithium transition metal oxides. In ordered (*e.g.,* layered) compounds, (a) the effective lithium ion-vacancy (Li–Va) interaction (J^{Li-Va}) controls the change of energy with concentration, which in turn controls the voltage slope (b). In disordered compounds, (c) the statistical distribution of local environments around Li sites results in a statistical distribution of ΔE_{site}, and (d) both J^{Li-Va} and $\sigma_{\Delta Esite}$ (the standard deviation of ΔE_{site}) contribute to the voltage slope. Reproduced from Refs.[192] With permission of ACS

Cation disorder is one of the parameters governing the voltage profile of alkali-ion transition metal compounds.[193] In the ordered layered system (*e.g.,* $LiCoO_2$), the voltage profile is affected by the effective alkali ion-vacancy (j^{A-Va}) interaction which controls the energy changes with alkali ion concentration (Fig. 16a-b). However, in the case of disordered (*e.g.,* $Li_{1+x}M_{1-x}O_2$), there is statistical distribution of local environments around alkali-ion sites, so the ΔE_{site} is various according to the diverse local environments. Therefore, the voltage profile is influenced by two factors, both j^{A-Va} and $\sigma_{\Delta Esite}$. As a result, as shown in Fig. 16d, the voltage curve becomes more sloped in the disordered structure. Good examples are the disordered rock-salt structures.[125,194–198] In addition to the disorder effect, when the three out of four face-sharing Li-ions around 0-TM tetrahedral sites are extracted during de-insertion process from the disordered rock-salt structures, the remaining Li-ion can migrate into and occupy the tetrahedral site. In this case, a higher energy is needed to extract the Li-ion from the tetrahedral site, consequently it results in the voltage increase at around the end of charge.[192]

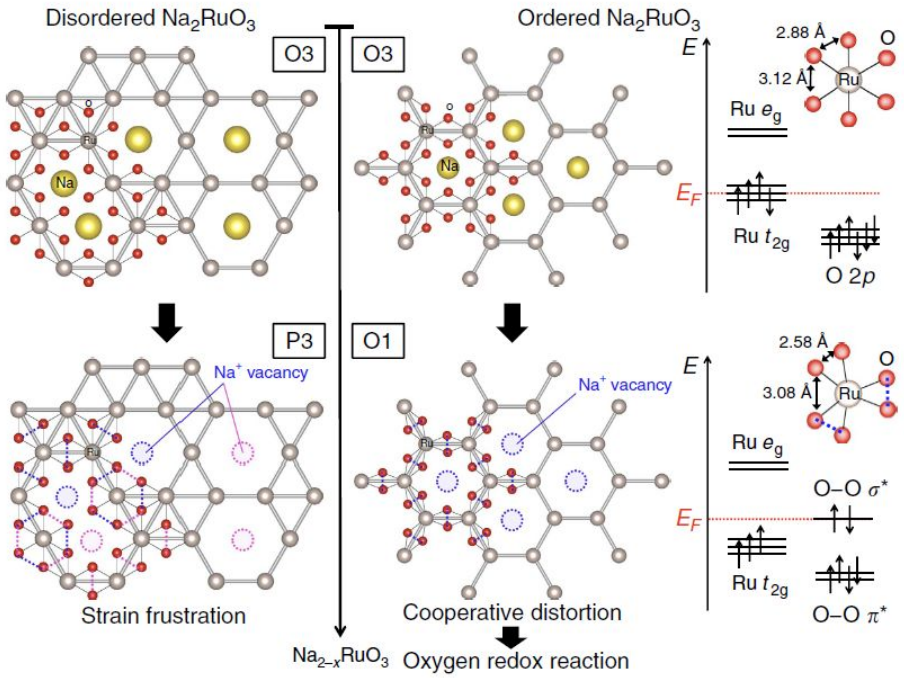

Fig. 17 Schematic representation of the structural changes during charge–discharge for disordered Na_2RuO_3 and ordered Na_2RuO_3. Ordered Na_2RuO_3 can distort cooperatively to raise the energy level of the antibonding s* orbital of the O–O bond, leading to the oxygen redox reaction. Disordered Na_1RuO_3 cannot accommodate the RuO_6 distortion due to strain frustration, which prevents the oxygen redox reaction. Reproduced from Refs.[199] With permission of NPG.

In Na_2MO_3, there is a structural disorder in a transition metal slab unlike the disordered rock-salts where both alkali and transition metal ions are randomly distributed in the entire structure. For example, a Na_2RuO_3 material can have two crystal structures like ordered and disordered Na_2RuO_3 depending on synthesis conditions.[200,201] In the ordered Na_2RuO_3 structure, the configuration of alkali- and transition metal ions in the $Na_{1/3}Ru_{2/3}O_2$ slabs exhibits a honeycomb ordering. In contrast, the disordered Na_2RuO_3 structure shows that both two cations are randomly distributed in the $Na_{1/3}Ru_{2/3}O_2$ slabs. Compared with the disordered structure, the ordered Na_2RuO_3 can deliver a higher capacity because the ordered intermediate of $NaRuO_3$ phase can accommodate the distortion of the RuO_6 octahedrons cooperatively that causes the reorganization of frontier orbitals triggering the anionic redox reaction. However, this reaction is impossible in the case of the disordered intermediate of $NaRuO_3$ phase owing to a strain frustration (Fig. 17).[199] For the distribution of transition metal ions in the framework, the cation ordered ($P4_332$) and disordered ($Fd3m$) spinel phases can be one of the examples. The disordered spinel exhibits higher electronic conductivity and better rate capability than the ordered one, which is due to the presence of Mn^{3+} ions that is without in the ordered structure.[202]

Generally, a high rate cycling leads to a reduction of capacity compared to a low rate cycling. However, the opposite phenomenon can happen when the crystal structure has a property that is prone to become a cation disordered state. For instance, the $Li_{1.15}Ni_{0.47}Sb_{0.38}O_2$ shows higher discharge capacities at faster rates, which is attributable to Ni migration into Li sites. At low rate, there is enough time for the Ni ions to migrate into other sites such as a contiguous tetrahedral site or octahedral sites in the Li layer. On the contrary, a rapid de-insertion at high rate causes the oxidation of Ni ions from Ni^{2+} to Ni^{3+} before they migrate to Li sites, and therefore a lot of Ni ions remain in their place where they are located in octahedral sites in the transition metal layer. Thus, Li-ions can move faster during high rate cycling than at lower current rates.[198] In many cases, transition metal migration into alkali-ion layer is harmful for alkali ion migration and electrochemical performance,

but in some cases, it is helpful in some aspects. For example, molybdenum migration into Li layer can reduce the *c*-axis expansion range in the early charge stage and suppress the collapse of structure at high charge state in the Li_2MoO_3 layered compound.[203]

Anion disorder

The concept of "disorder" is not confined to the cations only. The disorder on the anion sublattice can be created by an aliovalent anion doping.[204] For the $Na_xV_2(PO_4)_2O_{2y}F_{3-2y}$ compounds, the reversible capacity can increase by introducing disorder on the anion sublattice which interrupts the Na-vacancy ordering and thereby lowering Na migration barrier and polarization.[106] In the case of $KVPO_{4+x}F_{1-x}$ compounds, the oxygenated $KVPO_{4.36}F_{0.64}$ has various local coordination compared to the $KVPO_4F$. For example, the K and V sites of oxygenated $KVPO_{4.36}F_{0.64}$ have three and four different local coordination, respectively as follows: one KO_7F_2, one KO_8F, and one KO_9 for 9-coordinate K sites and two VO_4F_2, one VO_5F, and one VO_6 for four octahedral V sites. Contrariwise, the K and V sites of $KVPO_4F$ have two different local coordination, respectively as follows: KO_7F_2 for K sites and VO_4F_2 for V sites. In this case, the locally disordered fluorine-oxygen anion distribution allows the K sites have different energies, reducing the K-vacancy ordering. As the result, the anion disordered $KVPOF_4$ structure exhibits a smooth voltage profile and better rate capability.[51,52] In a broad sense, the fluorination in disordered rock-salt materials can be regarded as the introduction of disorder in the anion lattice. When the oxygen ion is replaced by fluorine ion in locally Li-rich environment within the disordered rock-salt oxides matrix, the capacity and cyclability can be improved.[205–208] For example, the Li percolation is restored and enhanced as the amount of F ion is increased in the $Li_xMn_{2-x}O_{2-y}F_y$ disordered rock-salt system, affecting the Li-ion transport properties of the material.[209] In addition, the fluorination leads to the increase in the ratio of low-valent transition metal ions functioning as an electron source. This enables the fluorinated disordered rock-salt materials to have increased transition metal redox capacity without a restriction of Li excess condition which is essential for the bulk Li percolation, reducing the dependence on O ion redox. Thus, the capacity and cycle life can be improved.[210]

2.2.3. Phase transition

During the electrochemical reactions, the alkali-ions are going in and out of the host crystal structure incessantly, and it gives an impetus for the host structure to change lattice parameters or trigger off phase transition reactions. The phase transition can be divided into two meaningful segments, one is an event that a system follows a desirable reaction route without destructive crystal structure change (*i.e.* reversible phase transition) and the other one is a phase transition correlated with a degradation of crystal structure that results in a capacity loss (*i.e.* irreversible phase transition). In the former case, single or multiple phase transition will be emerged as a major interest, while, in the latter case, issues about a deteriorative transformation from an original crystal structure to an impaired state that cannot carry out a normal electrochemical performance will be discussed.

Reversible phase transition

Reversible phase transition in crystalline implies recovery of the phase upon cycling. The word "reversible" feels like that it is unlikely to have any impact on structure, but in fact repetition of phase transition can affect to its particle as a form of stress. In case of layered $LiNiO_2$ cathode materials, it undergoes multiple reversible phase transition[172,211] during charge and discharge consisting of three hexagonal phase(H1, H2, H3) and a monoclinic phase (M) in the voltage range from 2.5 to 4.2 V. Although there is a controversial question[212] whether hexagonal phase changes to monoclinic phase, it is conceded that generic phase transition occurs from the original layered hexagonal structure (H1) to other layered hexagonal phases (H2, H3) in common. While the H2 phase emerges without significant lattice parameter difference compared with H1 phase, the H3 phase that appears above 4.2V does not. It maintains the O3 structural type but, locally complete deinsertion of the Li from the inter-slab space induces the formation of O1 stacking faults by gliding of the $[MO_2]$ slab due to weak binding of Van der Waals.[213] This results in anisotropic lattice variation especially along the *c*-axis with highly reduced value. The lattice mismatch between different phases

induces internal strain with large volume change, and therefore repeated cycling causes structural damage as a form of micro-cracks in particles.[214]

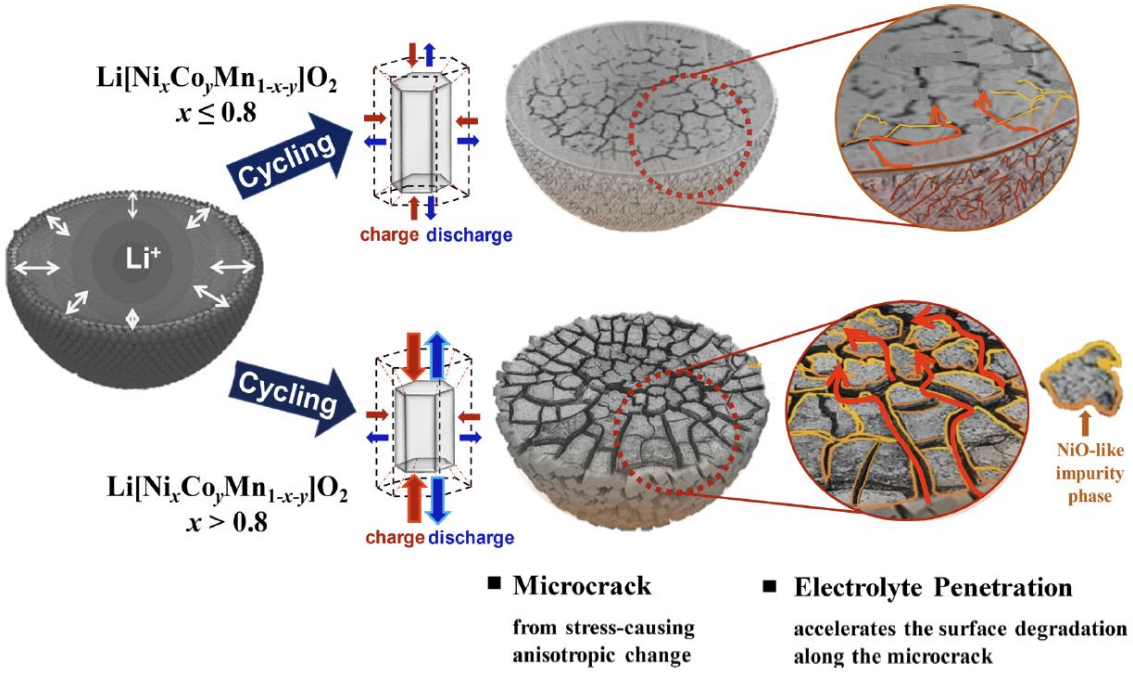

Fig. 18 Capacity fading scheme of Ni-rich $Li[Ni_xCo_yMn_{1-x-y}]O_2$ cathodes. Reproduced from Refs.[215] With permission of ACS.

In Ni-Co-Mn three component layered system, the material resembles the properties of $LiNiO_2$ as the portion of the nickel content increases so that Ni-rich cathode materials which contain more than 80% of nickel in transition metal layer also exhibit H2 to H3 phase transition at high state-of-charge. Although the voltage at which phase transition occurs is different, these materials also create harsh environment in particle which leads the particle to crack (Fig. 18).[215] This consequence makes the loss of contact among primary or secondary particles and provides new electrolyte penetration channel which can cause additional side reaction (*i.e.,* electrolyte decomposition and solid-electrolyte interphase formation).

Depending on the stacked arrangement of the oxygen atom layers, alkali-ions can occupy prismatic (P) or octahedral (O) sites.[216] Unlike Li compounds, where alkali-ions occupy octahedral or tetrahedral sites, Na compounds shows P- or O-type layered structure to accommodate the large size of alkali-ion compared with Li-ions as elucidated in chapter 2.1. Since both octahedral and prismatic site are energetically stable for Na-ion, Na transition metal oxides (Na_xMO_2) have various oxygen layer stacking sequences depending on the contents of Na ions due to Na-vacancy ordering caused by the strong Na-Na interactions.[217] For example, Lu *et al.* reported that P2-type $Na_{2/3}[Ni_{1/3}Mn_{2/3}]O_2$ shows a reversible phase transition from P2-type to O2-type in the voltage range from 2.0 - 4.4 V by XRD analysis.[218] $Na_x[Ni_{1/3}Mn_{2/3}]O_2$ remains the P2-type structure upon charging to 4.15 V which corresponds to x = 1/3, but after that two phase reaction occurs by forming a O2-type structure with a large plateau at 4.2 V. And finally it changes to a single phase O2-type structure at the end of charge, and reversibly come back at the following discharge. Since phase transition from P2 to O2-structure and vice versa requires the slab gliding of $[MO_2]$ slab, the content of Na-ions in the structure is a determining factor of the presence of this phenomenon. When the amount of Na-ions in the $Na_x[Ni_{1/3}Mn_{2/3}]O_2$ is less than 1/3, there exists enough repulsion between oxygen to oxygen, so that favorable environment are formed to introduce O2-type stacking faults by gliding of oxygen layer in the structure. Since neighboring oxygen planes are closely packed in O2-type structure, drastically decreased '*c*' lattice parameter (~20 %) is obtained in the structure compared with P2-type structure when the

remaining contents of Na-ions is less than 1/3 which corresponds to a long plateau at 4.2 V.[218] A large anisotropic lattice variation in this region severely affects to cyclability like above $LiNiO_2$ or high nickel NCM materials by inducing large volume change and strains. Within the voltage range which suffers from such a large lattice misfit (2.3 - 4.5 V), micro-cracks are present after 100 cycles at a C/20 rate, and the electrochemical cell test shows a very low cyclability (64 % of capacity retention compared with 1st discharge capacity after 10 cycles) even at the very slow rate of cycling (C/100).[169,219]

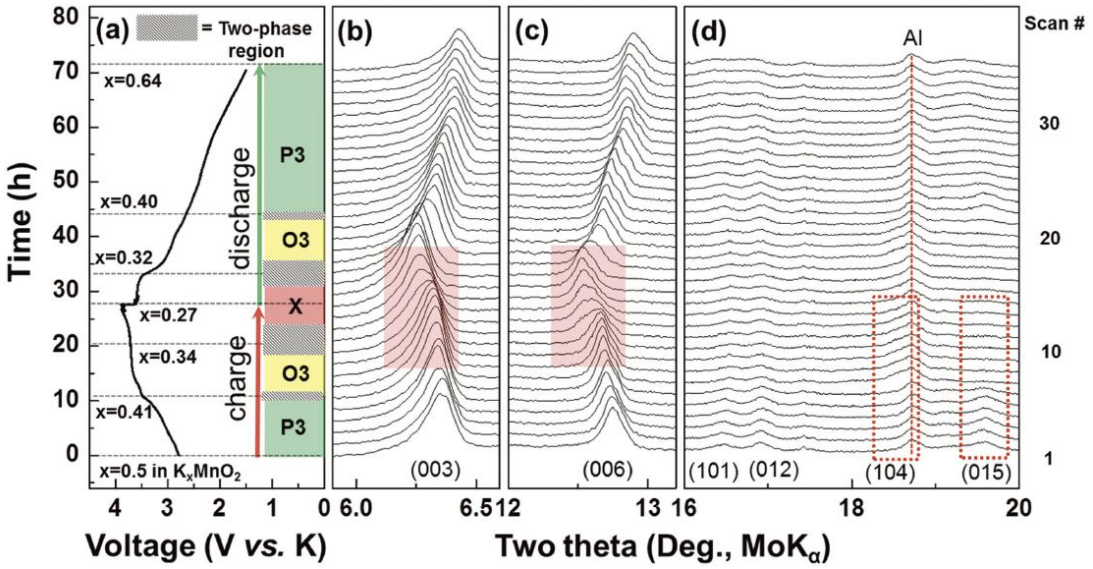

Fig. 19 Structural changes of P3-$K_{0.5}MnO_2$ during charge and discharge. (a) Typical charge/discharge profiles of P3-type $K_{0.5}MnO_2$ at a current rate of 2 mA g−1. (b–d) In situ XRD pattern taken for 2 h scanning rate per pattern. Reproduced from Refs.[31] With permission of Wiley.

Although few papers have reported as a cathode material for K-ion batteries, some electrochemical K-ion insertion host materials are recently being published due to the cost issue and similarity with Na-ion batteries.[27,220–223] Due to the larger ionic radii than Li-ion, K-ion layered materials have a crystal structure similar to Na transition metal compounds so that it also shows P- or O-type layered structure. Vaalma *et al.* showed the reasonable electrochemical performance of the P2-type $K_{0.3}MnO_2$, but it suffers low cyclability when it experiences low K content,[220] which can be speculated from the results of large volume change and layer gliding as like mentioned above Na-layered oxide. However, no direct evidence showing the structural evolution of the P2-$K_{0.3}MnO_2$ was suggested by Vaalma *et al*. In P3-K_xMnO_2 system, Kim *et al.* observed multiple phase transition and peak broadening, which is likely attributable to stacking disorder along the *c*-axis at the top of charge ($x < 0.27$ in K_xMnO_2) as shown in Fig. 19.[31] Such phase transition and stacking disorder may result in a poor cyclability of K_xMnO_2. Until now, various papers have reported that local lattice mismatch with large volume change in the structure causes internal/intergranular strains and crack formation by showing direct observation such as SEM, TEM, *etc* in Li layered compounds. Although Na- and K-ion compounds are relatively lacking in these visualizing studies so that additional experiments are likely to be necessary based on degraded Na-, K-ion compounds, it is clear that lattice mismatch in crystal structure leads to capacity loss and reduced cycle life.

Compared with layered structure materials of which lattice parameters vary anisotropically during the cycling as mentioned above, cathode materials which have a rigid host structures do not suffer the harsh environmental condition during cycling. One such representative cathode material is $LiFePO_4$ which have an olivine structure consisting of corner-shared FeO_6 octahedra and edge-shared LiO_6 octahedra interconnected by PO_4 tetrahedra. During charge and discharge, two phase reaction occurs in which charged ($FePO_4$) and discharged ($LiFePO_4$)

phase coexist, resulting in a plateau on the voltage profile at 3.4 V. Both $LiFePO_4$ and $FePO_4$ have the same olivine framework with slightly varied lattice parameters and a reduced (~6.8 %) unit cell volumes. By virtue of highly stable framework, excellent cyclability over thousands cycles can be obtained.[224]

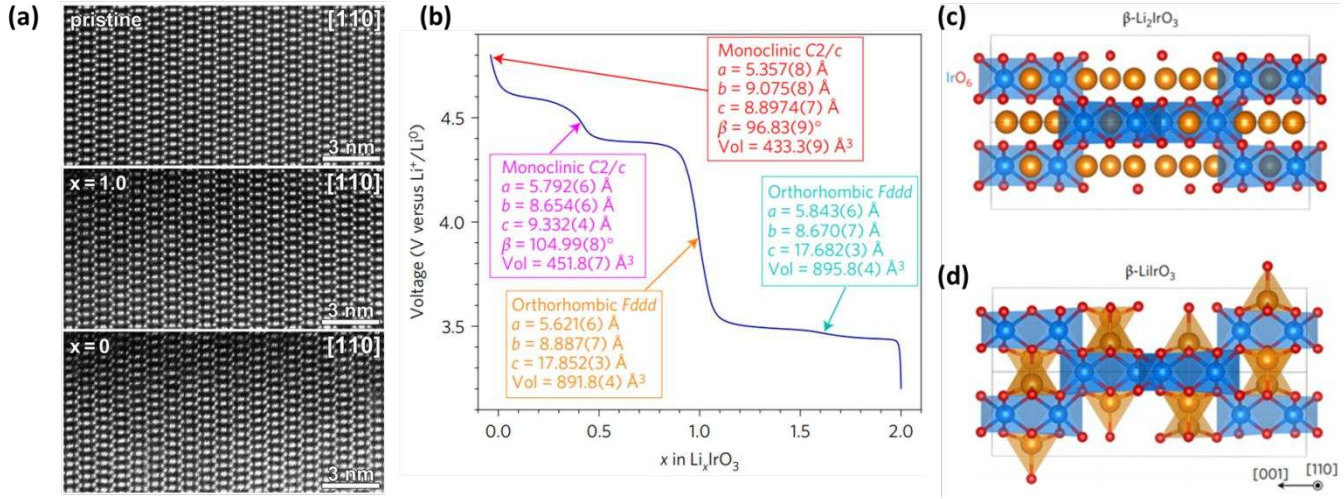

Fig. 20 (a) HAADF-STEM images of the β-Li_xIrO_3 at different states of charge. The arrangement of the Ir atoms in the structure is preserved even at x=0. (b) Charging voltage profile of β-Li_2IrO_3 with refinement result of the intermediate phases. Structures for (c) the β-Li_2IrO_3 structure and (d) the 4 V-charged β-$LiIrO_3$. For the structural models, Li is orange, Ir is blue, O is red. Note that Li is in octahedral position in β-Li_2IrO_3 and in tetrahedral positions in 4V-charged β-$LiIrO_3$. Reproduced from Refs.[167] With permission of NPG.

There are a few such kind of materials which do not change structure whether mobile ions exist or not due to the rigid host structure. β-Li_2IrO_3 which is a polymorph of a α-Li_2IrO_3 as already explained above chapter 2.2.1 (polymorph in crystal structure type) is another example of not undergoing significant changes in lattice upon (de)insertion of Li-ion. Unlike the α-Li_2IrO_3, which has a 2D-layered structure, β-Li_2IrO_3 has a highly stable hyperhoneycomb framework (IrO_3) of which structure has rigid 3D network. Therefore, its structure is maintained even when all mobile ions are extracted as can be identified by HAADF-STEM as shown in Fig. 20a, while showing neither cation migration nor plane gliding which are usually observed in layered material.[167] Given the four plateaus in the voltage profile, various phase transitions can be inferred, and each phase was identified by *in situ* XRD and Rietveld refinement analysis (Fig. 20b). XRD analysis demonstrates that when more than 1 mol of Li is extracted, *Fddd* orthorhombic (Fig. 20c,d) transforms to *C*2/*c* monoclinic (Fig. 20b) due to the distortions of the edge-sharing IrO_6 octahedrons. But, when comparing the unit cell by transforming orthorhombic to monoclinic unit cell, the lattice parameter difference is small and volume change is less than 3% upon charging to 4.8V. Therefore, overall structure is maintained due to the structural stability of the 3D structure with a little lattice and volume change, and exhibits high capacity retention compared with α-Li_2IrO_3 and rate capability (80% of the theoretical capacity at 4C) despite some existence of internal shear stress caused by monoclinic distortion during (de)insertion.

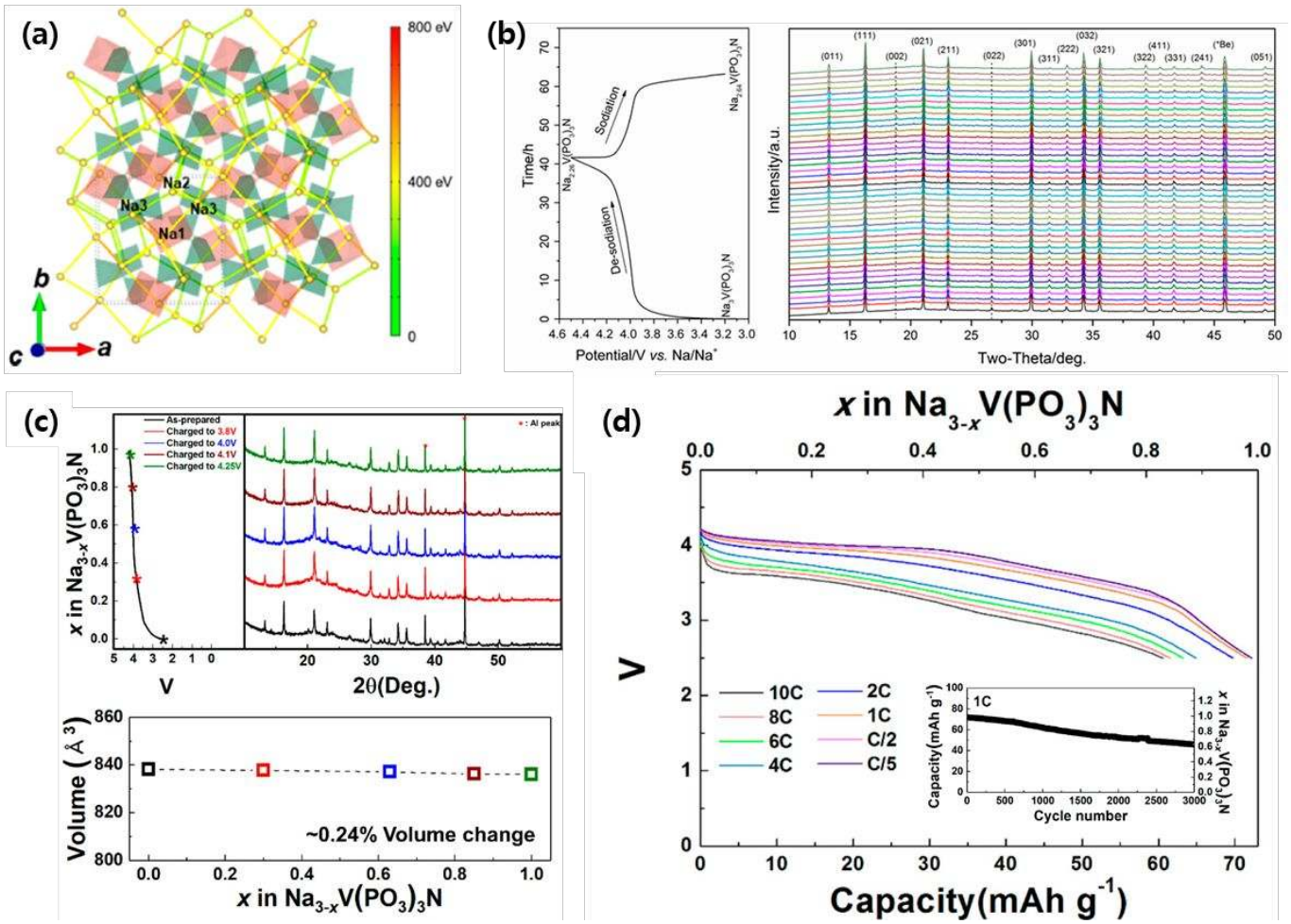

Fig. 21 (a) Illustration of the three-dimensional Na-ion diffusion pathways in $Na_3V(PO_3)_3N$. Note that the Na1−Na2 pathways are excluded in this figure because of their high activation barriers (~800 eV). (b) Voltage profile and in situ XRD patterns of $Na_3V(PO_3)_3N$ during the first cycle. (c) Ex situ XRD patterns and volume changes of $Na_{3-x}V(PO_3)_3N$ ($0 \leq x \leq 1$). (d) Electrochemical performances of various discharge capacities of $Na_3V(PO_3)_3N$ at different current rates (C/5, C/2, 1C, 2C, 4C, 6C, 8C, and 10C in the 2.5−4.25 V window, 1C = 73 mAh g^{-1}). Inset graph is cyclability test result at 1C during 3000 cycles. Reproduced from Refs. [225, 226] With permission of ACS and MDPI.

The fact that highly stable host structure would have high capacity retention during cycling can be also applied to Na compounds as well as Li compounds. $Na_3V(PO_3)_3N$ which have a cubic unit cell with composed of VO_6 tetrahedrons and PO_3N tetrahedrons[226] is a one of another examples that maintains the host structure during cycling. Among three distinct Na sites in this structure, only limited certain Na-ions are preferably mobile by attributed to the difference in site energies.[225,227] In this structure, Na-ions migrate via 3D ion channels for (de)insertion. While the authors speculated a two phase reaction between Na-rich and Na-poor from the plateau in electrochemical profile and *in-situ* XRD, they never distinguish the two phases in the XRD, which might come from a negligible change of peak position and intensity during cycling (Fig. 21a,b).[226] According to Kim *et al.*, the $Na_{3-x}V(PO_3)_3N$ ($0 \leq x \leq 1$) electrode shows very negligible volumetric change (~0.24 %) with 1.0 mol equivalents of Na (Fig. 21c).[225] They attributed remarkable power capability (~84 % of the theoretical capacity at 10C) and highly reversible capacity retention (maintained for the first 500 cycles without degradation and ~67 % of the initial capacity after 3000 cycles at the current condition of 1C) as shown in Fig. 21d to the 3D ion channels and negligible lattice variation of cubic unit cell.[225]

Reversible phase transition reaction is inherent property of the material system as alkali-ions are (de)inserted. One of major factors in which reversible phase variation affects the structure stability is coherency between phase boundaries that accommodate the misfit of the lattices. Therefore, cyclability is highly correlated with a factor influenced by the alignment between long-term repeated lattices within a material where reversible phase transitions occur. However, irreversible phase transition is a direct factor that prevents the alkali ion accessibility, and it could occur both in bulk and on surface.

Irreversible phase transition

Like the negative electrode materials which lose crystallinity and become amorphous due to conversion or alloying reaction, an irreversible phase transition of the material in the bulk can occur for insertion cathode materials if certain unstable and harsh conditions exist. One example that shows irreversible phase transition in the cathode is *Immm*-Li_2NiO_2, in which Li and Ni occupies the center of the tetrahedral site and rectangle site respectively between oxygen layers. In more specifically, during the 1st de-insertion of Li-ion, the bulk crystalline structure collapses and transforms into a layered *R*-3*m* with some degree of amorphization or very small crystallite size accompanying the oxygen evolution. Consequently, it never recovered again because NiO6 octahedrons in the layered structure is more stable thermodynamic state than NiO4 square plane in the pristine state.[228,229] That is, the changed stable state cannot accommodate mobile ions as in the original state. These irreversible phase transition in the bulk comes from the intrinsic property tending to be an energetically favorable state from original metastable state. Layered transition metal oxides also experience the irreversible phase transition when the material suffers from repeated cycling or at highly charged states. LiMnO2 layered material is a good example for the former one. In the layered $LiMnO_2$, the capacity decays during initial few cycles because of the transformation into the spinel-like phase at the surface.[230–232] Irreversible phase transition in the bulk is more common for layered materials which have relatively large possibility of slab gliding owing to intrinsic property (e.g. Na compounds[233]) or almost complete de-insertion process (e.g. typical $LiCoO_2$[234–236]). The irreversible phase transition may result in collapse of the structure and formation of the defects at the boundaries between the various domains, and therefore, it remains as a challenge. This fact reiterates the importance of the stable and rigid host structure with or without mobile ions as like polyanion materials.

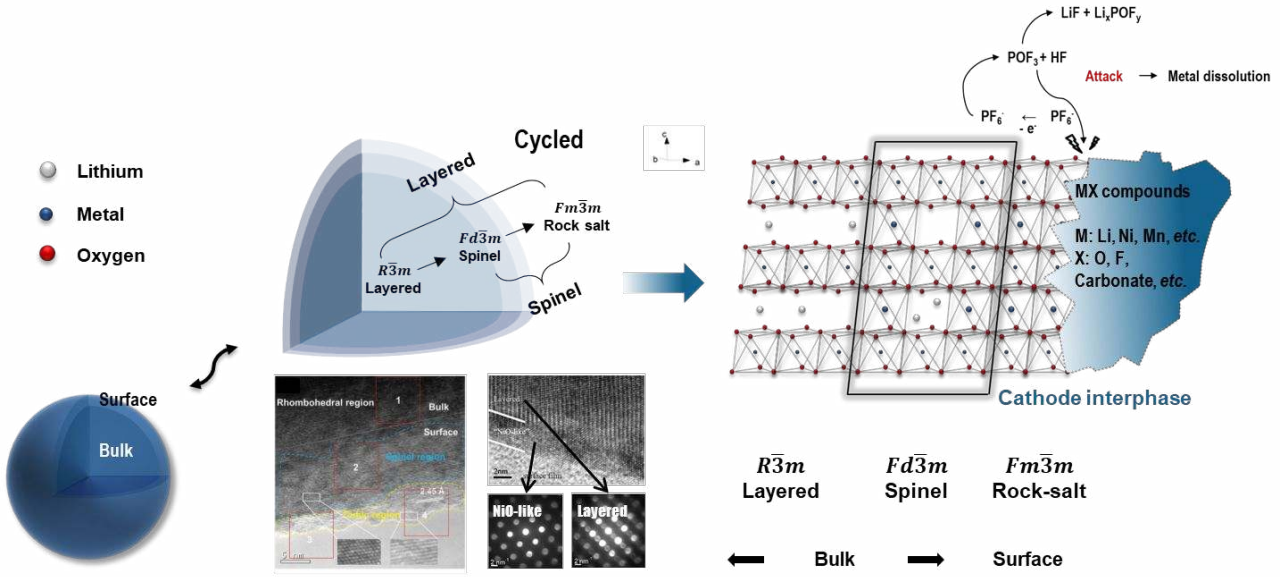

Fig. 22 Schematic illustration of degradation mechanism and factors for cathode materials. The crystal structure of high energy cathode materials can be degraded by cation migration, oxygen loss, metal dissolution etc. Reproduced from Refs.[9] With permission of Wiley.

However, irreversible phase transition on the surface can be affected by the extrinsic factors such as cutoff condition, cycle rate, operation

temperature condition or redox reaction with electrolyte, all of which are highly correlated and usually observed for the layered material. A main cause of surface phase transition is a cation migration as described in ion channel & disorder part at chapter 2.2.2. Migrating transition metal ion toward the mobile ion layer causes the irreversible structural transition with the concomitant formation of a layered to spinel and/or rock-salt phase in many cases.[237–239] This phenomenon is governed by the amount of empty alkali-ion site[240] because of the nature of vacancies promoting ion diffusion. Ni-rich layered materials ($LiNi_{1-x-y}Co_xMn_yO_2$) are representative examples of showing such a phenomenological result. The more Li-ions are extracted to the high state-of-charge, the more irreversible surface phase transition occurs from layered to spinel, and then to rock-salt phase (Fig. 22).[241,242] This was also confirmed through the different cycling rate experiment which induces varied amount of available vacancies. When layered materials are cycled for 200 cycles with different rates; one of which is slow cycling rate that enables the mobile ions thoroughly and highly reversibly to be (de)inserted and the other is fast cycling rates that impedes the full extraction of mobile ions leaving a Li residue in the structure; former and latter ones showed a structure evolution of the disordered rock-salt phase and spinel phase on the surface, respectively.[243] Actually, it is not only the structural reason (the vacancy of mobile ions around the transition metal) that causes surface structure transitions, but also result from the other chemical reactions. When transition metal orbital (*e.g.* $Co^{3+/4+}$ t_{2g} or $Ni^{3+/4+}$ e_g orbital) substantially overlaps the oxygen 2*p* orbital, which is when transition metal ions are in a highly oxidative environment, oxygen evolution could occur by redox reaction with transition metal ions, and then surface reconstruction occurs.[244] Since these reactions are the consecutive events during cycling, reconstructed surface layers (spinel and/or rock-salt phase) propagates into bulk lattice and act as a directly disturbing factor for capacity retention and rate capability due to its insulating property and reduced active sites (Fig. 22).[245] Irreversible phase transition on the surface can be summarized to the nature of the structure itself to be stabilized as a result of countermeasures against external changes. Therefore, it is commonly happened to layered materials (*e.g.* Li-rich or Na- compounds) or its analogue (*e.g.* spinel compound) and it is difficult to mitigate such irreversible phase transitions.

Strategies

It is obvious that phase transition of the material (in)directly affects to battery performance. Stable cycling life cannot be expected when there is irreversible phase transition or reversible phase transition with large lattice differences between phases. Hence, various strategies are commonly used to prevent or alleviate the phase transition by controlling the cell operating condition, by changing the composition of the cathode materials, or by coating.

Controlling cutoff condition is an easy way to achieve high capacity retention. Reducing the charging cutoff voltage can prevent all the undesirable circumstances from the structural collapse or side reactions, except at the high cycling rate condition which can trigger inhomogeneous reaction among particles resulting in partially overcharged state.[246] However, since high capacity retention is obtained by sacrificing capacity in the cutoff control case, common strategies are changing the inner or outer chemistry. By small amount of Co substitution to $LiMn_{1.5}Ni_{0.5}O_4$, $LiMn_{1.42}Ni_{0.42}Co_{0.16}O_4$ material exhibits enhanced cyclability and rate capacity as a result of reducing lattice parameter changes among the three different cubic phases.[247] According to Cho *et al.*'s argument, introducing nickel element (10%) in a Li layer as a screening ion between oxygen layer in $LiCoO_2$ alleviates the phase transition to O1 stacking, so that more capacity can be achieved.[248] Yang *et al.* claimed that low content of Li_2MnO_3 embedded in Ni-rich layered $LiNi_{0.8}Co_{0.1}Mn_{0.1}O_2$ suppresses the formation of H3 phase and thus enables the high voltage cycling resulting in high capacity retention without large lattice misfit in the structure.[249] Such kind of compositional changing method by doping of element or another material in the structure to suppress the transition and behave like solid solution by lowering the symmetry of the crystal is effectively now being progressed.[186,250–252] Outer chemistry which corresponds to coating method that is related with surface chemistry will be covered in chapter 2.3.1.

2.3. Crystallographic to microscopic scale

Particle size level based approaches ranging from crystallographic to microscopic scale enable to a more detailed understanding of the intrinsic/extrinsic factors affecting the reaction mechanisms and the electrochemical performance. In other words, multiscale approaches from crystal to particle scales will help to confer additional or complementary functions to the target materials for enhancing the electrochemical performance besides their intrinsic properties that originate from the factors between the atomic to crystal levels (Fig. 23).

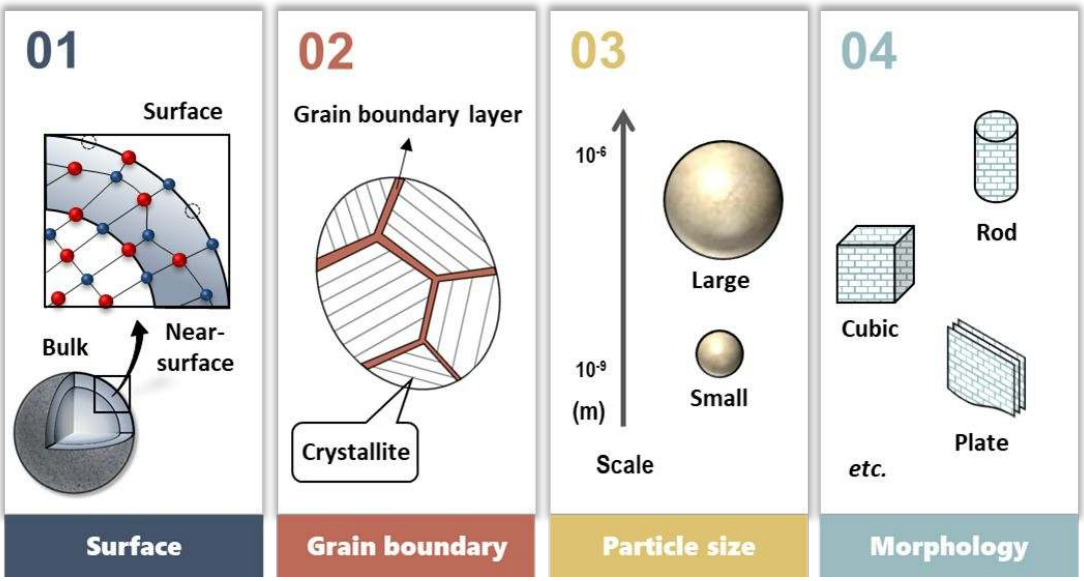

Fig. 23 Factors affecting battery performances range from crystallographic to microscopic scale.

2.3.1. Surface

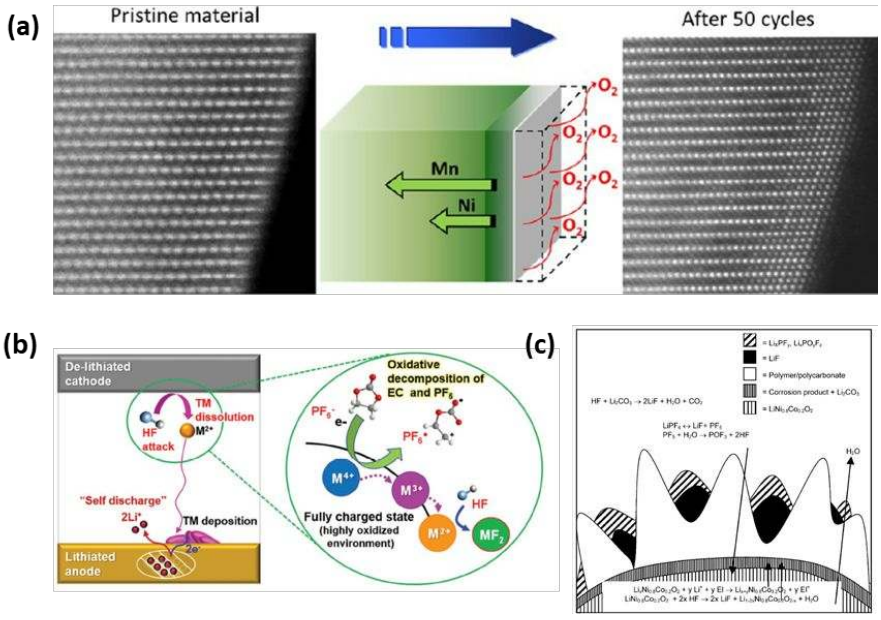

Fig. 24 (a) High-resolution STEM-HAADF images of pristine and cycled layered material.[237] Surface modification occurs through the migration of transition metal concomitant with oxygen evolution. Schematic illustration of (b) transition metal dissolution and side reactions[253] at high

voltage as well as forming (c) resistive CEI layer.[254] Reproduced from Refs.[237, 253, 254] with permission of ACS, Wiley, and Elsevier.

Surface chemistries between electrode and electrolyte are paramount issues for enhancing the performance of batteries. Although the bulk material exhibits a stable reaction during cycling, undesired side reactions at the surface highly hinder the battery performance: capacity, cyclability, rate capability as well as safety of the batteries. Knowing the interfacial reactions and their characteristics can play a crucial role in establishing effective strategies to improve the functionality of the surface layers, however, a full understanding of them has not been achieved due to the complexity of such reactions. Generally known surface chemical phenomena are surface reconstruction of the cathode, transition metal dissolution from the cathode, and cathode-electrolyte interphase (CEI) layer formation, all of which are highly correlated and continuously get worse over repeated cycles (Fig. 24). Surface reconstruction problem is in line with irreversible phase transition at the surface for usually layered materials and its analogue as already described in chapter 2.2.3. Its main root cause is the migration of transition metal ions for the thermodynamically stable state and oxygen evolution from the lattices and redox reaction with electrolyte at the highly charged state (Fig. 24a). This newly formed resistive surface builds up polarization of the battery cells and causes loss of capacity retention and rate capability.[255]

Transition metal dissolution, usually occurring at cathode-electrolyte interface, is another critical issue deteriorating electrochemical performance of the cathode materials. Such transition metal dissolution is originated from the disproportionation reaction of the transition metal ions and/or highly oxidized environment where transition metal ions are leached by acidic species. Manganese-based cathode materials are prone to experience this phenomenon because the unstable Mn^{3+} ions easily generate Mn^{2+},[79] which is soluble in organic electrolyte by disproportionation reaction as covered in chapter 2.1.2. and/or by HF attack. For example, main degradation mechanisms for lithium manganese oxides ($LiMn_2O_4$) with spinel structure[256] contains not only structural variation because of Jahn-Teller distortion, but also dissolution of divalent manganese ion in the electrolyte. High voltage spinel $LiNi_{0.5}Mn_{1.5}O_4$, improved from the $LiMn_2O_4$ through partial substitution of Mn with Ni, also suffers from Mn^{2+} dissolution even at charge state.[257] Also, the voltage fading, capacity degradation, and low rate capability of Li-rich and Mn-rich materials are attributable to the Mn ion dissolution issue at least some part. From the scanning transmission electron microscopy (STEM) combined with electron energy loss spectroscopy (EELS) results, Zheng *et al.*[258] claimed that the degraded performance for long cycled (300 cycles) $Li_{1.2}Ni_{0.2}Mn_{0.6}O_2$ ($0.5Li_2MnO_3$–$0.5LiNi_{0.5}Mn_{0.5}O_2$) comes from structure deformation by forming a sponge-like structure on the surface with fragmented pieces, in which Mn^{2+} species is a main component due to the disproportionate reaction of Mn^{3+}. This reaction can be accelerated by attack of the acidic species, HF in the electrolyte, and other researchers[259–261] also adverted the problem of Mn dissolution in Li-rich NMC materials. Although dissolution of Mn^{2+} ion is dominant, other transition metal ions also can be dissolved[262,263] in layered materials. Transition metal ion dissolution is also a cause of performance degradation in other structure types[264–267] as well as layered structure materials,[262,263,268] where all of the reactions are accelerated under high temperature and/or high voltage condition.

The formation of solid-electrolyte interphase (SEI) layer is well known interfacial phenomenon at the anode because of its mostly inevitable spontaneous reaction environment, *i.e.,* higher lithiated anode energy than lowest unoccupied molecular orbital (LUMO) of electrolyte components, and the electrochemical voltage window of electrolyte is enlarged once proper SEI layers are formed.[244,269] Although irreversible SEI layer formation at the anode entails a noticeable capacity loss by forming inorganic/organic compounds at the initial few cycles, it has been treated as a necessary evil because of its not only passivating and repairing ability[270] but also unexpected additional capacity[271], so that relevant research largely have been focused on.[272–277] Similarly, delithiated cathode energy, which is lower than highest occupied molecular orbital (HOMO) of the electrolyte, induces further decomposition of the electrolytes forming CEI layer at the cathode. While it is vital to understand the nature of CEI formation, the reaction mechanisms are complex and the surface sensitive analyzing technologies including direct *in situ* analysis[278] are limited far behind the demand. Therefore, tailoring the exact formation mechanisms and properties of the CEI layer is in difficulty until now. Preliminary works[254,279] indicated that the formation of CEI layers depends on the materials, with different

layer thickness and various resulted products. According to the papers reported to date, it was revealed that main cause of different CEI layer formation at high voltage comes from the complexity of electrolyte decomposition reaction involved with surface reconstruction reaction and metal dissolution from the nucleophilic attack of the electrolytes. Side reactions such as oxygen evolution from the cathode also have a significant influence on the CEI layer.[280] More specifically, $LiPF_6$-containing carbonate-based electrolytes, which are most commonly used, undergoes decomposition reaction (*i.e.* dissociation into LiF and PF_5),[281] thereby form a reactive species such as POF_3 and HF by reacting with H_2O. These products can deteriorate the cell performance by inducing above mentioned surface reconstruction and metal dissolution as well as decomposition of the solvents.[282] Also residual Li compounds (*e.g.* LiOH, Li_2CO_3, Li_2O, *etc.*) on the surface of cathode promote the unwanted surface side reaction.[283] The exothermic reactions that cause oxygen generation from the lattice (*e.g.* surface reconstruction reaction of the Ni-rich or Li-rich materials) not only expedite the reactions but also cause additional side reactions by which active oxygen radicals (reduced oxygen) attack carbonated solvents in the electrolyte[284] resulting in formation of by-products such as Li_2CO_3 and various organic compounds.[253] These vicious and consecutive complex reactions form a resistive CEI layer containing various inorganic/organic compounds[255] on the surface during repeated cycling and make it hard to accurate analysis, and currently such reactions for the sodium compounds are barely understood.[285]

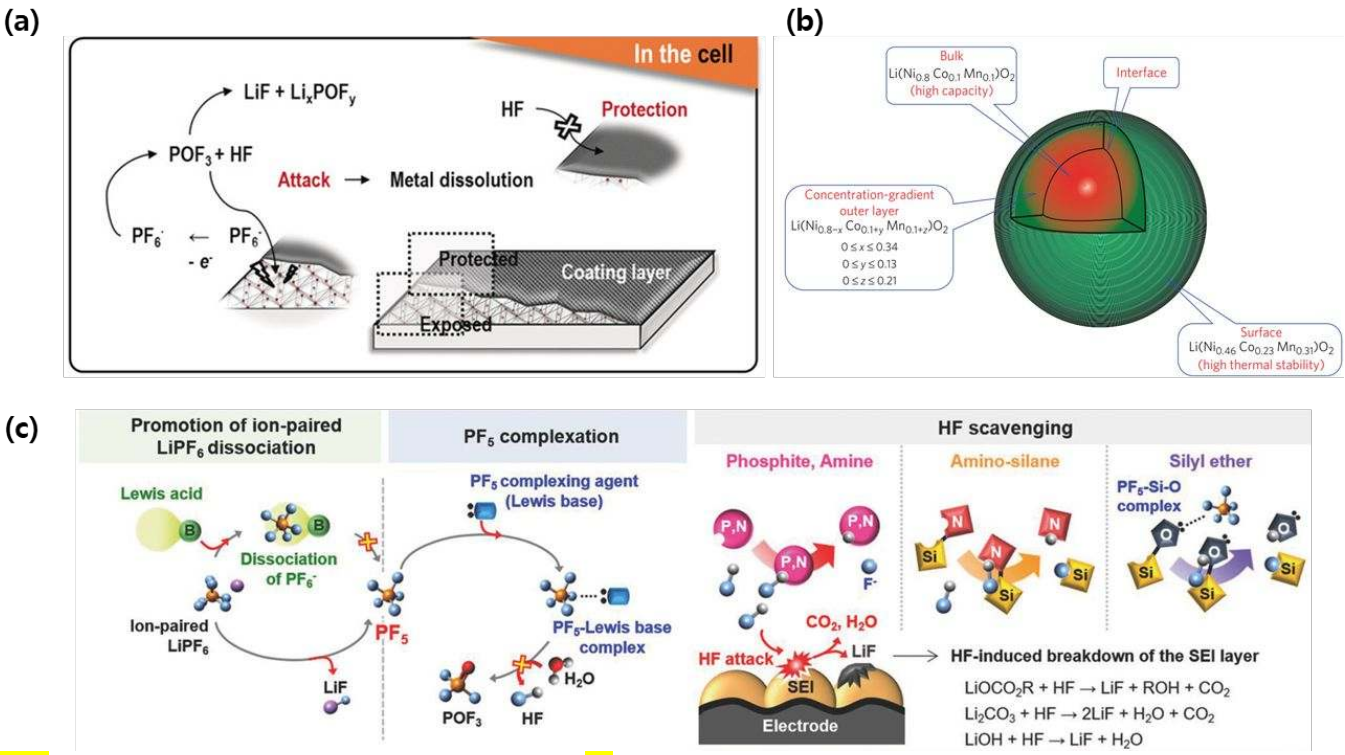

Fig. 25 Schematic illustration of (a) surface coating method,[9] (b) surface modification method by inducing deviation of composition at the surface, [298] (c) scavenging mechanisms of different electrolyte additives.[253] Reproduced from Refs.[9, 298, 253] with permission of Wiley and NPG.

Tremendous researches have been done to improve the electrochemical performance of the cathode materials by surface coating/modification or application of electrolyte additives (Fig. 25) because surface reactions, including CEI layer formation, are detrimental factors for battery performance as we mentioned above. A coating method that prevents direct contact between electrolyte and electrode could be an effective strategy (Fig. 25a). This method not only mitigates pernicious chemical production, but also prevents pulverization of particles, and can complement poor intrinsic properties depending on the type of coating materials. Representative example is carbon

coating by which direct surface area with electrolyte can decrease and electronic conductivity can be improved. Such carbon coating can enhance rate capability[286–289] of cathodes regardless of the kind of alkali-ion and host structure and can improve cycle life [290–292] and increase thermal stability of cathodes[287,293] by alleviating unwanted parasitic reactions such as oxygen evolution with decomposition of the electrolyte on the surface. In rare cases, it is reported that the surface wrapped with graphene can exhibit excess capacity beyond the theoretical capacity as well as the rate characteristic by providing additional Li storage sites between graphene sheets.[294] For cathode materials which experience severe all above mentioned surface reaction problems at high voltage, it is essential that having a more effective coating with moderate uniformity, coverage and thickness to be conserved from aggressive environments. Therefore, it has been explored with diverse kinds of coating species, notably resulting in improved electrochemical performance and thermal stability results[295] by Al_2O_3,[219,296–300] AlF_3,[301,302] Li_3PO_4,[303,304] $AlPO_4$,[305–308] *etc.*

There are other strategies to mitigate interfacial reaction through surface modification by composition change or atomic variation (Fig. 25b). For instance, Sun and co-workers synthesized and developed the particle with core-shell concentration gradient using co-precipitation method to mitigate the thermal instability and surface reconstruction reaction of Ni-rich cathode materials due to the migration of nickel ion. Particles with altered internal composition distribution, in which inner core and outer shell are relatively comprised of Ni-rich and Ni-poor, exhibited the highly enhanced performance compared to particles with uniformly distributed element.[309–312] Lin *et al*.[313] also reported that $LiNi_{0.4}Mn_{0.4}Co_{0.2}O_2$ spherical particles in which surface exhibits element segregation with nickel-depleted/manganese-rich deviating from nominal bulk composition on nanometer length scales have superior resistance to surface reconstruction. It was identified that both bulk element gradient and nanoscale surface element gradient effectively alleviate the surface side reactions in Ni-rich materials. There is also a method of complementing bulk active material by forming another beneficial phase to the surface in advance. Wang *et al*.[314] reported that TiO_2-modified high voltage spinel $LiNi_{0.5}Mn_{1.5}O_4$ forms reconstructed rock-salt like surface via migration of titanium ions at high temperature sintering, and the reconstructed surface mitigates the migration and dissolution of Mn ions into electrolyte at 55 °C cycling. Therefore, the modified $LiNi_{0.5}Mn_{1.5}O_4$ cathode exhibited enhanced capacity retention and Coulombic efficiency compared with bare $LiNi_{0.5}Mn_{1.5}O_4$ when cycled at high temperature (55 °C). Similarly, Han *et al.*[315] demonstrated that Zr doping induces $LiZr_2(PO_4)_3$-like phase on the surface of $Li_3V_2(PO_4)_3$, thereby improves rate capability and cyclability and similar results can be found for olivine material through off-stoichiometric variation method.[316]

In addition to controlling the surface of the positive electrodes, one can tune the nature of CEI layers by changing electrolyte composition. Since the uncontrollable complex surface reaction are highly related with the decomposition of $LiPF_6$, forming resistive CEI layer, the development of functional electrolyte additives that can scavenge decomposed material or substances is currently now being underway.[253] In more detail for the above mentioned contexts, $LiPF_6$ undergoes decomposition by hydrolysis reaction (*i.e.*, $LiPF_6(s) + H_2O(l) \rightarrow LiF(s) + POF_3(g) + 2HF(g)$), or undergoes dissociation (*i.e.*, $LiPF_6(s) \leftrightarrow LiF(g) + PF_5(g)$) for ion-paired $LiPF_6$ under presence of a Lewis acid.[317] Newly formed PF_5 also hydrolyzes to form POF_3 gas ($PF_5(g) + H_2O(l) \rightarrow POF_3(g) + 2HF(g)$), and it is sequentially converted into HF and by-products upon progressive hydrolysis reaction.[318–321] Acidic component, HF, leads to not only leaching transition metal dissolution, but also additional decomposition of interface components (*e.g.*, Li_2CO_3, LiOH, Li_2O, LiOR, $LiOCO_2R$), thereby generates additional triggering components (ROH and H_2O) for further hydrolysis of $LiPF_6$. [322,323] In addition, PF_5 does not only react with interface components (e.g., $PF_5(g) + Li_2CO_3(s) \rightarrow POF_3(g) + 2LiF(s) + CO_2(g)$),[324] but also decomposes the carbonate solvents in electrolytes,[325] resulting in accelerated cell degradation. Therefore, various additives are being developed for preventing the formation of detrimental factors such as HF and PF_5 by eliminating or deactivating the reactive species. Representative additives are: tris(pentafluorophenyl) borane (TPFPB); effectively complexes with PF_6^- anions and it hinders the formation of PF_5 and HF by trapping F^- from PF_6^- anions,[326] tris(trimethylsilyl) borate (TMSB); exhibits a high affinity for PF_6^- and F^- and thus facilitates the dissociation of $LiPF_6$ and stabilizes HF,[327] hexakis(2,2,2-trifluoroethoxy)cyclotriphosphazene (HFEPN); binds the hydrolyzed products of $LiPF_6$, HF or PF_5, due to the elevated electron donation ability of nitrogen,[328] heptamethyldisilazane (HMDS);

reacts with HF and results in its elimination,[329] 1-(trimethylsilyl)-imiddazole (1-TMSI); reacts with H_2O and blocks the hydrolysis of $LiPF_6$.[330] By using this method, additives are involved in the redox reaction prior to the consecutive detrimental reactions, so that enhanced CEI layer as well as safety can be achieved as shown in Fig. 25c.

2.3.2. Grain boundary

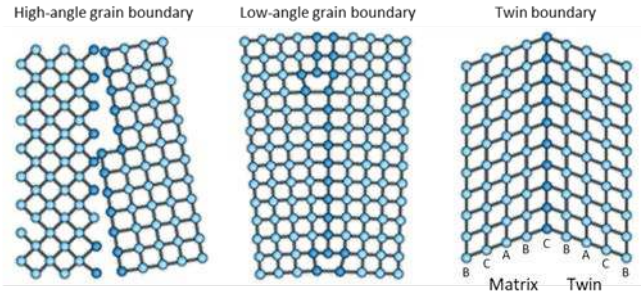

Fig. 26 Type of grain boundary according to the degree of misorientation of lattice.[331] Reproduced from Refs. [331] with permission of NPG.

Grain boundary, one of interfacial defects, is the interface between neighboring grains or crystals which have different structures or crystallographic orientations in the polycrystalline materials. Depending on the degree of misorientation of lattice between the grain interior structure at the grain boundary, the grain boundaries can be classified into high-angle grain boundary, low-angle grain boundary, or twin boundary (Fig. 26).[331] While some grain boundaries, including a mirror lattice symmetry (*i.e.* twin boundary), show fast ion migration[332–334] along the grain boundary, most of the grain boundaries suffer structural and chemical deviation due to energetically unfavorable environments of the end of grain atoms, giving rise to large resistance for ion migration across the grain boundary.[335] Therefore, even if transport along internal grain boundaries can be faster than through the bulk crystal at certain cases, ion migration from primary particle to another primary particle across the grain boundaries is inevitable, in which large activation energy is needed and causes low ion diffusivity. Therefore, grain boundaries have a disruptive influence on battery performance. This is not a phenomenon that solely occurs between particles, but also can occur within the primary particle. For example, in the case of triplite $LiFeSO_4F$, although which was expected to have high ionic conductivity value due to the low hopping energy from theoretical calculations, it actually shows poor (de)inserting performance.[152,336,337] According to Kang's group, it is attributed to the intrinsic nature of formation of pure corner-shared FeO_4F_2 octahedra regions with locally surrounded by the mixed corner/edge-shared regions.[164] Although crystals are coherently structured over the whole space in the single primary particle, the locally disordered regions induced from the lattice mismatch between pure and mixed region are widely distributed, thereby lead to high activation energy barrier for ion diffusion.[164] To sum up, several special boundaries can modify the energy between two grains to have energetically favorable environment but, in essence, grain boundary is the resistance for not only ion diffusion but also electronic conduction.[338]

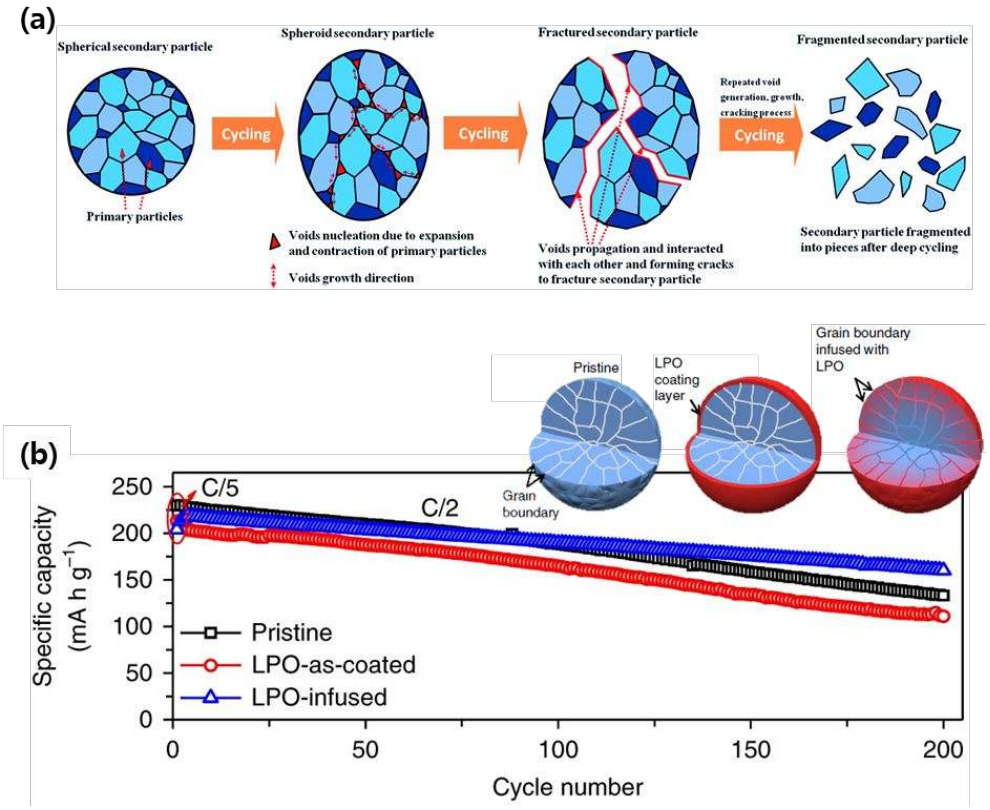

Fig. 27. (a) Schematic illustration of crack formation and fragmentation mechanisms of secondary particle during cycling.[339] (b) Cycling performance of $LiNi_{0.76}Mn_{0.14}Co_{0.10}O_2$ at 60 ℃ with different surface treatment. LPO-infused material shows[340] best performance by preventing crack formation along the grain boundaries. Reproduced from Refs. [339,340] with permission of RSC and NPG.

Grain boundaries also play a detrimental role in mechanical degradation. Secondary particles are composed of randomly oriented primary particles. The primary particles at the surface of secondary particles are exposed to direct ion and electron transport parameters (*i.e.* electrolyte and conductive additive), while subsurface primary particles are indirect. Furthermore, as each secondary particle is not uniform, all the insertion kinetics in the electrode are the result of non-cooperative inhomogeneous reaction of individual primary particles.[341] Therefore, stress or strain in the secondary particle induced from the volume expansion/contraction of the primary particles during cycling are not uniformly distributed and arranged along the grain boundaries. It results in the intergranular cracking in the secondary particle.[342] Fig. 27a illustrates the following mechanism. Even after first cycle, micro-cracks with large grain boundary layer in the secondary particle are formed,[343] and it propagates due to repeated stress during cycling.[339] If the primary particle experiences anisotropic lattice variation and volume change as like layered material during cycling, intergranular cracking can occur even at very low current rate, while cubic structures which show isotropic lattice variation during cycling can avoid it. However, at high current rate conditions, where severe inhomogeneous reaction among particles and/or lattice mismatch in the structure induced from concentration gradients of Li occurs, the formation of cracks in secondary particle is accelerated regardless of whether lattice change is isotropic or not.[342,344,345] As the crack formation along the grain boundaries induces disconnected transport kinetics resulting from the reduced contact area between primary particles and side reactions with penetration of electrolyte, it needs to be prevented in order to maintain capacity retention for a long cycling. Recently, as a way of grain boundary engineering and improve the battery performance, Yan *et al.*[340] suggested infusion of Li_3PO_4 (LPO) solid electrolyte into the grain

boundaries. The authors infused LPO into the grain boundaries of Ni-rich layered material ($LiNi_{0.76}Mn_{0.14}Co_{0.10}O_2$) using atomic layer deposition (ALD), and showed that the infused solid electrolyte prevents formation of intergranular cracking as well as interfacial side reaction at the grain boundaries. As a result, it makes increased kinetic network without detrimental factors of grain boundaries, and finally enhances the cycling stability of the cathode (Fig. 27b). And coating the single crystalline primary nanoparticles[346] with conducting additive can alleviate the grain boundary resistance by the enhanced transport kinetics, and mitigate the lattice change mechanically. Grain boundary engineering is effective, however, these strategies hitherto have not fully developed and more efforts need to be made.

2.3.3. Particle size

Tuning the particle size of the material, which can be controlled by changing the synthesis condition (*e.g.* sintering temperature and/or time, and *etc.*) could be a fruitful approach to improve the bad properties of the cathode materials by which enhancing or reducing chemical/physical effects change the electrochemical reaction in the electrode level. Size-dependent chemical properties compared with larger particles of the same material are highly related with the surface. As the particle size decreases towards the nanometer scale, material properties gradually follow the surface characteristics rather than the bulk structure characteristics, and, nano-sized particles tend to be agglomerated to lower the thermodynamically unstable surface energy [347] as a secondary particle. Despite the reduced surface area of each nanoparticle through agglomeration, total surface area of inner and outer secondary particles is usually increased because of porosity, and as the size of particle become dispersive, the greater the effect.[348] As a result, in nanosized particles, the surface reaction is promoted, which in turn lowers the cycle life and thermal stability for materials showing detrimental reactions at the surface.[348,349]

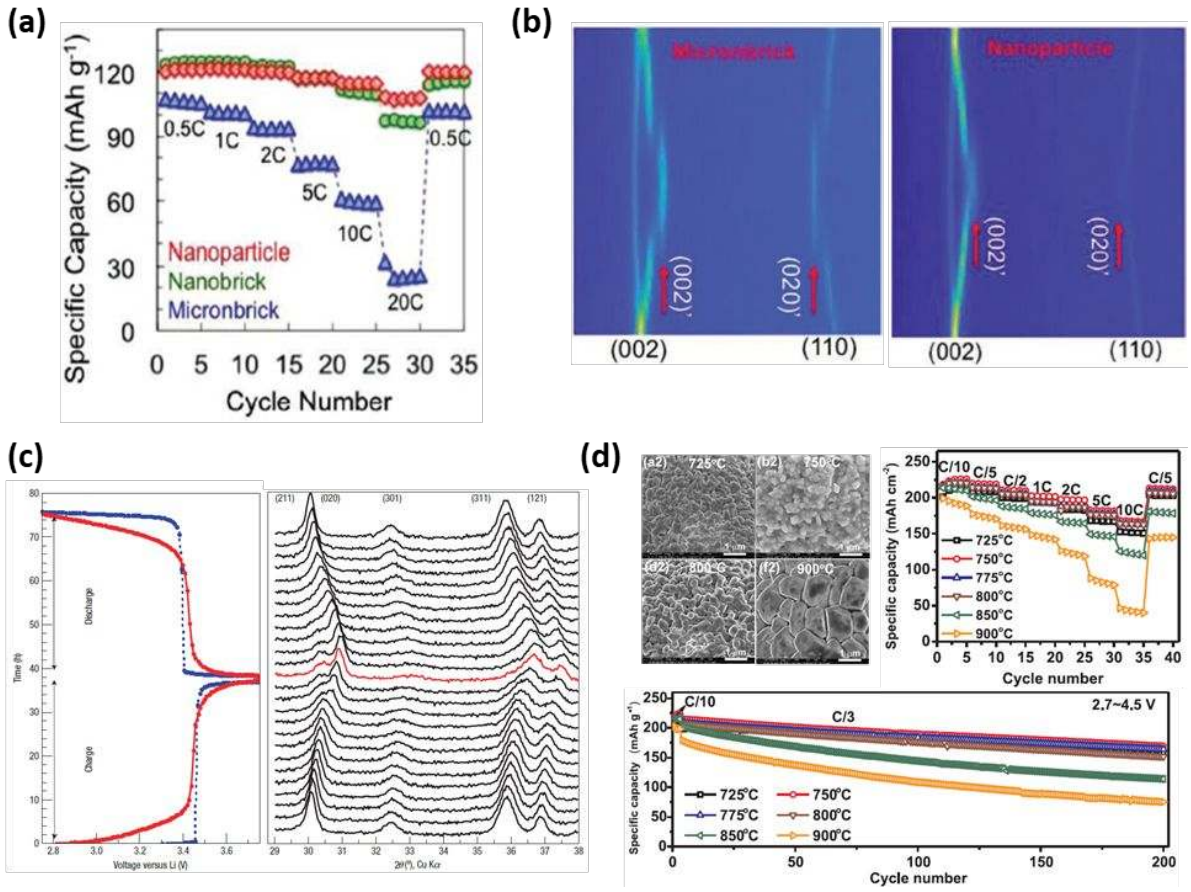

Fig. 28 In $Na_{1.5}VOPO_4F_{0.5}$ system, (a) Rate performance of with different size of particle and (b) *in situ* XRD results of micronbrick and

nanoparticle.[350] (c) *in situ* XRD measurement result of 40 nm particle size of $LiFePO_4$ during galvanostatic charge/discharge at C/40.[351] It shows solid solution structural variation. (d) SEM images and electrochemical test results of rate capability and cyclability of $LiNi_{0.76}Mn_{0.14}Co_{0.10}O_2$ with different particle sizes.[352] Reproduced from Refs. [350, 351, 352] with permission of Wiley, NPG and Elsevier.

Nevertheless, other apparent changed physical effects that are altered by reducing particle size can improve the battery performance, especially cyclability and rate capability in cooperation with a large surface area. For example, inferior packing of particles can mitigate the intergranular strain which is one of the main causes of poor cyclability as described in chapter 2.3.2. The short path length of transport parameters complement the electric conductivity and the low ionic diffusivity within the active primary particle, *etc.*[353]. This is especially effective for materials that have inherently slow kinetic properties, and $LiFePO_4$ is one of most widely known examples.[354] This phenomenon is not confined to specific mobile ion system, indicating that other alkali-ion insertion based materials (*i.e.* host material for Na[350,355] and K[356]) are also applied. In the case of $Na_{1.5}VOPO_4F_{0.5}$ system, for example, Lai *et al.*[350] reported that among the various particle sizes including micronbrick, nanobrick, and nanoparticle, the smallest nanoparticle expectedly delivers superior rate performance with high capacity (Fig. 28a).

Additional physical advantage of small particle size is alleviation of the stress/strain not only between particles, but also within the particles by reducing the miscibility gap. Gibot *et al.*[351] discovered that 40 nm particle size of $LiFePO_4$ exhibits solid solution behavior during charge/discharge even at very slow rate C/40 (Fig. 28c) through the *in situ* XRD analysis, in contrary to classical two phase insertion process.[357] Kobayashi *et al.*[358] and Meethong *et al.*[359] also found that decreasing particle size induces more solid solution like behavior during cycling and it results from the mutually constrained solubility of Li-ion between coexisting crystalline phases. The same phenomenon was also observed for the above mentioned Na system (Fig. 28b).[350] The micro-scale stress within the particles, which can be originated from the local ion concentration gradient change, is also a performance degradation factor similar to intergranular crack,[339] therefore, solid solution behavior can lessen the cyclic mechanical damages because it can avoid spatial heterogeneities. However, not all the materials show enhanced battery performance by lowering particle sizes, and to fully take advantages, several prerequisites have to be met, *e.g.*, the particles must be in good contact through an effective connection network within the electrode,[224,360,361] side reactions should be inconspicuous or mitigated via adequate engineering, *etc.* In addition, smaller particle size is not always better for battery performance, and the proper size can give the highest performance[352] by balanced synergic chemical/physical effects (Fig. 28d).

Increasing the size of the particles up to micrometer dimension with high purity can have another benefit as oppose to that reducing the size of the particles. As the size of the single crystalline particles increases, volumetric energy density is enhanced and other unwanted side reactions is reduced with decreased surface area. Also, absence of the void spaces in the particle prevents additional deteriorating reaction such as crack formation during cycling.[362] Dahn and co-workers[363,364] investigated the difference between large single crystalline particle and polycrystalline particle of $LiNi_{0.5}Mn_{0.3}Co_{0.2}O_2$, and reported that compared with latter one, the former shows the improved cycle life and thermal stability during cycling due to reduced parasitic reaction as above mentioned, though it trades off with the rate capability. Zhong *et al.*[365] also recently confirmed the same results. Therefore, it is necessary to find an appropriately optimized particle size for its purpose.

2.3.4. Morphology

Particle morphology control is an effective strategy to achieve enhanced battery performance. Morphology of the primary particle changes not only intrinsic characteristics of primary particle, but also interior structure of the secondary particles which consists of primary particle, so that it can change various physical/chemical properties and thus battery performance (*e.g.* capacity retention, rate capability, energy density). Controlled variables and effects are summarized as follows:

(i) **Exposed crystal planes of the primary particle:** Ion diffusion is dependent on the crystal plane. Exposure of favorable crystal plane

(along ion diffusion direction) enhances the rate capability (*e.g.* open surface of {010} facets for layered, (110) planes for spinel, (010) planes for olivine facilitate the ion diffusion).[366]

(ii) **Surface area in the secondary particle:** It has pros and cons. Large surface area leads to higher reaction rates, but can promote undesirable electrode/electrolyte reaction.

(iii) **Grain boundary between primary particles:** As described in 2.3.2, it is a resistance for transport parameters, and cause of cracking by volume change, so it needs to be reduced.

(iv) **Density of secondary particle:** Spatial distribution of the primary particles in secondary particle is correlated with surface area in the secondary particle, and it affects the energy density of the electrode.

(v) **Network system of transport parameters:** The more ion and electron conducting species are efficiently combined, the more improved battery performance is obtained. It is applicable for all the battery systems.[367]

Hence, controlling the particle morphology is a useful method to complement bad material characteristics or circumvent the undesirable environments (*e.g.* irreversible phase transition at the interface between particle and electrolyte) by modifying those five categories, and numerous papers have shown that the effective morphology design can get over the weakness or disadvantages of the materials.

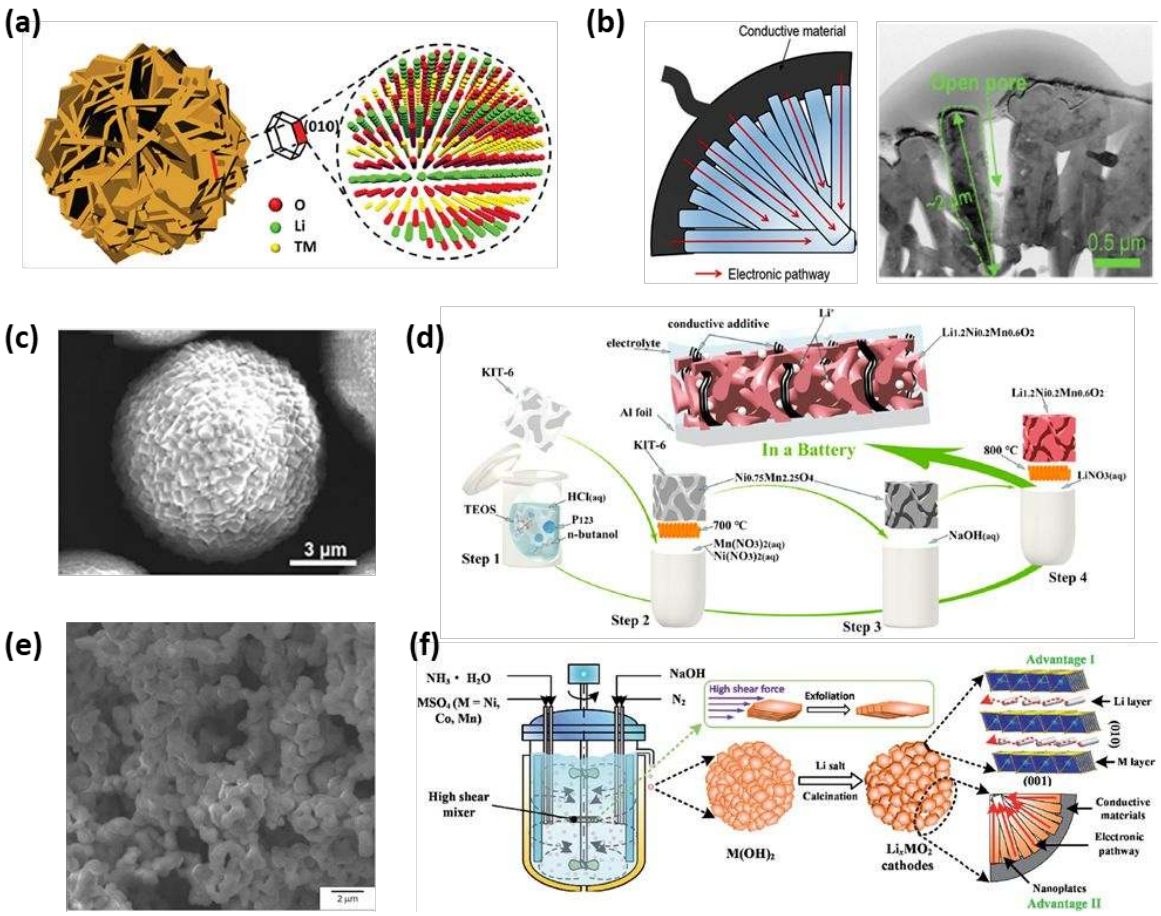

Fig. 29 (a-d) Morphology controlled $Li_{1.2}Ni_{0.2}Mn_{0.6}O_2$ particles. Schematic illustration or SEM image of (a) radially aligned primary nano-plates into hierarchical quasi-sphere,[368] (b) secondary particle composed of flake-shaped large primary particles,[338] (c) microsphere structure with

partially activated primary nano-cube particles,[369] (d) 3D reticular morphology with synthesizing route.[370] (e) SEM image of pristine macro-porous $LiNi_{1/3}Co_{1/3}Mn_{1/3}O_2$,[371] and (f) schematic illustration of synthesizing hierarchically structured nano-plate $LiNi_{1/3}Co_{1/3}Mn_{1/3}O_2$.[372] Reproduced from Refs. [368, 338, 369 ,370, 371, 372] with permission of Wiley, ACS, and RSC.

Strategy for achieving high rate capability by reducing the particle size[353] and reducing the diffusion length of Li-ion leads to a dilemma that results in performance degradation (*i.e.,* capacity decay) because of more side reactions by increased surface area.[348]As a way to solve rate and cyclability problems, many studies have found innovative results by developing new synthesis methods which control the particle morphology. For example, Chen *et al.*[368]synthesized $Li_{1.2}Ni_{0.2}Mn_{0.6}O_2$ ($0.5Li_2MnO_3$–$0.5LiNi_{0.5}Mn_{0.5}O_2$) with a radially aligned primary nano-plates into hierarchical quasi-sphere, whose surface is exposed with {010} facets to which the planes parallel to [001] direction (Fig. 29a). Therefore, they could achieve reduced electrode-electrolyte interface area and increased open surface for direct Li-ion diffusion for enhanced Li-ion transport, and thus it showed improved rate capability as well as cycling performance. [Strategy (i, ii)] Oh *et al.*[338] developed $Li_{1.2}Ni_{0.2}Mn_{0.6}O_2$ with 10 μm size flake-shaped particles with surface activation treatment (Fig. 29b) and the cathode exhibits high rate capability as well as high capacity retention (93 % for 600 cycles). Although a large particle size needs several activation cycles, increased tap density with reduced surface area results in high volumetric energy density and cycle retention. Also, long flake-shaped primary particles reduce electronic interfacial resistances among inner particles, which facilitate electron conduction and thus provide increased rate capability. [Strategy (ii, iii, iv, v)] Similarly, Li *et al.*[369] demonstrated that close-packed microsphere structure with partially activated primary nano-cube particles of $Li_{1.2}Ni_{0.2}Mn_{0.6}O_2$ (Fig. 29c) delivers enhanced cyclability and rate performance. [Strategy (ii, iv)] 3D reticular structure can also promote electrochemical performance of $Li_{1.2}Ni_{0.2}Mn_{0.6}O_2$ because of nano-sized 3D network and meso-pore channels (Fig. 29d) according to Li *et al.*[370] This structure is related with strategy (ii) and (v).

The morphology control is also effective for traditional layered materials ($LiMO_2$, M = transition metal). One example can be found in Bruce group's work.[371] They synthesized a disordered macro-porous form of $LiNi_{1/3}Co_{1/3}Mn_{1/3}O_2$ composed of fused individual primary particles (Fig. 29e) in the range of 0.5 – 1.0 μm within which the macro-pores range in size from around 1 – 5 μm. Despite the increased porosity, it remains relatively modest surface areas. Both dense contact between primary particles and efficient penetration of the electrolyte through the macro-pores form an expeditious environment for transport parameters. Therefore, excellent capacity retention even at high rate could be achieved. [Strategy (ii, iv, v)] Hua *et al.*[372] also developed $LiNi_{1/3}Co_{1/3}Mn_{1/3}O_2$ with self-assembled hierarchical structure composed of nano-plate with many exposed electrochemically active {010} facets by using a continuous stirred tank reactor (CSTR), in which a high-shear mixer is introduced (Fig. 29f). The secondary particle having large nano-plates and nano-pores shows reduced surface area with small grain boundary resistances, and forms a 3D network for ion and electron transport by combination of penetrated electrolyte and conductive additives around the particle. Efficient transport pathways with a short length in a 3D structure that has a reduced surface area and low grain boundary resistance enables excellent rate capability with high capacity retention performance (98.2 % capacity retention after 500 cycles at 20C). [Strategy (i), (ii), (iii), (v)]

Since above strategies are not limited only layered materials, but all types of electrode material, many studies have tried to find novel ways of synthesizing with efficient particle morphology. Because the problems associated with material properties vary depending on materials, each has had to find an efficient method. In the case of $LiFePO_4$, for example, although high structural stability is ensured, it has the disadvantage of low electronic conductivity. This shortcoming can be overcome by particle morphology change (*e.g.* nanowire,[373] nanoflake,[374] mesoporous structure,[375,376] *etc.*), as well as typical carbon coating method which is also included in the strategy (v) for forming efficient transport network.

New methods of synthesizing the functional structure of secondary particles that exhibit improved battery performance are continuously being developed. Table 1. summarizes the examples of showing enhanced battery performance by changing the particle morphology,

including Na, K compounds as well as Li compounds. However, designing appropriate structure of secondary particle considering all the above mentioned categories still remains a challenge because of difficulties in synthesis (*e.g.* controlling the particle growth during the sintering process, agglomeration of nanoparticles, and *etc.*), so that considerable effort needs to be devoted in this research area.

Material	Morphology	Strategies[a]					Voltage range (V)	Long-term cycled capacity[b] (retention, cycle #) @ current rate	Low rate – High rate capacity[b] (current rate)	Ref
		(i)	(ii)	(iii)	(iv)	(v)				
$LiNi_{1/3}Co_{1/3}Mn_{1/3}O_2$	Macroporous		✓		✓	✓	2.5-4.6	190 (99.99%, 20 to 220) @ 0.5C	203 (0.25C) – 173 (12C)	371
	Hierarchical nanoplate	✓	✓	✓		✓	2.7-4.3	(98.2%, 500) @ 20C	~170 (0.1C) – 120.88 (20C)	372
$Li_{1.2}Ni_{0.2}Mn_{0.6}O_2$	Nanoplate	✓	✓				2.0-4.8	216.2(95.5%, 60) @ 1C 183.6(86.6%, 60) @ 2C	230.8 (1C) – 141.7(20C)	368
	Flake shaped		✓	✓	✓	✓	2.0-4.6	(93%, 600) @ 1C	242 (0.1C) – ~100 (12C)	338
	Hierarchical nanocube		✓		✓		2.0-4.8	243(81.4%, 200) @ 0.1C (20mA/g)	283.1 (0.1C) – 122.6 (5C)	369
	3D-reticular		✓	✓		✓	2.0-4.8	241(93%, 25) @ 0.1C 187(95.6%, 50) @ 1C	261.2 (0.1C) – 135.4 (5C)	370
$LiMn_2O_4$	Nanowire	✓	✓				3.1-4.5	100 (92.6%, 100) @ 5 A/g	118 (0.1 A/g) – 88 (20 A/g)	377
	Porous core-shell microellipsoid		✓	✓			3.0-4.5	(90.1%, 400) @ 5 C	110.7 (0.1C) – 70.2 (10C)	378
$LiFePO_4$	Nanowire	✓	✓			✓	2.5-4.3	146 (97.3%, 100) @ 1C	169 (0.1C) – 93 (10C)	373
	Mesoporous microsphere		✓		✓	✓	2.0-4.5	140 (100%, 50) @ 1C	153 (0.1C) – 86 (20C)	376
	Macro-Mesoporous		✓			✓	2.0-4.0	166.1 (95.6%, 200) @ 0.2C	156.9 (0.1C) – 110.9 (10C)	375
	Nanorod	✓	✓				2.0-4.3	—	169 (0.05C) – 139 (10C)	379
LiV_3O_8	Nanowire		✓			✓	1.5-4.0	271.7 (84.7%, 100) @ 100 mA/g	320.6 (100 mA/g) – 202.8 (2 A/g)	380
$Na_{0.6}Mn_{0.98}Mo_{0.02}O_2$	Multilayer nanoplate	✓					2.0-4.0	143.9 (89.6%, 100) @ 1C 66.65(86%, 1200) @ 10C	166.8 (0.2C) – 77.5 (10C)	381
$Na_{2/3}Fe_{1/2}Mn_{1/2}O_2$	Hierarchical nanofiber		✓			✓	1.5-4.2	166 (86.4%, 80) @ 0.1 C	195 (0.1C) – ~50 (15C)	382
NaV_3O_8	Nanosheet		✓	✓		✓	1.5-4.0	99 (77.3%, 60) @ 0.23 C	140 (0.23C) – 63 (3.68C)	383
$Na_{1.25}V_3O_8$	Zigzag nanowire		✓	✓		✓	1.5-4.0	92.2 (87%, 1000) @ 1 A/g	171.9 (100 mA/g) – 79.1 (2 A/g)	384
$Na_3V_2(PO_4)_3$	Mesoporous		✓			✓	2.8-3.8	63.64 (74%, 450) @ 0.4 A/g (3.64 C)	98 (0.1 A/g) – 63 (1 A/g)	385
	3D hierarchical nanowall		✓	✓		✓	2.5-4.0	80.05 (74.4%, 600) @ 1 C	114.8 (0.1 C) – 94.9 (5 C)	386
	3D nanofiber		✓	✓		✓	2.3-3.9	105.49 (95.9%, 1000) @ 10 C	113 (1 C) – 94 (100 C)	387
	Nanoflake		✓	✓		✓	2.5-4.0	62.1 (62.5%, 30000) @ 50 C	115.2 (1 C) – 75.9 (200 C)	388
	Hierarchically porous hollow nanosphere		✓	✓		✓	2.3-3.9	93 (90.9%, 10000) @ 1 C	106 (0.1 C) – 84 (400 C)	389
	Branch shaped nanofiber	✓	✓			✓	2.5-4.0	107.2 (>100%, 125) @ 0.2C	115.0 (0.1C) – 103.0 (2 C)	390
$K_{0.7}Fe_{0.5}Mn_{0.5}O_2$	Nanowire		✓			✓	2.0-4.5	59.2 (87%, 450) @ 1000 mA/g	178 (20 mA/g) – 68 (1 A/g)	221
$K_3V_2(PO_4)_3$	Mesoporous		✓			✓	1.5-4.3	52 (96%, 100) @ 20 mA/g	54 (20 mA/g) – ~20 (200 mA/g)	391

Table 1. Summary of the results of enhanced electrochemical characteristics of morphology controlled cathode materials

[a] Strategies are controlling (i): Exposed crystal planes of the primary particle, (ii): Surface area in the secondary particle, (iii): Grain boundary between primary particles, (iv): Density of secondary particle, (v): Network system of transport parameters. [b] Unit of capacity is mAh g^{-1}

3. Concluding remarks and perspectives

Thanks to pioneers in the alkali-ion rechargeable batteries, energy consumption patterns have undergone substantial changes, and the necessity for more energy and less carbon has led advances in energy-efficient and environment-saving technologies. The cathode, after all, is the most important part of the rechargeable batteries in consideration of the five requirements as energy, power, safety, life, and cost. The progress in synthesis and analysis technology enables a more complete understanding of what governs the properties and performance of the cathode materials. The fundamental understanding provided by diverse approaches from nano to micro level has already helped to bridge the gap between industrial and academic research field for the improvement and commercialization of the state-of-the-art cathode materials. Each level offers its own challenges and attractions, but understanding how different level of changes are linked to and influence each other is needed with a holistic approach. This review has discussed the influencing factors on the properties and performance of the cathode materials ranging widely from atomic through microscopic levels. The main factors to consider for designing cathode materials at each level are as follows:

- **Atomic to molecular levels:** The electrochemical properties of the cathode materials vary depending on the size of insertion ion and interaction between them (*e.g.*, Li-Li, Na-Na, and K-K interaction) even in the same crystal structure. From the host structure point of view, the manipulation of the interaction among transition metal ions and anions by considering electronegativity enables a delicate controlling of the redox potential. Moreover, in addition to the electronic structures of transition metal ions and anions, the local environment of them provide a lot of predictable information such as available number of electrons (*e.g.*, redox active species) and structural stability (*e.g.*, Jahn-Teller distortion and disproportionation) of the cathode materials, which govern the electrochemical performance of cathodes.

- **Molecular to crystallographic levels:** Notwithstanding same chemical compositions, the redox potential, electron and ion conductivity, and structural stability differ considerably among crystal structures. Crystal structure controls reaction mechanisms in the ion transport and redox chemistry, and these are deeply linked to the ion channel and disorder in the crystal structure. The size of ion channel is directly related to the diffusivity of mobile ions. Generally, a larger ion diffusion channel is considered as a favorable environment for mobile ions to diffuse, but optimized void size for each alkali-ion is an important factor. The term 'disorder' often connotes a sense of negative effect in the crystal structure of insertion cathode materials. The immobile ions located in the alkali-ion channel obstruct alkali-ions diffusion, so it is considered one of the deleterious factors lowering the rate performance of the alkali-ion rechargeable batteries. However, not all the defects on the crystal structure are detrimental. For example, certain type of disorder in the layered structure system can function as a pillar preventing the ion channel from collapsing. Moreover, it can extend the dimensionality (*i.e.*, 1D to 3D) of diffusion channels by percolating the crossover pathway between the ion channels or enable the materials with a disordered rock-salt structure to transport mobile ions by forming a percolating 0-TM network. Furthermore, the local disorder around anions can activate the redox activity of anions by making localized non-bonding O 2*p* states. During the electrochemical reactions, cathode materials go through a change in crystal structures by a phase transition. In case of multi-phase transition, reducing the lattice parameter differences between each phase or suppressing a dramatic change in the phase and the emergence of irreversible phase are essential.

- **Crystallographic to microscopic levels:** Both chemical properties and physical properties of cathodes mainly affect the cell performance. Side reaction on the surface of the cathode materials is usually cooperated with electrolyte decomposition and it causes a degradation in cell performance during the charge/discharge process. Coating and chemical compositional changes can reduce such side reaction. As electrolytes penetrate into the grain boundaries between particles, subsurface of particle also experiences side reactions. During cycling with a dynamic structural change, not only are its influence amplified due to the crack

formation and propagation along the grain boundaries, but they also cause contact loss among the primary or secondary particles. To complement the shortcomings for each material, therefore, controlling particle size and morphology, which are the main factors that govern the physicochemical aspects such as diffusion path, surface reaction area, transport network system, *etc.*, could be profitable strategies.

These factors in the respective levels are not independent and are intimately linked with one another. For instance, the constituent elements do not only determine the redox potentials and available electron numbers of the cathode materials but also influence the ion channels and structural disorder according to the electronic structure and atomic configuration in crystal structures, and therethrough affect as far as the phase transitions (Fig. 9). The undesirable phase transitions during cycling can incur deterioration in the electrochemical performance through the formation of crack or even the loss of contact among particles.

In addition to the expectation of the rapid growth of renewable energy in the global energy system, the enormous market potential of electric vehicles is encouraging the electricity storage technologies to advance a great deal in the foreseeable future together. The multiscale approaches can access to key factors, overcoming the limits of cathode materials by combining different levels of parameters, bringing a new perspective to electrode material design (Fig. 30).

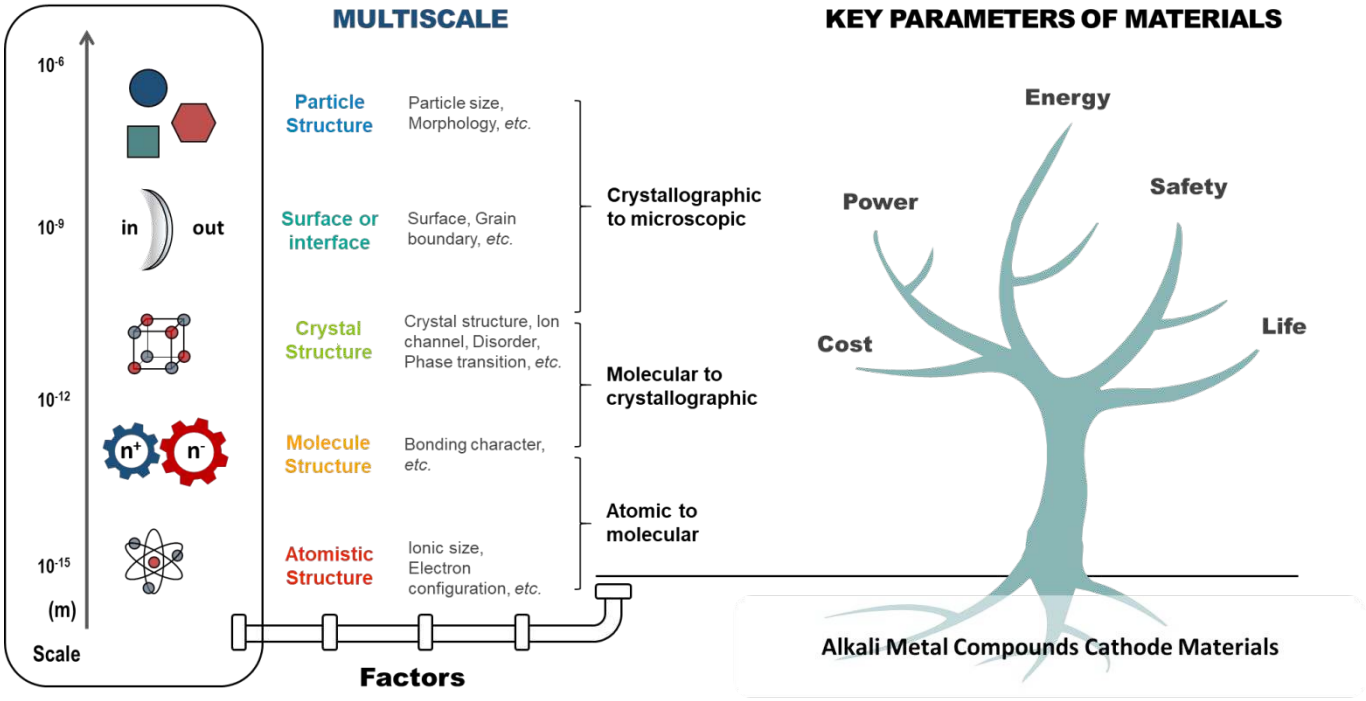

Fig. 30 Summary of the factors from atomic to microscopic levels.

Conflicts of interest

There are no conflicts to declare.

Acknowledgements

This work was supported by a National Research Foundation of Korea (NRF) grant funded by the Korean government (MSIP) (No. NRF-2017R1A4A1015770 and No. NRF-2019R1A2C2003731).

References

1 BP Energy Outlook, *BP Energy Outlook 2019, https//www.bp.com/en/global/corporate/energy-economics/energy-outlook.html*.

2 IRENA, *Electr. Storage Renewables Costs Mark. to 2030, https//www.irena.org/publications/2017/Oct/Electricity-storage-and-renewables-costs-and-markets*.

3 C. M. Hayner, X. Zhao and H. H. Kung, *Annu. Rev. Chem. Biomol. Eng.*, 2012, **3**, 445–471.

4 J. W. Choi and D. Aurbach, *Nat. Rev. Mater.*, 2016, **1**, 16013.

5 J. Xu, F. Lin, M. M. Doeff and W. Tong, *J. Mater. Chem. A*, 2017, **5**, 874–901.

6 C. Daniel, D. Mohanty, J. Li and D. L. Wood, in *AIP Conference Proceedings*, 2014, vol. 1597, pp. 26–43.

7 C. Aucher, *ALISE-Advanced Lithium Sulphur Batter. xEV, http//www.avicenne.com/articles_energy.php*.

8 N. Nitta, F. Wu, J. T. Lee and G. Yushin, *Mater. Today*, 2015, **18**, 252–264.

9 W. Lee, S. Muhammad, C. Sergey, H. Lee, J. Yoon, Y. M. Kang and W. S. Yoon, *Angew. Chemie - Int. Ed.*, 2020, 59, 2578–2605.

10 G. Assat and J.-M. Tarascon, *Nat. Energy*, 2018, **3**, 373–386.

11 M. Ben Yahia, J. Vergnet, M. Saubanère and M.-L. Doublet, *Nat. Mater.*, , DOI:10.1038/s41563-019-0318-3.

12 S. Dargaville and T. W. Farrell, *J. Electrochem. Soc.*, 2010, **157**, A830.

13 R. E. Garćıa, Y.-M. Chiang, W. Craig Carter, P. Limthongkul and C. M. Bishop, *J. Electrochem. Soc.*, 2005, **152**, A255.

14 A. G. Kashkooli, S. Farhad, D. U. Lee, K. Feng, S. Litster, S. K. Babu, L. Zhu and Z. Chen, *J. Power Sources*, 2016, **307**, 496–509.

15 P. Ramadass, B. Haran, R. White and B. N. Popov, *J. Power Sources*, 2003, **123**, 230–240.

16 S. Pannala, J. A. Turner, S. Allu, W. R. Elwasif, S. Kalnaus, S. Simunovic, A. Kumar, J. J. Billings, H. Wang and J. Nanda, *J. Appl. Phys.*, , DOI:10.1063/1.4927817.

17 A. A. Franco, A. Rucci, D. Brandell, C. Frayret, M. Gaberscek, P. Jankowski and P. Johansson, *Chem. Rev.*, 2019, **119**, 4569–4627.

18 P. Barai, Z. Feng, H. Kondo and V. Srinivasan, *J. Phys. Chem. B*, 2019, **123**, 3291–3303.

19 Y. Ding, Z. P. Cano, A. Yu, J. Lu and Z. Chen, *Electrochem. Energy Rev.*, 2019, **2**, 1–28.

20 A. Kwade, W. Haselrieder, R. Leithoff, A. Modlinger, F. Dietrich and K. Droeder, *Nat. Energy*, 2018, **3**, 290–300.

21 W. B. Hawley and J. Li, *J. Energy Storage*, 2019, **25**, 100862.

22 X. Zeng, M. Li, D. Abd El-Hady, W. Alshitari, A. S. Al-Bogami, J. Lu and K. Amine, *Adv. Energy Mater.*, 2019, **9**, 1–25.

23 A. A. Franco, *Physical Multiscale Modeling and Numerical Simulation of Electrochemical Devices for Energy Conversion and Storage - From Theory to Engineering to Practice*, 2015.

24 K. Li and D. Xue, *J. Phys. Chem. A*, 2006, **110**, 11332–11337.

25 R. D. Shannon, *Acta Crystallogr. Sect. A*, 1976, **32**, 751–767.

26 K. Saravanan, C. W. Mason, A. Rudola, K. H. Wong and P. Balaya, *Adv. Energy Mater.*, 2013, **3**, 444–450.

27 H. Kim, J. C. Kim, S. H. Bo, T. Shi, D. H. Kwon and G. Ceder, *Adv. Energy Mater.*, 2017, **7**, 2–7.

28 N. Wu, H. Wu, W. Yuan, S. Liu, J. Liao and Y. Zhang, *J. Mater. Chem. A*, 2015, **3**, 13648–13652.

29 X. Chen, X. Zhou, M. Hu, J. Liang, D. Wu, J. Wei and Z. Zhou, *J. Mater. Chem. A*, 2015, **3**, 20708–20714.

30 Y. Peng, R. Tan, J. Ma, Q. Li, T. Wang and X. Duan, *J. Mater. Chem. A*, 2019, **7**, 14681–14688.

31 H. Kim, D. H. Seo, J. C. Kim, S. H. Bo, L. Liu, T. Shi and G. Ceder, *Adv. Mater.*, 2017, **29**, 1–6.

32 S. Kumakura, Y. Tahara, K. Kubota, K. Chihara and S. Komaba, *Angew. Chemie - Int. Ed.*, 2016, **55**, 12760–12763.

33 H. Q. Pham, E. H. Hwang, Y. G. Kwon and S. W. Song, *Chem. Commun.*, 2019, **55**, 1256–1258.

34 L. Shen, Z. Wang and L. Chen, *Chem. - A Eur. J.*, 2014, **20**, 12559–12562.

35 M. Bianchini, N. Brisset, F. Fauth, F. Weill, E. Elkaim, E. Suard, C. Masquelier and L. Croguennec, *Chem. Mater.*, 2014, **26**, 4238–4247.

36 A. Ueda, *J. Electrochem. Soc.*, 1994, **141**, 2010.

37 M. Okubo, D. Asakura, Y. Mizuno, J. D. Kim, T. Mizokawa, T. Kudo and I. Honma, *J. Phys. Chem. Lett.*, 2010, **1**, 2063–2071.

38 T. Deng, X. Fan, J. Chen, L. Chen, C. Luo, X. Zhou, J. Yang, S. Zheng and C. Wang, *Adv. Funct. Mater.*, 2018, **28**, 1–9.

39 P. Barpanda, G. Oyama, S. I. Nishimura, S. C. Chung and A. Yamada, *Nat. Commun.*, , DOI:10.1038/ncomms5358.

40 B. Kang and G. Ceder, *Nature*, 2009, **458**, 190–193.

41 F. Chen, V. M. Kovrugin, R. David, O. Mentré, F. Fauth, J. Chotard and C. Masquelier, *Small Methods*, 2019, **3**, 1800218.

42 X. Bie, K. Kubota, T. Hosaka, K. Chihara and S. Komaba, *J. Mater. Chem. A*, 2017, **5**, 4325–4330.

43 J. J. Ding, Y. N. Zhou, Q. Sun, X. Q. Yu, X. Q. Yang and Z. W. Fu, *Electrochim. Acta*, 2013, **87**, 388–393.

44 H. Kim, D.-H. Seo, A. Urban, J. Lee, D.-H. Kwon, S.-H. Bo, T. Shi, J. K. Papp, B. D. McCloskey and G. Ceder, *Chem. Mater.*, 2018, **30**, 6532–6539.

45 Y. You, X. L. Wu, Y. X. Yin and Y. G. Guo, *Energy Environ. Sci.*, 2014, **7**, 1643–1647.

46 C.-Y. Yu, J.-S. Park, H.-G. Jung, K.-Y. Chung, D. Aurbach, Y.-K. Sun and S.-T. Myung, *Energy Environ. Sci.*, 2015, **8**, 2019–2026.

47 X. Lin, J. Huang, H. Tan, J. Huang and B. Zhang, *Energy Storage Mater.*, 2019, **16**, 97–101.

48 L. Wang, J. Song, R. Qiao, L. A. Wray, M. A. Hossain, Y.-D. Chuang, W. Yang, Y. Lu, D. Evans, J.-J. Lee, S. Vail, X. Zhao, M. Nishijima, S.

Kakimoto and J. B. Goodenough, *J. Am. Chem. Soc.*, 2015, **137**, 2548–2554.

49 J. Song, L. Wang, Y. Lu, J. Liu, B. Guo, P. Xiao, J. J. Lee, X. Q. Yang, G. Henkelman and J. B. Goodenough, *J. Am. Chem. Soc.*, 2015, **137**, 2658–2664.

50 L. Xue, Y. Li, H. Gao, W. Zhou, X. Lü, W. Kaveevivitchai, A. Manthiram and J. B. Goodenough, *J. Am. Chem. Soc.*, 2017, **139**, 2164–2167.

51 H. Kim, D. H. Seo, M. Bianchini, R. J. Clément, H. Kim, J. C. Kim, Y. Tian, T. Shi, W. S. Yoon and G. Ceder, *Adv. Energy Mater.*, 2018, **8**, 1–12.

52 H. Kim, H. Ji, J. Wang and G. Ceder, *Trends Chem.*, 2019, 1–11.

53 J. M. Paulsen, J. R. Mueller-Neuhaus and J. R. Dahn, *J. Electrochem. Soc.*, 2000, **147**, 508–516.

54 B. Peng, Z. Sun, S. Jiao, J. Li, G. Wang, Y. Li, X. Jin, X. Wang, J. Li and G. Zhang, *J. Mater. Chem. A*, 2019, **7**, 13922–13927.

55 H. Kim, Y. Ishado, Y. Tian and G. Ceder, *Adv. Funct. Mater.*, 2019, **1902392**, 1–8.

56 V. A. Nikitina, S. S. Fedotov, S. Y. Vassiliev, A. S. Samarin, N. R. Khasanova and E. V. Antipov, *J. Electrochem. Soc.*, 2017, **164**, A6373–A6380.

57 S. S. Fedotov, A. S. Samarin, V. A. Nikitina, D. A. Aksyonov, S. A. Sokolov, A. Zhugayevych, K. J. Stevenson, N. R. Khasanova, A. M. Abakumov and E. V. Antipov, *J. Mater. Chem. A*, 2018, **6**, 14420–14430.

58 N. Recham, G. Rousse, M. T. Sougrati, J. N. Chotard, C. Frayret, S. Mariyappan, B. C. Melot, J. C. Jumas and J. M. Tarascon, *Chem. Mater.*, 2012, **24**, 4363–4370.

59 S. Komaba, N. Yabuuchi, T. Nakayama, A. Ogata, T. Ishikawa and I. Nakai, *Inorg. Chem.*, 2012, **51**, 6211–6220.

60 S. P. Ong, V. L. Chevrier, G. Hautier, A. Jain, C. Moore, S. Kim, X. Ma and G. Ceder, *Energy Environ. Sci.*, 2011, **4**, 3680–3688.

61 F. Zhou, M. Cococcioni, K. Kang and G. Ceder, *Electrochem. commun.*, 2004, **6**, 1144–1148.

62 A. Gutierrez, N. A. Benedek and A. Manthiram, *Chem. Mater.*, 2013, **25**, 4010–4016.

63 Y. Nanba, T. Iwao, B. M. De Boisse, W. Zhao, E. Hosono, D. Asakura, H. Niwa, H. Kiuchi, J. Miyawaki, Y. Harada, M. Okubo and A. Yamada, *Chem. Mater.*, 2016, **28**, 1058–1065.

64 S. B. Schougaard, J. Bréger, M. Jiang, C. P. Grey and J. B. Goodenough, *Adv. Mater.*, 2006, **18**, 905–909.

65 N. Yabuuchi, M. Yano, H. Yoshida, S. Kuze and S. Komaba, *J. Electrochem. Soc.*, 2013, **160**, 3131–3137.

66 Shriver and Atkins, *Oxford Univ.*, , DOI:10.1016/0375-9601(91)90960-G.

67 C. A. Marianetti, G. Ceder and D. Morgan, *Phys. Rev. B - Condens. Matter Mater. Phys.*, 2001, **63**, 1–15.

68 X. Li, Y. Xu and C. Wang, *J. Alloys Compd.*, 2009, 479, 310–313.

69 P. Lucas and C. A. Angell, *J. Electrochem. Soc.*, 2000, **147**, 4459–4463.

70 R. Prasad, R. Benedek and M. M. Thackeray, *Phys. Rev. B - Condens. Matter Mater. Phys.*, 2005, **71**, 1–11.

71 Y. Il Jang, B. Huang, H. Wang, D. R. Sadoway and Y. M. Chiang, *J. Electrochem. Soc.*, 1999, **146**, 3217–3223.

72 D. Choi, D. Wang, I. T. Bae, J. Xiao, Z. Nie, W. Wang, V. V. Viswanathan, Y. J. Lee, J. G. Zhang, G. L. Graff, Z. Yang and J. Liu, *Nano Lett.*, 2010, **10**, 2799–2805.

73 M. Yonemura, A. Yamada, Y. Takei, N. Sonoyama and R. Kanno, *J. Electrochem. Soc.*, 2004, **151**, A1352.

74 X. Li, Y. Wang, D. Wu, L. Liu, S. H. Bo and G. Ceder, *Chem. Mater.*, 2016, **28**, 6575–6583.

75 H. Kim, G. Yoon, I. Park, K. Y. Park, B. Lee, J. Kim, Y. U. Park, S. K. Jung, H. D. Lim, D. Ahn, S. Lee and K. Kang, *Energy Environ. Sci.*, 2015, **8**, 3325–3335.

76 H. Kim, I. Park, S. Lee, H. Kim, K. Y. Park, Y. U. Park, H. Kim, J. Kim, H. D. Lim, W. S. Yoon and K. Kang, *Chem. Mater.*, 2013, **25**, 3614–3622.

77 S. H. Bo, X. Li, A. J. Toumar and G. Ceder, *Chem. Mater.*, 2016, **28**, 1419–1429.

78 W. Li, B. Song and A. Manthiram, *Chem. Soc. Rev.*, 2017, **46**, 3006–3059.

79 M. M. Thackeray, P. J. Johnson, L. A. de Picciotto, P. G. Bruce and J. B. Goodenough, *Mater. Res. Bull.*, 1984, **19**, 179–187.

80 C. Zhan, T. Wu, J. Lu and K. Amine, *Energy Environ. Sci.*, 2018, **11**, 243–257.

81 M. Balasubramanian, J. McBreen, I. J. Davidson, P. S. Whitfield and I. Kargina, *J. Electrochem. Soc.*, 2002, **149**, 176–184.

82 M. H. Cao, Y. Wang, Z. Shadike, J. L. Yue, E. Hu, S. M. Bak, Y. N. Zhou, X. Q. Yang and Z. W. Fu, *J. Mater. Chem. A*, 2017, **5**, 5442–5448.

83 B. Ammundsen, J. Paulsen, I. Davidson, R. S. Liu, C. H. Shen, J. M. Chen, L. Y. Jang and J. F. Lee, *J. Electrochem. Soc.*, 2002, **149**, 431–436.

84 P. J. Reeves, I. D. Seymour, K. J. Griffith and C. P. Grey, *Chem. Mater.*, 2019, **31**, 2814–2821.

85 C. Delmas and I. Saadoune, *Solid State Ionics*, 1992, **53–56**, 370–375.

86 N. IMANISHI, M. TOYODA, Y. TAKEDA and O. YAMAMOTO, *Solid State Ionics*, 1992, **58**, 333–338.

87 T. Ohzuku, S. Takeda and M. Iwanaga, *J. Power Sources*, 1999, **81–82**, 90–94.

88 C. M. Julien and A. Mauger, *Review of 5-V electrodes for Li-ion batteries: Status and trends*, 2013, vol. 19.

89 A. Kraytsberg and Y. Ein-Eli, *Adv. Energy Mater.*, 2012, **2**, 922–939.

90 L. A. de Picciotto, M. M. Thackeray, W. I. F. David, P. G. Bruce and J. B. Goodenough, *Mater. Res. Bull.*, 1984, **19**, 1497–1506.

91 H. Arai, S. Okada, Y. Sakurai and J. I. Yamaki, *Solid State Ionics*, 1998, **106**, 45–53.

92 J. Barker, M. Y. Saidi and J. L. Swoyer, *Solid State Ionics*, 2003, **158**, 261–267.

93 Q. Zhong, A. Bonakdarpour, M. Zhang, Y. Gao and J. R. Dahn, *J. Electrochem. Soc.*, 1997, **144**, 205–213.

94 J. R. Croy, A. Abouimrane and Z. Zhang, *MRS Bull.*, 2014, **39**, 407–415.

95 Z. M. Xu, S. H. Bo and H. Zhu, *ACS Appl. Mater. Interfaces*, 2018, **10**, 36941–36953.

96 Y. Kim, K. S. Park, S. H. Song, J. Han and J. B. Goodenough, *J. Electrochem. Soc.*, , DOI:10.1149/1.3151856.

97 M. S. WHITTINGHAM, *Science*, 1976, **192**, 1126–1127.

98 B. C. Melot and J. M. Tarascon, *Acc. Chem. Res.*, 2013, **46**, 1226–1238.

99 K. Chen and D. Xue, *J. Mater. Chem. A*, 2016, **4**, 7522–7537.

100 A. Yamada, S. C. Chung and K. Hinokuma, *J. Electrochem. Soc.*, 2001, **148**, 224–229.

101 G. Weirum, G. Barcaro, A. Fortunelli, F. Weber, R. Schennach, S. Surnev and F. P. Netzer, *J. Phys. Chem. C*, 2010, **114**, 15432–15439.

102 M. Reynaud, M. Ati, B. C. Melot, M. T. Sougrati, G. Rousse, J. N. Chotard and J. M. Tarascon, *Electrochem. commun.*, 2012, **21**, 77–80.

103 C. Masquelier and L. Croguennec, *Chem. Rev.*, 2013, **113**, 6552–6591.

104 M. Armand and M. E. Arroyo Y De Dompablo, *J. Mater. Chem.*, 2011, **21**, 10026–10034.

105 C. Masquelier and L. Croguennec, *Chem. Rev.*, 2013, **113**, 6552–6591.

106 M. Bianchini, P. Xiao, Y. Wang and G. Ceder, *Adv. Energy Mater.*, 2017, **7**, 1–9.

107 L. Croguennec, C. Pouillerie, A. N. Mansour and C. Delmas, *J. Mater. Chem.*, 2001, **11**, 131–141.

108 W. S. Yoon, K. B. Kim, M. G. Kim, M. K. Lee, H. J. Shin, J. M. Lee, J. S. Lee and C. H. Yo, *J. Phys. Chem. B*, 2002, **106**, 2526–2532.

109 Z. W. Lebens-Higgins, N. V. Faenza, M. D. Radin, H. Liu, S. Sallis, J. Rana, J. Vinckeviciute, P. J. Reeves, M. J. Zuba, F. Badway, N. Pereira, K. W. Chapman, T.-L. Lee, T. Wu, C. P. Grey, B. C. Melot, A. Van Der Ven, G. G. Amatucci, W. Yang and L. F. J. Piper, *Mater. Horizons*, , DOI:10.1039/c9mh00765b.

110 M. M. Thackeray, S. H. Kang, C. S. Johnson, J. T. Vaughey, R. Benedek and S. A. Hackney, *J. Mater. Chem.*, 2007, **17**, 3112–3125.

111 H. Koga, L. Croguennec, M. Menetrier, K. Douhil, S. Belin, L. Bourgeois, E. Suard, F. Weill and C. Delmas, *J. Electrochem. Soc.*, 2013, **160**, 786–792.

112 S. Muhammad, H. Kim, Y. Kim, D. Kim, J. H. Song, J. Yoon, J.-H. Park, S.-J. Ahn, S.-H. Kang, M. M. Thackeray and W.-S. Yoon, *Nano Energy*, 2016, **21**, 172–184.

113 K. Luo, M. R. Roberts, R. Hao, N. Guerrini, D. M. Pickup, Y.-S. Liu, K. Edström, J. Guo, A. V. Chadwick, L. C. Duda and P. G. Bruce, *Nat. Chem.*, 2016, **8**, 684–691.

114 N. Yabuuchi, M. Nakayama, M. Takeuchi, S. Komaba, Y. Hashimoto, T. Mukai, H. Shiiba, K. Sato, Y. Kobayashi, A. Nakao, M. Yonemura, K. Yamanaka, K. Mitsuhara and T. Ohta, *Nat. Commun.*, 2016, **7**, 13814.

115 A. D. Robertson and P. G. Bruce, *Chem. Mater.*, 2003, **15**, 1984–1992.

116 M. Sathiya, G. Rousse, K. Ramesha, C. P. Laisa, H. Vezin, M. T. Sougrati, M.-L. Doublet, D. Foix, D. Gonbeau, W. Walker, A. S. Prakash, M. Ben Hassine, L. Dupont and J.-M. Tarascon, *Nat. Mater.*, 2013, **12**, 827–835.

117 E. McCalla, A. M. Abakumov, M. Saubanère, D. Foix, E. J. Berg, G. Rousse, M. L. Doublet, D. Gonbeau, P. Novák, G. Van Tendeloo, R.

Dominko and J. M. Tarascon, *Science*, 2015, **350**, 1516–1521.

118 J. Hong, W. E. Gent, P. Xiao, K. Lim, D. H. Seo, J. Wu, P. M. Csernica, C. J. Takacs, D. Nordlund, C. J. Sun, K. H. Stone, D. Passarello, W. Yang, D. Prendergast, G. Ceder, M. F. Toney and W. C. Chueh, *Nat. Mater.*, 2019, **18**, 256–265.

119 A. J. Perez, Q. Jacquet, D. Batuk, A. Iadecola, M. Saubanère, G. Rousse, D. Larcher, H. Vezin, M. L. Doublet and J. M. Tarascon, *Nat. Energy*, 2017, **2**, 954–962.

120 N. Yabuuchi, Y. Tahara, S. Komaba, S. Kitada and Y. Kajiya, *Chem. Mater.*, 2016, **28**, 416–419.

121 T. Matsuhara, Y. Tsuchiya, K. Yamanaka, K. Mitsuhara, T. Ohta and N. Yabuuchi, *Electrochemistry*, 2016, **84**, 797–801.

122 M. Saubanère, E. McCalla, J. M. Tarascon and M. L. Doublet, *Energy Environ. Sci.*, 2016, **9**, 984–991.

123 D.-H. Seo, J. Lee, A. Urban, R. Malik, S. Kang and G. Ceder, *Nat. Chem.*, 2016, **8**, 692–697.

124 E. McCalla, A. S. Prakash, E. Berg, M. Saubanère, A. M. Abakumov, D. Foix, B. Klobes, M.-T. Sougrati, G. Rousse, F. Lepoivre, S. Mariyappan, M.-L. Doublet, D. Gonbeau, P. Novak, G. Van Tendeloo, R. P. Hermann and J.-M. Tarascon, *J. Electrochem. Soc.*, 2015, **162**, A1341–A1351.

125 Q. Jacquet, A. Perez, D. Batuk, G. Van Tendeloo, G. Rousse and J. M. Tarascon, *Chem. Mater.*, 2017, **29**, 5331–5343.

126 W. E. Gent, K. Lim, Y. Liang, Q. Li, T. Barnes, S. J. Ahn, K. H. Stone, M. McIntire, J. Hong, J. H. Song, Y. Li, A. Mehta, S. Ermon, T. Tyliszczak, D. Kilcoyne, D. Vine, J. H. Park, S. K. Doo, M. F. Toney, W. Yang, D. Prendergast and W. C. Chueh, *Nat. Commun.*, , DOI:10.1038/s41467-017-02041-x.

127 W. Lee, S. Muhammad, T. Kim, H. Kim, E. Lee, M. Jeong, S. Son, J.-H. Ryou and W.-S. Yoon, *Adv. Energy Mater.*, 2018, **8**, 1701788.

128 E. G. Tulsky and J. R. Long, *Chem. Mater.*, 2001, **13**, 1149–1166.

129 K. Kang, *Science*, 2006, **311**, 977–980.

130 U. Maitra, R. A. House, J. W. Somerville, N. Tapia-Ruiz, J. G. Lozano, N. Guerrini, R. Hao, K. Luo, L. Jin, M. A. Pérez-Osorio, F. Massel, D. M. Pickup, S. Ramos, X. Lu, D. E. McNally, A. V. Chadwick, F. Giustino, T. Schmitt, L. C. Duda, M. R. Roberts and P. G. Bruce, *Nat. Chem.*, 2018, **10**, 288–295.

131 J. Lee, A. Urban, X. Li, D. Su, G. Hautier and G. Ceder, *Science*, 2014, **343**, 519–522.

132 S. Patoux, L. Daniel, C. Bourbon, H. Lignier, C. Pagano, F. Le Cras, S. Jouanneau and S. Martinet, *J. Power Sources*, 2009, **189**, 344–352.

133 Y. Janssen, D. Santhanagopalan, D. Qian, M. Chi, X. Wang, C. Hoffmann, Y. S. Meng and P. G. Khalifah, *Chem. Mater.*, 2013, **25**, 4574–4584.

134 M. Reynaud, G. Rousse, J. N. Chotard, J. Rodríguez-Carvajal and J. M. Tarascon, *Inorg. Chem.*, 2013, 52, 10456–10466.

135 M. Sato, T. Ishigaki, K. Uematsu, K. Toda and H. Okawa, *Acta Crystallogr. Sect. E Struct. Reports Online*, , DOI:10.1107/S1600536812035040.

136 V. Legagneur, Y. An, A. Mosbah, R. Portal, A. Le Gal La Salle, A. Verbaere, D. Guyomard and Y. Piffard, *Solid State Ionics*, 2001, **139**, 37–46.

137 W. Dong, L. N. Zhu, H. Bin Song, D. Z. Liao, Z. H. Jiang, S. P. Yan, P. Cheng and S. Gao, *Inorg. Chem.*, 2004, **43**, 2465–2467.

138 H. Zhou, S. Upreti, N. A. Chernova and M. S. Whittingham, *Acta Crystallogr. Sect. E Struct. Reports Online*, , DOI:10.1107/S1600536811038451.

139 S. S. Fedotov, N. R. Khasanova, A. S. Samarin, O. A. Drozhzhin, D. Batuk, O. M. Karakulina, J. Hadermann, A. M. Abakumov and E. V. Antipov, *Chem. Mater.*, 2016, **28**, 411–415.

140 M. Sun, G. Rousse, D. D. Corte, M. Saubanère, M. L. Doublet and J. M. Tarascon, *Chem. Mater.*, 2016, **28**, 1607–1610.

141 C. Delmas, A. Nadiri and J. L. Soubeyroux, *Solid State Ionics*, 1988, **28–30**, 419–423.

142 C. Masquelier, A. K. Padhi, K. S. Nanjundaswamy and B. Goodenough, *J. Solid State Chem.*, 1998, **135**, 228–234.

143 G. Rousse, J. Rodriguez-Carvajal, S. Patoux and C. Masquelier, *Chem. Mater.*, 2003, **15**, 4082–4090.

144 M. Tamaru, S. C. Chung, D. Shimizu, S. I. Nishimura and A. Yamada, *Chem. Mater.*, 2013, **25**, 2538–2543.

145 P. Barpanda, S. I. Nishimura and A. Yamada, *Adv. Energy Mater.*, 2012, 2, 841–859.

146 J. Barker, M. Y. Saidi and J. L. Swoyer, *J. Electrochem. Soc.*, 2003, **150**, A1394.

147 J. Gaubicher, C. Wurm, G. Goward, C. Masquelier and L. Nazar, *Chem. Mater.*, 2000, **12**, 3240–3242.

148 A. Manthiram and J. B. Goodenough, *J. Power Sources*, 1989, **26**, 403–408.

149 K. S. Nanjundaswamy, A. K. Padhi, J. B. Goodenough, S. Okada, H. Ohtsuka, H. Arai and J. Yamaki, *Solid State Ionics*, 1996, **92**, 1–10.

150 N. Recham, J.-N. Chotard, L. Dupont, C. Delacourt, W. Walker, M. Armand and J.-M. Tarascon, *Nat. Mater.*, 2010, **9**, 68–74.

151 G. Rousse and J. M. Tarascon, *Chem. Mater.*, 2014, **26**, 394–406.

152 P. Barpanda, M. Ati, B. C. Melot, G. Rousse, J. N. Chotard, M. L. Doublet, M. T. Sougrati, S. A. Corr, J. C. Jumas and J. M. Tarascon, *Nat. Mater.*, 2011, **10**, 772–779.

153 M. Ben Yahia, F. Lemoigno, G. Rousse, F. Boucher, J. M. Tarascon and M. L. Doublet, *Energy Environ. Sci.*, 2012, **5**, 9584–9594.

154 M. Anji Reddy, V. Pralong, V. Caignaert, U. V. Varadaraju and B. Raveau, *Electrochem. commun.*, 2009, 11, 1807–1810.

155 C. Sirisopanaporn, C. Masquelier, P. G. Bruce, A. R. Armstrong and R. Dominko, *J. Am. Chem. Soc.*, 2011, **133**, 1263–1265.

156 A. R. Armstrong, C. Lyness, M. Ménétrier and P. G. Bruce, *Chem. Mater.*, 2010, **22**, 1892–1900.

157 M. E. Arroyo-de Dompablo, M. Armand, J. M. Tarascon and U. Amador, *Electrochem. commun.*, 2006, 8, 1292–1298.

158 A. R. Armstrong, C. Lyness, M. Ménétrier and P. G. Bruce, *Chem. Mater.*, 2010, **22**, 1892–1900.

159 D. H. Seo, Y. U. Park, S. W. Kim, I. Park, R. A. Shakoor and K. Kang, *Phys. Rev. B - Condens. Matter Mater. Phys.*, 2011, **83**, 1–8.

160 H. Tokoro and S. I. Ohkoshi, *Dalt. Trans.*, 2011, **40**, 6825–6833.

161 B. Wang, Y. Han, X. Wang, N. Bahlawane, H. Pan, M. Yan and Y. Jiang, *iScience*, 2018, **3**, 110–133.

162 R. Tripathi, G. Popov, X. Sun, D. H. Ryan and L. F. Nazar, *J. Mater. Chem. A*, 2013, **1**, 2990–2994.

163 M. Ati, B. C. Melot, J. N. Chotard, G. Rousse, M. Reynaud and J. M. Tarascon, *Electrochem. commun.*, 2011, **13**, 1280–1283.

164 D. H. Seo, K. Y. Park, H. Kim, S. K. Jung, M. S. Park and K. Kang, *Adv. Energy Mater.*, 2018, **8**, 1–9.

165 L. Lander, M. Reynaud, G. Rousse, M. T. Sougrati, C. Laberty-Robert, R. J. Messinger, M. Deschamps and J. M. Tarascon, *Chem. Mater.*, 2014, **26**, 4178–4189.

166 L. Lander, M. Reynaud, J. Carrasco, N. A. Katcho, C. Bellin, A. Polian, B. Baptiste, G. Rousse and J. M. Tarascon, *Phys. Chem. Chem. Phys.*, 2016, **18**, 14509–14519.

167 P. E. Pearce, A. J. Perez, G. Rousse, M. Saubanère, D. Batuk, D. Foix, E. McCalla, A. M. Abakumov, G. Van Tendeloo, M.-L. Doublet and J.-M. Tarascon, *Nat. Mater.*, 2017, **16**, 580–586.

168 K. Kang and G. Ceder, *Phys. Rev. B*, 2006, **74**, 094105.

169 D. H. Lee, J. Xu and Y. S. Meng, *Phys. Chem. Chem. Phys.*, 2013, **15**, 3304–3312.

170 C. Delmas, A. Maazaz, C. Fouassier, J. M. Réau and P. Hagenmuller, *Mater. Res. Bull.*, 1979, **14**, 329–335.

171 H. Y. P. Hong, *Mater. Res. Bull.*, 1976, **11**, 173–182.

172 T. Ohzuku, A. Ueda and M. Nagayama, *J. Electrochem. Soc.*, 1993, **140**, 1862–1870.

173 Q. Zhong, A. Bonakclarpour, M. Zhang and J. R. Dahn, *J. Electrochem. Soc.*, 1997, **144**, 205–213.

174 D. . Abraham, R. . Twesten, M. Balasubramanian, I. Petrov, J. McBreen and K. Amine, *Electrochem. commun.*, 2002, **4**, 620–625.

175 W. Lee, D. Lee, Y. Kim, W. Choi and W. S. Yoon, *J. Mater. Chem. A*, 2020, **8**, 10206–10216.

176 W. Lee, S. Yun, H. Li, J. Kim, H. Lee, K. Kwon, J. Y. Lee, Y. Choi and W. Yoon, *Small*, 2020, **16**, 1905875.

177 C. Pouillerie, L. Croguennec, P. Biensan, P. Willmann and C. Delmas, *J. Electrochem. Soc.*, 2000, **147**, 2061.

178 J. P. Peres, C. Delmas, A. Rougier, M. Broussely, F. Perton, P. Biensan and P. Willmann, *J. Phys. Chem. Solids*, 1996, **57**, 1057–1060.

179 C. Delmas, J. P. Pérès, A. Rougier, A. Demourgues, F. Weill, A. V. Chadwick, M. Broussely, F. Perton, P. Biensan and P. Willmann, *J. Power Sources*, 1997, **68**, 120–125.

180 Y. U. Park, D. H. Seo, B. Kim, K. P. Hong, H. Kim, S. Lee, R. A. Shakoor, K. Miyasaka, J. M. Tarascon and K. Kang, *Sci. Rep.*, 2012, **2**, 1–7.

181 M. Gu, I. Belharouak, J. Zheng, H. Wu, J. Xiao, A. Genc, K. Amine, S. Thevuthasan, D. R. Baer, J. G. Zhang, N. D. Browning, J. Liu and C. Wang, *ACS Nano*, 2013, **7**, 760–767.

182 D. Mohanty, J. Li, D. P. Abraham, A. Huq, E. A. Payzant, D. L. Wood and C. Daniel, *Chem. Mater.*, 2014, **26**, 6272–6280.

183 K. Kleiner, B. Strehle, A. R. Baker, S. J. Day, C. C. Tang, I. Buchberger, F. F. Chesneau, H. A. Gasteiger and M. Piana, *Chem. Mater.*, 2018, **30**, 3656–3667.

184 D. Eum, B. Kim, S. J. Kim, H. Park, J. Wu, S. P. Cho, G. Yoon, M. H. Lee, S. K. Jung, W. Yang, W. M. Seong, K. Ku, O. Tamwattana, S. K. Park, I. Hwang and K. Kang, *Nat. Mater.*, , DOI:10.1038/s41563-019-0572-4.

185 M. R. Jo, Y. Kim, J. Yang, M. Jeong, K. Song, Y. Il Kim, J. M. Lim, M. Cho, J. H. Shim, Y. M. Kim, W. S. Yoon and Y. M. Kang, *Nat.*

Commun., 2019, **10**, 1–9.

186 Y. Kim, J. Yoo, D. Jang, S. Muhammad, M. Jeong, W. Choi and W. S. Yoon, *J. Mater. Chem. A*, 2018, **6**, 13743–13750.

187 J. Kim, B. Lee, H. Kim, H. Kim and K. Kang, *Chem. Mater.*, 2016, **28**, 6894–6899.

188 J. M. Clark, P. Barpanda, A. Yamada and M. S. Islam, *J. Mater. Chem. A*, 2014, **2**, 11807–11812.

189 J. C. Kim, D. H. Seo and G. Ceder, *Energy Environ. Sci.*, 2015, **8**, 1790–1798.

190 K. Y. Park, I. Park, H. Kim, G. Yoon, H. Gwon, Y. Cho, Y. S. Yun, J. J. Kim, S. Lee, D. Ahn, Y. Kim, H. Kim, I. Hwang, W. S. Yoon and K. Kang, *Energy Environ. Sci.*, 2016, **9**, 2902–2915.

191 M. Sathiya, A. M. Abakumov, D. Foix, G. Rousse, K. Ramesha, M. Saubanère, M. L. Doublet, H. Vezin, C. P. Laisa, A. S. Prakash, D. Gonbeau, G. VanTendeloo and J.-M. Tarascon, *Nat. Mater.*, 2015, **14**, 230–238.

192 A. Abdellahi, A. Urban, S. Dacek and G. Ceder, *Chem. Mater.*, 2016, **28**, 5373–5383.

193 A. Abdellahi, A. Urban, S. Dacek and G. Ceder, *Chem. Mater.*, 2016, **28**, 3659–3665.

194 N. Yabuuchi, M. Takeuchi, M. Nakayama, H. Shiiba, M. Ogawa, K. Nakayama, T. Ohta, D. Endo, T. Ozaki, T. Inamasu, K. Sato and S. Komaba, *Proc. Natl. Acad. Sci. U. S. A.*, 2015, **112**, 7650–7655.

195 R. Wang, X. Li, L. Liu, J. Lee, D. H. Seo, S. H. Bo, A. Urban and G. Ceder, *Electrochem. commun.*, 2015, **60**, 70–73.

196 J. Lee, D. H. Seo, M. Balasubramanian, N. Twu, X. Li and G. Ceder, *Energy Environ. Sci.*, 2015, **8**, 3255–3265.

197 S. L. Glazier, J. Li, J. Zhou, T. Bond and J. R. Dahn, *Chem. Mater.*, 2015, **27**, 7751–7756.

198 N. Twu, M. Metzger, M. Balasubramanian, C. Marino, X. Li, H. Chen, H. Gasteiger and G. Ceder, *Chem. Mater.*, 2017, **29**, 2584–2593.

199 B. Mortemard De Boisse, G. Liu, J. Ma, S. I. Nishimura, S. C. Chung, H. Kiuchi, Y. Harada, J. Kikkawa, Y. Kobayashi, M. Okubo and A. Yamada, *Nat. Commun.*, 2016, **7**, 1–9.

200 K. M. Mogare, K. Friese, W. Klein and M. Jansen, *Zeitschrift fur Anorg. und Allg. Chemie*, 2004, **630**, 547–552.

201 M. Tamaru, X. Wang, M. Okubo and A. Yamada, *Electrochem. commun.*, 2013, **33**, 23–26.

202 M. Kunduraci, J. F. Al-Sharab and G. G. Amatucci, *Chem. Mater.*, 2006, **18**, 3585–3592.

203 Y. N. Zhou, J. Ma, E. Hu, X. Yu, L. Gu, K. W. Nam, L. Chen, Z. Wang and X. Q. Yang, *Nat. Commun.*, 2014, **5**, 1–8.

204 S. T. Dacek, W. D. Richards, D. A. Kitchaev and G. Ceder, *Chem. Mater.*, 2016, **28**, 5450–5460.

205 J. Lee, J. K. Papp, R. J. Clément, S. Sallis, D. H. Kwon, T. Shi, W. Yang, B. D. McCloskey and G. Ceder, *Nat. Commun.*, 2017, **8**, 981

206 R. A. House, L. Jin, U. Maitra, K. Tsuruta, J. W. Somerville, D. P. Förstermann, F. Massel, L. Duda, M. R. Roberts and P. G. Bruce, *Energy Environ. Sci.*, 2018, **11**, 926–932.

207 J. Lee, D. A. Kitchaev, D.-H. Kwon, C.-W. Lee, J. K. Papp, Y.-S. Liu, Z. Lun, R. J. Clément, T. Shi, B. D. McCloskey, J. Guo, M. Balasubramanian and G. Ceder, *Nature*, 2018, **556**, 185–190.

208 Z. Lun, B. Ouyang, D. A. Kitchaev, R. J. Clément, J. K. Papp, M. Balasubramanian, Y. Tian, T. Lei, T. Shi, B. D. McCloskey, J. Lee and G. Ceder, *Adv. Energy Mater.*, 2019, **9**, 1802959.

209 Z. Lun, B. Ouyang, Z. Cai, R. J. Clément, D. H. Kwon, J. Huang, J. K. Papp, M. Balasubramanian, Y. Tian, B. D. McCloskey, H. Ji, H. Kim, D. A. Kitchaev and G. Ceder, *Chem*, 2020, **6**, 153–168.

210 R. J. Clément, Z. Lun and G. Ceder, *Energy Environ. Sci.*, 2020, **13**, 345–373.

211 W. Li, J. N. Reimers and J. R. Dahn, *Solid State Ionics*, 1993, **67**, 123–130.

212 X. Q. Yang, X. Sun and J. McBreen, *Electrochem. commun.*, 1999, **1**, 227–232.

213 L. Croguennec, C. Pouillerie and C. Delmas, *Solid State Ionics*, 2000, **135**, 259–266.

214 C. S. Yoon, D. W. Jun, S. T. Myung and Y. K. Sun, *ACS Energy Lett.*, 2017, **2**, 1150–1155.

215 H. H. Ryu, K. J. Park, C. S. Yoon and Y. K. Sun, *Chem. Mater.*, 2018, **30**, 1155–1163.

216 C. Delmas, C. Fouassier and P. Hagenmuller, *Phys. B+C*, 1980, **99**, 81–85.

217 A. J. Toumar, S. P. Ong, W. D. Richards, S. Dacek and G. Ceder, *Phys. Rev. Appl.*, 2015, **4**, 1–9.

218 Z. Lu and J. R. Dahn, *J. Electrochem. Soc.*, 2001, **148**, 1225–1229.

219 J. Alvarado, C. Ma, S. Wang, K. Nguyen, M. Kodur and Y. S. Meng, *ACS Appl. Mater. Interfaces*, 2017, **9**, 26518–26530.

220 C. Vaalma, G. A. Giffin, D. Buchholz and S. Passerini, *J. Electrochem. Soc.*, 2016, **163**, A1295–A1299.

221 X. Wang, X. Xu, C. Niu, J. Meng, M. Huang, X. Liu, Z. Liu and L. Mai, *Nano Lett.*, 2017, **17**, 544–550.

222 Y. Hironaka, K. Kubota and S. Komaba, *Chem. Commun.*, 2017, **53**, 3693–3696.

223 H. Kim, J. C. Kim, M. Bianchini, D. H. Seo, J. Rodriguez-Garcia and G. Ceder, *Adv. Energy Mater.*, 2018, **8**, 1–19.

224 W. J. Zhang, *J. Power Sources*, 2011, **196**, 2962–2970.

225 J. Kim, G. Yoon, M. H. Lee, H. Kim, S. Lee and K. Kang, *Chem. Mater.*, 2017, **29**, 7826–7832.

226 H. Zhang, D. Buchholz and S. Passerini, *Energies*, , DOI:10.3390/en10070889.

227 M. Kim and S. J. Kim, *Acta Crystallogr. Sect. E Struct. Reports Online*, , DOI:10.1107/S1600536813012427.

228 K. Kang, C. H. Chen, B. J. Hwang and G. Ceder, *Chem. Mater.*, 2004, **16**, 2685–2690.

229 C. K. Back, R. Z. Yin, S. J. Shin, Y. S. Lee, W. Choi and Y. S. Kim, *J. Electrochem. Soc.*, 2012, **159**, 0–6.

230 G. Vitins and K. West, *J. Electrochem. Soc.*, 1997, **144**, 2587–2592.

231 Y. Shao-Horn, S. A. Hackney, A. R. Armstrong, P. G. Bruce, R. Gitzendanner, C. S. Johnson and M. M. Thackeray, *J. Electrochem. Soc.*, 1999, **146**, 2404–2412.

232 J. Reed, G. Ceder and A. Van Der Ven, *Electrochem. Solid-State Lett.*, 2001, **4**, 78–81.

233 P. F. Wang, Y. You, Y. X. Yin and Y. G. Guo, *Adv. Energy Mater.*, 2018, **8**, 1–23.

234 J. N. Reimers and J. R. Dahn, *J. Electrochem. Soc.*, 1992, **139**, 2091.

235 G. G. Amatucci, J. M. Tarascon, and L.C. Klein, *J. Electrochem. Soc.,* 1996, **143**, 1114–1123.

236 X. Lu, Y. Sun, Z. Jian, X. He, L. Gu, Y. S. Hu, H. Li, Z. Wang, W. Chen, X. Duan, L. Chen, J. Maier, S. Tsukimoto and Y. Ikuhara, *Nano Lett.*, 2012, **12**, 6192–6197.

237 A. Boulineau, L. Simonin, J.-F. Colin, C. Bourbon and S. Patoux, *Nano Lett.*, 2013, **13**, 3857–3863.

238 S.-K. Jung, H. Gwon, J. Hong, K.-Y. Park, D.-H. Seo, H. Kim, J. Hyun, W. Yang and K. Kang, *Adv. Energy Mater.*, 2014, **4**, 1300787.

239 L. Wang, T. Maxisch and G. Ceder, *Chem. Mater.*, 2007, **19**, 543–552.

240 G. Ceder and A. Van Der Ven, *Electrochim. Acta*, 1999, **45**, 131–150.

241 S. K. Jung, H. Gwon, J. Hong, K. Y. Park, D. H. Seo, H. Kim, J. Hyun, W. Yang and K. Kang, *Adv. Energy Mater.*, 2014, **4**, 1–7.

242 S. Hwang, W. Chang, S. M. Kim, D. Su, D. H. Kim, J. Y. Lee, K. Y. Chung and E. A. Stach, *Chem. Mater.*, 2014, **26**, 1084–1092.

243 L. Zou, W. Zhao, Z. Liu, H. Jia, J. Zheng, G. Wang, Y. Yang, J. G. Zhang and C. Wang, *ACS Energy Lett.*, 2018, **3**, 2433–2440.

244 J. B. Goodenough and Y. Kim, *Chem. Mater.*, 2010, **22**, 587–603.

245 L. Zou, Z. Liu, W. Zhao, H. Jia, J. Zheng, Y. Yang, G. Wang, J. G. Zhang and C. Wang, *Chem. Mater.*, 2018, **30**, 7016–7026.

246 M. Lewerenz, A. Warnecke and D. U. Sauer, *J. Power Sources*, 2017, **369**, 122–132.

247 T. A. Arunkumar and A. Manthiram, *Electrochem. Solid-State Lett.*, 2005, **8**, 403–405.

248 W. Cho, S. Myeong, N. Kim, S. Lee, Y. Kim, M. Kim, S. J. Kang, N. Park, P. Oh and J. Cho, *Adv. Mater.*, , DOI:10.1002/adma.201605578.

249 J. Yang and Y. Xia, *ACS Appl. Mater. Interfaces*, 2016, **8**, 1297–1308.

250 M. D. Radin, J. Alvarado, Y. S. Meng and A. Van Der Ven, *Nano Lett.*, 2017, **17**, 7789–7795.

251 H. Duncan, B. Hai, M. Leskes, C. P. Grey and G. Chen, *Chem. Mater.*, 2014, **26**, 5374–5382.

252 P. Vassilaras, D. H. Kwon, S. T. Dacek, T. Shi, D. H. Seo, G. Ceder and J. C. Kim, *J. Mater. Chem. A*, 2017, **5**, 4596–4606.

253 J. Han, K. Kim, Y. Lee and N. Choi, *Adv. Mater.*, 2019, **31**, 1804822.

254 K. Edström, T. Gustafsson and J. O. Thomas, *Electrochim. Acta*, 2004, **50**, 397–403.

255 D. Aurbach, *J. Power Sources*, 2000, **89**, 206–218.

256 J. Vetter, P. Novák, M. R. Wagner, C. Veit, K.-C. Möller, J. O. Besenhard, M. Winter, M. Wohlfahrt-Mehrens, C. Vogler and A. Hammouche, *J. Power Sources*, 2005, **147**, 269–281.

257 R. Qiao, Y. Wang, P. Olalde-Velasco, H. Li, Y. S. Hu and W. Yang, *J. Power Sources*, 2015, **273**, 1120–1126.

258 J. Zheng, M. Gu, J. Xiao, P. Zuo, C. Wang and J. G. Zhang, *Nano Lett.*, 2013, **13**, 3824–3830.

259 S. K. Martha, J. Nanda, Y. Kim, R. R. Unocic, S. Pannala and N. J. Dudney, *J. Mater. Chem. A*, 2013, **1**, 5587–5595.

260 J. G. Han, S. J. Lee, J. Lee, J. S. Kim, K. T. Lee and N. S. Choi, *ACS Appl. Mater. Interfaces*, 2015, **7**, 8319–8329.

261 S. Zhang, H. Gu, H. Pan, S. Yang, W. Du, X. Li, M. Gao, Y. Liu, M. Zhu, L. Ouyang, D. Jian and F. Pan, *Adv. Energy Mater.*, 2017, **7**, 1601066.

262 H. Zheng, Q. Sun, G. Liu, X. Song and V. S. Battaglia, *J. Power Sources*, 2012, **207**, 134–140.

263 B. Song, Z. Liu, M. O. Lai and L. Lu, *Phys. Chem. Chem. Phys.*, 2012, **14**, 12875–83.

264 K. Amine, J. Liu and I. Belharouak, *Electrochem. commun.*, 2005, **7**, 669–673.

265 A. R. Cho, J. N. Son, V. Aravindan, H. Kim, K. S. Kang, W. S. Yoon, W. S. Kim and Y. S. Lee, *J. Mater. Chem.*, 2012, **22**, 6556–6560.

266 K. Kalaga, F. N. Sayed, M. T. F. Rodrigues, G. Babu, H. Gullapalli and P. M. Ajayan, *J. Power Sources*, 2018, **390**, 100–107.

267 I. Källquist, A. J. Naylor, C. Baur, J. Chable, J. Kullgren, M. Fichtner, K. Edström, D. Brandell and M. Hahlin, *Chem. Mater.*, 2019, **31**, 6084–6096.

268 N. V. Faenza, Z. W. Lebens-Higgins, P. Mukherjee, S. Sallis, N. Pereira, F. Badway, A. Halajko, G. Ceder, F. Cosandey, L. F. J. Piper and G. G. Amatucci, *Langmuir*, 2017, **33**, 9333–9353.

269 A. Wang, S. Kadam, H. Li, S. Shi and Y. Qi, *npj Comput. Mater.*, , DOI:10.1038/s41524-018-0064-0.

270 H. Park, T. Yoon, Y. Kim, J. G. Lee, J. Kim, H. S. Kim, J. H. Ryu, J. J. Kim and S. M. Oh, *J. Electrochem. Soc.*, 2015, **162**, A892–A896.

271 H. Kim, W. Choi, J. Yoon, J. H. Um, W. Lee, J. Kim, J. Cabana and W. S. Yoon, *Chem. Rev.*, , DOI:10.1021/acs.chemrev.9b00618.

272 S. Laruelle, S. Grugeon, P. Poizot, M. Dollé, L. Dupont and J. M. Tarascon, *J. Electrochem. Soc.*, 2002, **149**, 627–634.

273 Y. Y. Hu, Z. Liu, K. W. Nam, O. J. Borkiewicz, J. Cheng, X. Hua, M. T. Dunstan, X. Yu, K. M. Wiaderek, L. S. Du, K. W. Chapman, P. J. Chupas, X. Q. Yang and C. P. Grey, *Nat. Mater.*, 2013, **12**, 1130–1136.

274 S. J. Rezvani, R. Gunnella, A. Witkowska, F. Mueller, M. Pasqualini, F. Nobili, S. Passerini and A. Di Cicco, *ACS Appl. Mater. Interfaces*, 2017, **9**, 4570–4576.

275 B. Philippe, M. Valvo, F. Lindgren, H. Rensmo and K. Edström, *Chem. Mater.*, 2014, **26**, 5028–5041.

276 B. Tian, J. Światowska, V. Maurice, S. Zanna, A. Seyeux, L. H. Klein and P. Marcus, *J. Phys. Chem. C*, 2013, **117**, 21651–21661.

277 R. Dedryvère, S. Laruelle, S. Grugeon, P. Poizot, D. Gonbeau and J. M. Tarascon, *Chem. Mater.*, 2004, **16**, 1056–1061.

278 J. Yang, S. Muhammad, M. R. Jo, H. Kim, K. Song, D. A. Agyeman, Y. Il Kim, W. S. Yoon and Y. M. Kang, *Chem. Soc. Rev.*, 2016, **45**, 5717–5770.

279 D. Aurbach, K. Gamolsky, B. Markovsky, G. Salitra, Y. Gofer, U. Heider, R. Oesten and M. Schmidt, *J. Electrochem. Soc.*, 2000, **147**, 1322–1331.

280 X. Yu and A. Manthiram, *Energy Environ. Sci.*, 2018, **11**, 527–543.

281 H. Yang, G. V. Zhuang and P. N. Ross, *J. Power Sources*, 2006, **161**, 573–579.

282 S. E. Sloop, J. B. Kerr and K. Kinoshita, *J. Power Sources*, 2003, **119–121**, 330–337.

283 K. Tasaki, A. Goldberg, J. J. Lian, M. Walker, A. Timmons and S. J. Harris, *J. Electrochem. Soc.*, 2009, **156**, 1019–1027.

284 N. S. Choi, J. G. Han, S. Y. Ha, I. Park and C. K. Back, *RSC Adv.*, 2015, **5**, 2732–2748.

285 P. K. Nayak, L. Yang, W. Brehm and P. Adelhelm, *Angew. Chemie - Int. Ed.*, 2018, **57**, 102–120.

286 J. S. Ko, V. V. T. Doan-Nguyen, H. S. Kim, X. Petrissans, R. H. Deblock, C. S. Choi, J. W. Long and B. S. Dunn, *J. Mater. Chem. A*, 2017, **5**, 18707–18715.

287 H. S. Kim, M. Kong, K. Kim, I. J. Kim and H. B. Gu, *J. Power Sources*, 2007, **171**, 917–921.

288 M. M. Doeff, J. D. Wilcox, R. Kostecki and G. Lau, *J. Power Sources*, 2006, **163**, 180–184.

289 X. Zhou, F. Wang, Y. Zhu and Z. Liu, *J. Mater. Chem.*, 2011, **21**, 3353–3358.

290 S. J. Shi, J. P. Tu, Y. J. Mai, Y. Q. Zhang, C. D. Gu and X. L. Wang, *Electrochim. Acta*, 2012, **63**, 112–117.

291 T. Yang, N. Zhang, Y. Lang and K. Sun, *Electrochim. Acta*, 2011, **56**, 4058–4064.

292 H. Lee, S. B. Lim, J. Y. Kim, M. Jeong, Y. J. Park and W. S. Yoon, *ACS Appl. Mater. Interfaces*, 2018, **10**, 10804–10818.

293 Y. Huang, N. A. Chernova, Q. Yin, Q. Wang, N. F. Quackenbush, M. Leskes, J. Fang, F. Omenya, R. Zhang, M. J. Wahila, L. F. J. Piper, G. Zhou, C. P. Grey and M. S. Whittingham, *Inorg. Chem.*, 2016, **55**, 4335–4343.

294 B. Lung-Hao Hu, F.-Y. Wu, C.-T. Lin, A. N. Khlobystov and L.-J. Li, *Nat. Commun.*, 2013, **4**, 1687.

295 W. Li, B. Song and A. Manthiram, *Chem. Soc. Rev.*, , DOI:10.1039/C6CS00875E.

296 S. T. Myung, K. Izumi, S. Komaba, Y. K. Sun, H. Yashiro and N. Kumagai, *Chem. Mater.*, 2005, **17**, 3695–3704.

297 A. M. Wise, C. Ban, J. N. Weker, S. Misra, A. S. Cavanagh, Z. Wu, Z. Li, M. S. Whittingham, K. Xu, S. M. George and M. F. Toney, *Chem. Mater.*, 2015, **27**, 6146–6154.

298 J. Liao and A. Manthiram, *J. Power Sources*, 2015, **282**, 429–436.

299 M. Xu, Z. Chen, L. Li, H. Zhu, Q. Zhao, L. Xu, N. Peng and L. Gong, *J. Power Sources*, 2015, **281**, 444–454.

300 P. Yan, J. Zheng, X. Zhang, R. Xu, K. Amine, J. Xiao, J. Zhang and C. Wang, *Chem. Mater.*, 2016, **28**, 857–863.

301 B. C. Park, H. B. Kim, H. J. Bang, J. Prakash and Y. K. Sun, *Ind. Eng. Chem. Res.*, 2008, **47**, 3876–3882.

302 J. Zheng, M. Gu, J. Xiao, B. J. Polzin, P. Yan, X. Chen, C. Wang and J. G. Zhang, *Chem. Mater.*, 2014, **26**, 6320–6327.

303 H. Konishi, K. Suzuki, S. Taminato, K. Kim, Y. Zheng, S. Kim, J. Lim, M. Hirayama, J. Y. Son, Y. Cui and R. Kanno, *J. Power Sources*, 2014, **269**, 293–298.

304 H. Liu, J. Huang, D. Qian, S. Hy, C. Fang, J. Luo and Y. S. Meng, *J. Electrochem. Soc.*, 2016, **163**, A971–A973.

305 J. Cho, T. J. Kim, J. Kim, M. Noh and B. Park, *J. Electrochem. Soc.*, 2004, **151**, 1899–1904.

306 K. S. Tan, M. V. Reddy, G. V. S. Rao and B. V. R. Chowdari, *J. Power Sources*, 2005, **141**, 129–142.

307 J. Liu and A. Manthiram, *Chem. Mater.*, 2009, **21**, 1695–1707.

308 F. Wu, X. Zhang, T. Zhao, L. Li, M. Xie and R. Chen, *ACS Appl. Mater. Interfaces*, 2015, **7**, 3773–3781.

309 Y. K. Sun, S. T. Myung, B. C. Park, J. Prakash, I. Belharouak and K. Amine, *Nat. Mater.*, 2009, **8**, 320–324.

310 Y. K. Sun, Z. Chen, H. J. Noh, D. J. Lee, H. G. Jung, Y. Ren, S. Wang, C. S. Yoon, S. T. Myung and K. Amine, *Nat. Mater.*, 2012, **11**, 942–947.

311 B. B. Lim, S. J. Yoon, K. J. Park, C. S. Yoon, S. J. Kim, J. J. Lee and Y. K. Sun, *Adv. Funct. Mater.*, 2015, **25**, 4673–4680.

312 U.-H. Kim, E.-J. Lee, C. S. Yoon, S.-T. Myung and Y.-K. Sun, *Adv. Energy Mater.*, 2016, **6**, 1601417.

313 F. Lin, D. Nordlund, Y. Li, M. K. Quan, L. Cheng, T.-C. Weng, Y. Liu, H. L. Xin and M. M. Doeff, *Nat. Energy*, 2016, **1**, 15004.

314 H. Wang, L. Ben, H. Yu, Y. Chen, X. Yang and X. Huang, *J. Mater. Chem. A*, 2017, **5**, 822–834.

315 D. W. Han, S. J. Lim, Y. Il Kim, S. H. Kang, Y. C. Lee and Y. M. Kang, *Chem. Mater.*, 2014, **26**, 3644–3650.

316 J. C. Kim, X. Li, B. Kang and G. Ceder, *Chem. Commun.*, 2015, **51**, 13279–13282.

317 C. G. Barlow, *Electrochem. Solid-State Lett.*, 1999, **2**, 362–364.

318 A. V. Plakhotnyk, L. Ernst and R. Schmutzler, *J. Fluor. Chem.*, 2005, **126**, 27–31.

319 S. F. Lux, I. T. Lucas, E. Pollak, S. Passerini, M. Winter and R. Kostecki, *Electrochem. commun.*, 2012, **14**, 47–50.

320 V. A. Agubra and J. W. Fergus, *J. Power Sources*, 2014, **268**, 153–162.

321 Y. M. Song, C. K. Kim, K. E. Kim, S. Y. Hong and N. S. Choi, *J. Power Sources*, 2016, **302**, 22–30.

322 A. M. Andersson and K. Edström, *J. Electrochem. Soc.*, 2001, **148**, 1100–1109.

323 S. Shiraishi, K. Kanamura and Z. I. Takehara, *Langmuir*, 1997, **13**, 3542–3549.

324 R. Wang, X. Li, Z. Wang and H. Zhang, *Nano Energy*, 2017, **34**, 131–140.

325 C. Xu, S. Renault, M. Ebadi, Z. Wang, E. Björklund, D. Guyomard, D. Brandell, K. Edström and T. Gustafsson, *Chem. Mater.*, 2017, **29**, 2254–2263.

326 X. Sun, H. S. Lee, X. Q. Yang and J. McBreen, *Electrochem. Solid-State Lett.*, 2002, **5**, 248–251.

327 Z. Cai, Y. Liu, J. Zhao, L. Li, Y. Zhang and J. Zhang, *J. Power Sources*, 2012, **202**, 341–346.

328 C. K. Kim, D. S. Shin, K. E. Kim, K. Shin, J. J. Woo, S. Kim, S. Y. Hong and N. S. Choi, *ChemElectroChem*, 2016, **3**, 913–921.

329 Y. Li, R. Zhang, J. Liu and C. Yang, *J. Power Sources*, 2009, **189**, 685–688.

330 A. S. Wotango, W. N. Su, E. G. Leggesse, A. M. Haregewoin, M. H. Lin, T. A. Zegeye, J. H. Cheng and B. J. Hwang, *ACS Appl. Mater. Interfaces*, 2017, **9**, 2410–2420.

331 K. Lu, *Nat. Rev. Mater.*, , DOI:10.1038/natrevmats.2016.19.

332 H. Moriwake, A. Kuwabara, C. A. J. Fisher, R. Huang, T. Hitosugi, Y. H. Ikuhara, H. Oki and Y. Ikuhara, *Adv. Mater.*, 2013, **25**, 618–622.

333 N. Balke, S. Jesse, A. N. Morozovska, E. Eliseev, D. W. Chung, Y. Kim, L. Adamczyk, R. E. García, N. Dudney and S. V. Kalinin, *Nat. Nanotechnol.*, 2010, **5**, 749–754.

334 S. Yang, B. Yan, L. Lu and K. Zeng, *RSC Adv.*, 2016, **6**, 94000–94009.

335 C. Ma, K. Chen, C. Liang, C. W. Nan, R. Ishikawa, K. More and M. Chi, *Energy Environ. Sci.*, 2014, **7**, 1638–1642.

336 M. Ati, M. Sathiya, S. Boulineau, M. Reynaud, A. Abakumov, G. Rousse, B. Melot, G. Van Tendeloo and J. M. Tarascon, *J. Am. Chem. Soc.*, 2012, **134**, 18380–18387.

337 Y. Sun, L. Liu, J. P. Dong, B. Zhang and X. J. Huang, *Chinese Phys. B*, , DOI:10.1088/1674-1056/20/12/126101.

338 P. Oh, S. Myeong, W. Cho, M. J. Lee, M. Ko, H. Y. Jeong and J. Cho, *Nano Lett.*, 2014, **14**, 5965–5972.

339 B. Song, T. Sui, S. Ying, L. Li, L. Lu and A. M. Korsunsky, *J. Mater. Chem. A*, 2015, **3**, 18171–18179.

340 P. Yan, J. Zheng, J. Liu, B. Wang, X. Cheng, Y. Zhang, X. Sun, C. Wang and J. G. Zhang, *Nat. Energy*, 2018, **3**, 600–605.

341 W. E. Gent, Y. Li, S. Ahn, J. Lim, Y. Liu, A. M. Wise, C. B. Gopal, D. N. Mueller, R. Davis, J. N. Weker, J. H. Park, S. K. Doo and W. C. Chueh, *Adv. Mater.*, 2016, 6631–6638.

342 H. Liu, M. Wolf, K. Karki, Y. S. Yu, E. A. Stach, J. Cabana, K. W. Chapman and P. J. Chupas, *Nano Lett.*, 2017, **17**, 3452–3457.

343 S. Zheng, R. Huang, Y. Makimura, Y. Ukyo, C. A. J. Fisher, T. Hirayama and Y. Ikuhara, *J. Electrochem. Soc.*, 2011, **158**, 357–362.

344 K. Zhao, M. Pharr, J. J. Vlassak and Z. Suo, *J. Appl. Phys.*, 2010, **108**, 1–7.

345 H. M. Wu, I. Belharouak, H. Deng, A. Abouimrane, Y. K. Sun and K. Amine, *J. Electrochem. Soc.*, 2009, **156**, 1047–1050.

346 S. Lee, Y. Cho, H. K. Song, K. T. Lee and J. Cho, *Angew. Chemie - Int. Ed.*, 2012, **51**, 8748–8752.

347 R. Y. S. Zampiva, C. G. Kaufmann Junior, J. S. Pinto, P. C. Panta, A. K. Alves and C. P. Bergmann, *Appl. Surf. Sci.*, 2017, **422**, 321–330.

348 M. Zhang, H. Liu, Z. Liu, C. Fang and Y. S. Meng, *ACS Appl. Energy Mater.*, 2018, **1**, 3369–3376.

349 J. Jiang and J. R. Dahn, *Electrochim. Acta*, 2004, **49**, 2661–2666.

350 C. (Matt) Lai, D. S. Ashby, N. H. Bashian, J. Schoiber, T. Liu, G. S. Lee, S. Chen, P. Wu, B. C. Melot and B. S. Dunn, *Adv. Energy Mater.*, 2019, **9**, 1900226.

351 P. Gibot, M. Casas-Cabanas, L. Laffont, S. Levasseur, P. Carlach, S. Hamelet, J. M. Tarascon and C. Masquelier, *Nat. Mater.*, 2008, **7**, 741–747.

352 J. Zheng, P. Yan, L. Estevez, C. Wang and J. G. Zhang, *Nano Energy*, 2018, **49**, 538–548.

353 A. S. Aricò, P. Bruce, B. Scrosati, J.-M. Tarascon and W. van Schalkwijk, *Nat. Mater.*, 2005, **4**, 366–377.

354 R. Malik, D. Burch, M. Bazant and G. Ceder, *Nano Lett.*, 2010, **10**, 4123–4127.

355 Y. Jiang, S. Yu, B. Wang, Y. Li, W. Sun, Y. Lu, M. Yan, B. Song and S. Dou, *Adv. Funct. Mater.*, 2016, **26**, 5315–5321.

356 M. Morant-Giner, R. Sanchis-Gual, J. Romero, A. Alberola, L. García-Cruz, S. Agouram, M. Galbiati, N. M. Padial, J. C. Waerenborgh, C. Martí-Gastaldo, S. Tatay, A. Forment-Aliaga and E. Coronado, *Adv. Funct. Mater.*, 2018, **28**, 1706125.

357 J. Lim, Y. Li, D. H. Alsem, H. So, S. C. Lee, P. Bai, D. A. Cogswell, X. Liu, N. Jin, Y. S. Yu, N. J. Salmon, D. A. Shapiro, M. Z. Bazant, T. Tyliszczak and W. C. Chueh, *Science*, 2016, **353**, 566–571.

358 G. Kobayashi, S. I. Nishimura, M. S. Park, R. Kanno, M. Yashima, T. Ida and A. Yamada, *Adv. Funct. Mater.*, 2009, **19**, 395–403.

359 N. Meethong, Y. H. Kao, M. Tang, H. Y. Huang, W. Craig Carter and Y. M. Chiang, *Chem. Mater.*, 2008, **20**, 6189–6198.

360 W. C. Chueh, F. El Gabaly, J. D. Sugar, N. C. Bartelt, A. H. McDaniel, K. R. Fenton, K. R. Zavadil, T. Tyliszczak, W. Lai and K. F. McCarty, *Nano Lett.*, 2013, **13**, 866–872.

361 Y. Li, S. Meyer, J. Lim, S. C. Lee, W. E. Gent, S. Marchesini, H. Krishnan, T. Tyliszczak, D. Shapiro, A. L. D. Kilcoyne and W. C. Chueh, *Adv. Mater.*, 2015, **27**, 6591–6597.

362 J. Kim, H. Lee, H. Cha, M. Yoon, M. Park and J. Cho, *Adv. Energy Mater.*, 2018, **8**, 1702028.

363 J. Li, A. R. Cameron, H. Li, S. Glazier, D. Xiong, M. Chatzidakis, J. Allen, G. A. Botton and J. R. Dahn, *J. Electrochem. Soc.*, 2017, **164**, A1534–A1544.

364 J. E. Harlow, X. Ma, J. Li, E. Logan, Y. Liu, N. Zhang, L. Ma, S. L. Glazier, M. M. E. Cormier, M. Genovese, S. Buteau, A. Cameron, J. E. Stark and J. R. Dahn, *J. Electrochem. Soc.*, 2019, **166**, A3031–A3044.

365 Z. Zhong, L. Chen, S. Huang, W. Shang, L. Kong, M. Sun, L. Chen and W. Ren, *J. Mater. Sci.*, , DOI:10.1007/s10853-019-04133-z.

366 S. Zhou, T. Mei, X. Wang and Y. Qian, *Nanoscale*, 2018, **10**, 17435–17455.

367 C. Zhu, R. E. Usiskin, Y. Yu and J. Maier, *Science*, DOI:10.1126/science.aao2808.

368 L. Chen, Y. Su, S. Chen, N. Li, L. Bao, W. Li, Z. Wang, M. Wang and F. Wu, *Adv. Mater.*, 2014, **26**, 6756–6760.

369 Y. Li, Y. Bai, X. Bi, J. Qian, L. Ma, J. Tian, C. Wu, F. Wu, J. Lu and K. Amine, *ChemSusChem*, 2016, **9**, 728–735.

370 L. Li, L. Wang, X. Zhang, Q. Xue, L. Wei, F. Wu and R. Chen, *ACS Appl. Mater. Interfaces*, 2017, **9**, 1516–1523.

371 K. M. Shaju and P. G. Bruce, *Adv. Mater.*, 2006, **18**, 2330–2334.

372 W. Hua, Z. Wu, M. Chen, M. Knapp, X. Guo, S. Indris, J. R. Binder, N. N. Bramnik, B. Zhong, H. Guo, S. Chou, Y. M. Kang and H. Ehrenberg, *J. Mater. Chem. A*, 2017, **5**, 25391–25400.

373 C. Zhu, Y. Yu, L. Gu, K. Weichert and J. Maier, *Angew. Chemie - Int. Ed.*, 2011, **50**, 6278–6282.

374 Z. Li, Z. Peng, H. Zhang, T. Hu, M. Hu, K. Zhu and X. Wang, *Nano Lett.*, 2016, **16**, 795–799.

375 Q. Zhang, S. Z. Huang, J. Jin, J. Liu, Y. Li, H. E. Wang, L. H. Chen, B. J. Wang and B. L. Su, *Sci. Rep.*, 2016, **6**, 1–12.

376 M. Y. Cho, K. B. Kim, J. W. Lee, H. Kim, H. Kim, K. Kang and K. Chul Roh, *RSC Adv.*, 2013, **3**, 3421–3427.

377 E. Hosono, T. Kudo, I. Honma, H. Matsuda and H. Zhou, *Nano Lett.*, 2009, **9**, 1045–1051.

378 J. Deng, J. Pan, Q. Yao, Z. Wang, H. Zhou and G. Rao, *J. Power Sources*, 2015, **278**, 370–374.

379 C. Nan, J. Lu, L. Li, L. Li, Q. Peng and Y. Li, *Nano Res.*, 2013, **6**, 469–477.

380 W. Ren, Z. Zheng, Y. Luo, W. Chen, C. Niu, K. Zhao, M. Yan, L. Zhang, J. Meng and L. Mai, *J. Mater. Chem. A*, 2015, **3**, 19850–19856.

381 Q. Zhao, Z. Guo, L. Wang, Y. Wu, F. K. Butt, Y. Zhu, X. Xu, X. Ma and C. Cao, *ACS Appl. Mater. Interfaces*, 2019, **11**, 30819–30827.

382 S. Kalluri, K. Hau Seng, W. Kong Pang, Z. Guo, Z. Chen, H. K. Liu and S. X. Dou, *ACS Appl. Mater. Interfaces*, 2014, **6**, 8953–8958.

383 H. Kang, Y. Liu, M. Shang, T. Lu, Y. Wang and L. Jiao, *Nanoscale*, 2015, **7**, 9261–9267.

384 Y. Dong, S. Li, K. Zhao, C. Han, W. Chen, B. Wang, L. Wang, B. Xu, Q. Wei, L. Zhang, X. Xu and L. Mai, *Energy Environ. Sci.*, 2015, **8**, 1267–1275.

385 T. F. Hung, W. J. Cheng, W. S. Chang, C. C. Yang, C. C. Shen and Y. L. Kuo, *Chem. - A Eur. J.*, 2016, **22**, 10620–10626.

386 H. Li, X. Bi, Y. Bai, Y. Yuan, R. Shahbazian-Yassar, C. Wu, F. Wu, J. Lu and K. Amine, *Adv. Mater. Interfaces*, 2016, **3**, 1–8.

387 W. Ren, Z. Zheng, C. Xu, C. Niu, Q. Wei, Q. An, K. Zhao, M. Yan, M. Qin and L. Mai, *Nano Energy*, 2016, **25**, 145–153.

388 X. Cao, A. Pan, S. Liu, J. Zhou, S. Li, G. Cao, J. Liu and S. Liang, *Adv. Energy Mater.*, 2017, **7**, 1–10.

389 T. Wei, G. Yang and C. Wang, *Nano Energy*, 2017, **39**, 363–370.

390 H. Li, Y. Bai, F. Wu, Y. Li and C. Wu, *J. Power Sources*, 2015, **273**, 784–792.

391 J. Han, G.-N. Li, F. Liu, M. Wang, Y. Zhang, L. Hu, C. Dai and M. Xu, *Chem. Commun.*, 2017, **53**, 1805–1808.